THE FRACABILITY EVALUATION OF DADAŞ SHALE IN SOUTHEASTERN TURKEY BASED ON ITS GEOMECHANICAL PROPERTIES

A THESIS SUBMITTED TO
THE GRADUATE SCHOOL OF NATURAL AND APPLIED SCIENCES
OF
MIDDLE EAST TECHNICAL UNIVERSITY

BY

OĞUZ CİHANER

IN PARTIAL FULFILLMENT OF THE REQUIREMENTS
FOR
THE DEGREE OF MASTER OF SCIENCE
IN
PETROLEUM AND NATURAL GAS ENGINEERING

SEPTEMBER 2023

Approval of the thesis:

THE FRACABILITY EVALUATION OF DADAŞ SHALE IN SOUTHEASTERN TURKEY BASED ON ITS GEOMECHANICAL PROPERTIES

submitted by **OĞUZ CİHANER** in partial fulfillment of the requirements for the degree of **Master of Science** in **Petroleum and Natural Gas Engineering, Middle East Technical University** by,

Prof. Dr. Halil Kalıpçılar
Dean, Graduate School of **Natural and Applied Sciences** _____

Assist Prof. Dr. İsmail Durgut
Head of the Department, **Petroleum and Natural Gas Engineering** _____

Assist. Prof. Dr. Betül Yıldırım
Supervisor, **Petroleum and Natural Gas Engineering, METU** _____

Examining Committee Members:

Assoc. Prof. Dr. Çağlar Sınayuç
Petroleum and Natural Gas Engineering Dept., METU _____

Assist. Prof. Dr. Betül Yıldırım
Petroleum and Natural Gas Engineering Dept., METU _____

Assoc. Prof. Dr. Şükrü Merey
Petroleum and Natural Gas Engineering Dept., Batman University _____

Date: 08.09.2023

I hereby declare that all information in this document has been obtained and presented in accordance with academic rules and ethical conduct. I also declare that, as required by these rules and conduct, I have fully cited and referenced all material and results that are not original to this work.

Name Last name: Oğuz Cihaner

Signature:

ABSTRACT

THE FRACABILITY EVALUATION OF DADAŞ SHALE IN SOUTHEASTERN TURKEY BASED ON ITS GEOMECHANICAL PROPERTIES

Cihaner, Oğuz
Master of Science, Petroleum and Natural Gas Engineering
Supervisor: Assist. Prof. Dr. Betül Yıldırım

September 2023, 124 pages

In an unconventional shale reservoir system, the source rock, the reservoir rock, and the caprock are all represented by the same shale formation. Shale reservoirs have poor natural productivity due to their extremely heterogeneous structures with ultra-low permeability. Therefore, an overwhelming majority of shale oil/gas wells requires horizontal drilling technologies combined with multi-stage hydraulic fracturing. Hydraulic fracturing of horizontal wells has been commonly used worldwide for the last 25 years to increase the stimulated reservoir volume (SRV).

The primary and sustained productivity of a shale reservoir is strongly dependent on geomechanical parameters. The fracability, which is stated as the most critical parameter in unconventional reservoir geomechanics, can be defined in its simplest form as the degree of a formation’s ability to be fractured effectively. Accordingly, the fracability index (FI) term can be used as a theoretical benchmark to mathematically calculate the tendency of rocks to be fractured. For hydraulic fracturing (HF) operations, FI can reflect a formation's tendency to initiate & propagate fractures and its ability to generate complex fracture network systems. Consequently, for unconventional reservoirs, fracability plays a crucial role in characterization of sweet spots and fracture barriers and in optimization of HF.

This study mainly aims at calculating the fracability index (FI) of Dadaş shale as a function of mechanical brittleness index (BI_{mech}), fracture toughness (K_C), minimum horizontal stress (σ_h), and differential horizontal stress (DHS, $\Delta\sigma$). To this end, firstly, a digitization study has been performed on the available logs (Gamma-ray log, Sonic (DT) log, and Density log) of Çalıktepe-2 well to obtain the crucial mechanical rock properties such as Young's Modulus (YM, E) and Poisson Ratio (PR, ν), geological principal stresses, DHS ($\Delta\sigma$), fracture toughness (K_C), unconfined compressive strength (UCS), tensile strength (To), internal friction angle (φ), and cohesion (C_O). Then, these geomechanical parameters have been utilized to evaluate the fracability from deterministic and probabilistic aspects. In this context, four fracability models, namely Rickman's et al.'s model (2008), Yuan et al.'s model (2017), Dou et al.'s model (2022), and newly proposed model in this study (2023) were implemented. This new fracability model obtained by modifying Dou et al.'s model includes mechanical brittleness index (BI_{mech}), mode-I and mode-II fracture toughness (K_{IC} & K_{IIC}), minimum horizontal stress (σ_h), and DHS ($\Delta\sigma$).

To achieve abovementioned goals, a comparative analysis between Marcellus shale and Dadaş shale was performed by examining FI results, which deterministically estimated from all studied models. Additionally, using Proposed model, FI values of some other shale formations (Barnett, Haynesville, Bakken, and Eagle Ford) were obtained to observe the correlation between FI and BI_{mech} and to validate successful HF performances applied in the U.S.'s productive shale reservoirs. In stochastic process, firstly Monte Carlo simulation with 10,000 iterations was applied to perform probabilistic risk analysis for FI. Next, for all studied fracability models, the effect of fracability components on output data (FI) was examined by sensitivity analysis using tornado chart and spider chart, accordingly, critical input parameters were determined for each model. Finally, all FI results of Dadaş shale was analyzed as a whole to compare deterministic method and stochastic method.

Interestingly, it was observed that the FI values obtained from Rickman et al.'s model (depends on normalized YM and PR) are significantly close to FI values of Yuan et al.'s model (depends on normalized YM and PR, K_{IC} and K_{IIC}, and minimum horizontal stress (σ_{min})). On the other hand, it was analyzed that values of Dou et al.'s model and Proposed model are obviously larger than those of two other models. Accordingly, this result may reflect that DHS ($\Delta\sigma$) has a strong effect on the fracability of Dadaş shale. Besides, it was found that the results of proposed model are highly close to results in Dou et al.'s model. From this point of view, it may be inferred that mode-II fracture toughness (K_{IIC}) plays a noticeable but small role in FI evaluation for Dadaş shale. The low effect of K_{IIC} on FI may be attributed to the fact that the initiation and propagation of fractures are more related to tensile fractures rather than shear fractures. All these findings mentioned above indicate that the Proposed model emphasizes the importance of differential horizontal stress and mode-II fracture toughness in fracability evaluation of shale reservoirs, which especially reside in strike-slip (SS) faulting and reverse faulting (RF) environments.

The relatively high deterministic FI results of Marcellus shale may be used as a supportive argument to successful hydraulic fracturing (HF) operations applied in this formation. From a comparative aspect, Marcellus shale has larger FI values than Dadaş-I shale in all studied models (especially in Rickman et al.'s model and Yuan et al.'s model). This can be explained by that Marcellus shale has a much more desirable geomechanical structure compared to Dadaş-I shale. On the other hand, deterministic FI results of Marcellus shale indicated close values with those of Dadaş-I shale for Dou et al.'s model and the Proposed model. It was also observed in this study that all examined formations in the U.S. was graded as highly fracable according to Proposed model despite their relatively not much bigger BI values. By this way, Dou et al.'s fracability model was verified by Proposed model. Additionally, it was found that Dadaş Shale shows a similar tendency with Barnett Shale and Haynesville Shale in regards to FI and BI_{mech}. The results also showed that there is not always a positive correlation between FI and BI.

In brief, according to Rickman et al.'s model and Yuan et al.'s model, it was identified that Dadaş shale is a low-level fracable formation, and it is difficult to obtain an effective HF performance from this formation. However, Rickman et al.'s model only contains the mechanical brittleness in FI equation. The reliability degree of Yuan et al.'s model is disputable due to the absence of DHS in fracability equation, and close FI values observed between this model and Rickman et al.'s model. On the other hand, Dou et al.'s model and the Proposed model showed in Dadaş shale that there is a high probability of effectually applying HF and a high tendency of obtaining complex fracture networks. Besides, compared to all other zones, L2 zone has more favorable petrophysical, geochemical (in terms of reservoir quality), and geomechanical properties (in terms of completion quality). From this viewpoint, it was concluded that L2 zone is the most likely ideal option in the matter of the effective stimulation of Dadaş shale by HF.

In light of the findings above, the Proposed model may be presented as an alternative FI method to determine sweet spots in an HF operation; yet, the results of this study should be extended by experimental data and numerical modelings. In the future, this research is expected to serve as a geomechanical benchmark in HF optimization of Turkey's pioneering unconventional shale resources.

Keywords: Dadaş Formation, Fracability, Fracability Index, Geomechanical Properties, Hydraulic Fracturing,

ÖZ

GÜNEYDOĞU TÜRKİYE'DEKİ DADAŞ ŞEYLİNİN JEOMEKANİK ÖZELLİKLERİNE GÖRE ÇATLATILABİLİRLİK DEĞERLENDİRMESİ

Cihaner, Oğuz
Yüksek Lisans, Petrol ve Doğal Gaz Mühendisliği
Tez Yöneticisi: Dr. Öğr. Üyesi Betül Yıldırım

Eylül 2023, 124 sayfa

Ankonvansiyonel (geleneksel olmayan) bir şeyl rezervuar sisteminde, kaynak kayaç, rezervuar kayaç ve örtü kayaç, aynı şeyl formasyonu tarafından temsil edilir. Şeyl rezervuarları, ultra düşük geçirgenliğe sahip son derece heterojen yapıları nedeniyle zayıf bir doğal üretkenliğe sahiptir. Bu nedenle, şeyl petrol/gaz kuyularının ezici bir çoğunluğu, çok aşamalı hidrolik çatlatma ile birlikte yatay sondaj teknolojilerine ihtiyaç duymaktadır. Yatay kuyuların hidrolik çatlatılması, uyarılmış rezervuar hacmini artırmak için son 25 yıldır dünya genelinde yaygın olarak kullanılmaktadır.

Bir şeyl rezervuarının birincil ve sürekli üretkenliği büyük ölçüde jeomekanik parametrelere bağlıdır. Ankonvansiyonel rezervuar jeomekaniğinde en kritik parametre olarak ifade edilen çatlatılabilirlik, en basit haliyle, bir formasyonun etkili bir şekilde kırılma/çatlama kabiliyetinin derecesi olarak tanımlanabilir. Buna göre çatlatılabilirlik indeksi (Çİ) terimi, kayaçların kırılma/çatlama eğilimini matematiksel olarak hesaplamak için teorik bir ölçüt olarak kullanılabilir. Hidrolik çatlatma (HÇ) operasyonları için Çİ, bir formasyonun çatlakları başlatma ve yayma eğilimini ve karmaşık kırılma ağı sistemleri oluşturma yeteneğini yansıtabilir. Sonuç olarak, geleneksel olmayan rezervuarlar için çatlatılabilirlik, tatlı noktaların ve

kırılma bariyerlerinin karakterizasyonunda ve HÇ optimizasyonunda çok önemli bir rol oynar.

Bu çalışma, temel olarak Dadaş şeylinin çatlatılabilirlik indeksini (Çİ) kırılganlık indeksinin (Kİ), kırılma tokluğunun (K_{I-II}), minimum yatay gerilmenin (σ_h) ve diferansiyel yatay gerilmenin ($\Delta\sigma$) bir fonksiyonu olarak hesaplamayı amaçlamaktadır. Bu amaç doğrultusunda, Young modülü (E), Poisson katsayısı (ν), jeolojik asal gerilmeler, diferansiyel yatay gerilme (DYG, $\Delta\sigma$), kırılma toklukları (Kıc and Kııc), serbest basınç dayanımı (UCS), çekme dayanımı (To), iç sürtünme açısı (φ) ve kohezyon (C) gibi önemli mekanik kayaç özelliklerini elde etmek amacıyla, öncelikle Çalıktepe-2 kuyusunun mevcut logları (gama-ışını logu, sonik DT logu ve özkütle logu) üzerinde bir sayısallaştırma çalışması yapılmıştır. Akabinde bu jeomekanik parametreler, çatlatılabilirliği deterministik ve olasılıksal açılardan değerlendirmek için kullanılmıştır. Bu bağlamda, Rickman v.d. modeli (2008), Yuan v.d. modeli (2017), Dou v.d. modeli (2022) ve bu çalışmada yeni önerilen model (2023) olmak üzere dört çatlatılabilirlik modeli uygulanmıştır. Dou v.d. modelinin değiştirilmesiyle elde edilen bu yeni çatlatılabilirlik modeli, mekanik kırılganlık indeksini ($Kİ_{mek}$), mod-I ve mod-II kırılma tokluğunu (K_{IC} & K_{IIC}), minimum yatay gerilimi (σh) ve DYG'yi ($\Delta\sigma$) içerir.

Yukarıda belirtilen hedeflere ulaşmak için, çalışılan tüm modellerden deterministik olarak tahmin edilen Çİ sonuçları incelenerek Marcellus şeyli ile Dadaş şeyli arasında karşılaştırmalı bir analiz yapıldı. Ek olarak, Çİ ve $Kİ_{mek}$ arasındaki korelasyonu gözlemlemek ve ABD'nin verimli şeyl rezervuarlarında uygulanan başarılı HÇ performanslarını doğrulamak için, Önerilen model kullanılarak diğer bazı şeyl formasyonlarının (Barnett, Haynesville, Bakken ve Eagle Ford) Çİ değerleri elde edildi. Stokastik süreçte, öncelikle Çİ için olasılıksal risk analizi gerçekleştirmek amacıyla 10,000 iterasyonlu Monte Carlo simülasyonu uygulandı. Daha sonra, incelenen tüm çatlatılabilirlik modelleri için, çatlatılabilirlik bileşenlerinin çıktı verisi (FI) üzerindeki etkisi, kasırga grafiği ve örümcek grafiği kullanılarak duyarlılık analizi ile incelenmiş ve buna göre her model için kritik girdi

parametreleri belirlenmiştir. Son olarak Dadaş şeylinin tüm Çİ sonuçları deterministik yöntem ile stokastik yöntemi karşılaştırmak amacıyla bir bütün olarak analiz edildi.

İlginç bir şekilde, Rickman v.d. modelinden (normalize edilmiş Young modülü (E) ve Poisson katsayısına (ν) bağlı olan) elde edilen Çİ değerlerinin Yuan v.d. modelindeki (normalize edilmiş Young modülü (E) ve Poisson katsayısına (ν), mod-I ve mod-II kırılma tokluklarına (Kıc and Kııc) ve minimum yatay gerilmeye (σh) bağlı olan) Çİ değerlerine önemli ölçüde yakın olduğu gözlemlenmiştir. Öte yandan Dou v.d. modelinin ve Önerilen modelin değerlerinin diğer iki modelden açıkça daha büyük olduğu analiz edilmiştir. Buna göre, bu sonuç Dadaş şeylinin çatlatılabilirliği üzerinde DYG'nin (Δσ) güçlü bir etkiye sahip olduğunu yansıtabilir. Ayrıca, Önerilen modelin sonuçlarının Dou v.d. modelindeki sonuçlara oldukça yakın olduğu bulunmuştur. Bu bakış açısından hareketle, Dadaş şeylinin Çİ değerlendirmesinde mod-II kırılma tokluğunun (K_{IIC}) gözle görülür fakat küçük bir rol oynadığı söylenebilir. K_{IIC}'nun Çİ üzerindeki etkisinin düşük olması, çatlakların başlaması ve ilerlemesinin kayma kırıklarından ziyade çekme kırıklarıyla daha fazla ilişkili olmasına bağlanabilir. Yukarıda bahsedilen tüm bu bulgular, Önerilen modelin, özellikle doğrultu atımlı (SS) faylanma ve ters faylanma (RF) ortamlarında bulunan şeyl rezervuarlarının çatlatılabilirlik değerlendirmesinde diferansiyel yatay gerilmenin ve mod-II kırılma tokluğunun önemini vurguladığını göstermektedir.

Marcellus şeylinin nispeten yüksek deterministik Çİ sonuçları, bu formasyonda uygulanan başarılı hidrolik çatlatma (HÇ) operasyonlarını destekleyici bir argüman olarak kullanılabilir. Karşılaştırmalı olarak bakıldığında, Marcellus şeyli, incelenen tüm modellerde (özellikle Rickman v.d. modelinde ve Yuan v.d. modelinde) Dadaş-I şeyline göre daha yüksek Çİ değerlerine sahiptir. Bu durum, Marcellus şeylinin Dadaş-I şeyline göre çok daha cazip bir jeomekanik yapıya sahip olmasıyla açıklanabilir. Öte yandan, Marcellus şeylinin deterministik Çİ sonuçları Dou v.d. modeli ve Önerilen model için Dadaş-I şeylinin değerlerine yakın değerler göstermiştir. Bu çalışmada ayrıca ABD'de incelenen tüm formasyonların Kİ

değerleri nispeten büyük olmasa da Önerilen modele göre yüksek derecede çatlatılabilir olarak derecelendirildiği gözlenmiştir. Böylece, Dou v.d. çatlatılabilirlik modeli Önerilen model ile doğrulanmıştır. Ek olarak, Dadaş şeylinin Çİ ve $Kİ_{mek}$ açısından Barnett şeyli ve Haynesville şeyli ile benzer eğilim gösterdiği bulunmuştur. Sonuçlar ayrıca Çİ ve Kİ arasında her zaman pozitif bir korelasyon olmadığını göstermiştir.

Özetle, Rickman v.d. modeli ile Yuan v.d. modeline göre Dadaş şeylinin düşük seviyeli çatlatılabilir bir formasyon olduğu ve bu formasyondan etkin bir HÇ performansı elde etmenin zor olduğu tespit edilmiştir. Ancak Rickman v.d. modeli FI denkleminde yalnızca mekanik kırılganlığı içermektedir. Yuan v.d. modelinin güvenilirlik derecesi, çatlatılabilirlik denkleminde DYG'nin bulunmaması ve bu model ile Rickman v.d. modeli arasında yakın Çİ değerlerinin gözlenmesi nedeniyle tartışmaya açıktır. Öte yandan, Dou v.d. modeli ve Önerilen model, Dadaş şeylinde HÇ'nın etkili bir şekilde uygulanma olasılığının ve karmaşık kırılma ağları elde etme eğiliminin yüksek olduğunu göstermiştir. Ayrıca L2 bölgesi diğer tüm bölgelere göre kıyasla daha elverişli petrofiziksel, jeokimyasal (rezervuar kalitesi açısından) ve jeomekanik (tamamlama kalitesi açısından) özelliklere sahiptir. Bu açıdan bakıldığında Dadaş şeylinin HÇ ile etkin bir şekilde uyarılması konusunda en olası ideal seçeneğin L2 bölgesi olduğu sonucuna varılmıştır.

Yukarıdaki bulguların ışığında, Önerilen model, bir HÇ operasyonundaki tatlı noktaları belirlemek için alternatif bir Çİ yöntemi olarak sunulabilir; ancak bu çalışmanın sonuçlarının deneysel veriler ve sayısal modellemelerle genişletilmesi gerekmektedir. Gelecekte bu araştırmanın, Türkiye'nin öncü geleneksel olmayan şeyl kaynaklarının HÇ optimizasyonunda jeomekanik bir referans noktası olarak hizmet etmesi beklenmektedir.

Anahtar Kelimeler: Dadaş Formasyonu, Çatlatılabilirlik, Çatlatılabilirlik İndeksi, Jeomekanik Özellikler, Hidrolik Çatlatma,

To my wife, my parents and my brothers

ACKNOWLEDGMENTS

I would sincerely like to express my deepest gratitude to my supervisor, Assist. Prof. Dr. Betül YILDIRIM, for her guidance, unique insight, beneficial advices, constructive feedbacks, and encouraging interpretations throughout this research.

I would also like to express my gratitude to Assoc. Prof. Dr. Çağlar Sınayuç and Assoc. Prof. Dr. Şükrü Merey, who served as my M.S. committee members, for their valuable comments, suggestions, and contributions.

I must express my endless thanks to my wife Ayşe Nur Cihaner, who continuously supported and motivated me in my master's study process.

Last but not the least, I would like to thank my friend and colleague Mehmet Soylu, who provided important contributions by generously allocating his time and effort.

TABLE OF CONTENTS

ABSTRACT v

ÖZ ix

ACKNOWLEDGMENTS xiv

TABLE OF CONTENTS xv

LIST OF TABLES xvii

LIST OF FIGURES xix

LIST OF ABBREVIATIONS xxiv

LIST OF SYMBOLS xxvi

CHAPTERS

1 INTRODUCTION 1

2 BACKGROUND INFORMATION 7

2.1 General Energy Perspective of the World 7

2.2 Conventional Reservoirs versus Unconventional Reservoirs 9

2.3 Geological Characterization of Shale Reservoirs 11

2.4 Unconventional Shale Reservoirs in the World 15

2.5 Overview of Energy Distribution in Turkey 20

2.6 Major Shale Basins in Turkey 22

2.7 Dadaş Shale in the Southeast Anatolia Basin 23

3 THEORETICAL FRAMEWORK 35

3.1 The Role of Geomechanics in Hydraulic Fracturing for Unconventional Shale Reservoirs 35
3.2 Mechanical Earth Model 35
3.3 Geomechanical Properties 36
3.3.1 Young's Modulus & Poisson's Ratio 37
3.3.2 Geological Principal Stresses 38
3.3.3 Biot's Coefficient 45
3.3.4 Pore Pressure 45
3.3.5 Strength Parameters 47
3.3.6 Brittleness and Brittleness Index 50
3.3.7 Fracture Toughness 53
4 LITERATURE REVIEW FOR FRACABILITY AND FRACABILITY INDEX 59
5 STATEMENT OF PROBLEM 67
6 RESEARCH METHODOLOGY 69
7 RESULTS & DISCUSSIONS FOR DADAŞ SHALE CASE STUDY 71
7.1 Deterministic Method 79
7.2 Stochastic (Probabilistic) Method 87
8 CONCLUSIONS 103
9 RECOMMENDATIONS 107
10 REFERENCES 109

LIST OF TABLES

TABLES

Table 2.1 Important Parameters in Evaluating Shale Reservoirs (Zee Ma, 2016). 13
Table 2.2 Top 10 Countries with Technically Recoverable Shale Resources (EIA, 2013). 19
Table 2.3 Shale Gas & Oil Properties of Dadaş Formation (EIA, 2015). 25
Table 2.4 The geological & petrophysical properties of Dadaş I shale gas/oil reservoirs (Merey, 2019). 29
Table 2.5 Reservoir Parameters of Dadaş Units and Dadaş-I Subunits Obtained from Log Analyses in Çalıktepe-2 well (Kara & Isik, 2021). 33
Table 3.1 Empirical relationships between unconfined compressive strength (UCS) and other physical properties in shale (Chang et al., 2006). 49
Table 3.2 Fracture Toughness Prediction Models for Unconventional Reservoirs. 56
Table 7.1 The list of geomechanical parameters used in the fracability evaluation. 74
Table 7.2 Selected fracability models for this study. 75
Table 7.3 The averaged input data of Dadaş-I for deterministic fracability evaluation. 79
Table 7.4 Deterministic fracability index results of all zones in Dadaş-I for studied models. 80
Table 7.5 The mineralogical distribution of Dadaş Shale from various sources. .. 81
Table 7.6 Poisson's ratio and Young's modulus values of some of the most productive North American shales and Dadaş shale (Modified after Dobson & Houseworth, 2014). 82
Table 7.7 Averaged geomechanical input data of Dadaş-I (all zones) and Marcellus shales. 84
Table 7.8 Deterministic fracability index results of Dadaş-I shale (all zones) and Marcellus shale for all studied models. 85

Table 7.9 Fracability Index and mechanical brittleness index values of some of the most productive North American shales and Dadaş shale. 86
Table 7.10 Distribution types of input parameters for each zone. 87
Table 8.1 The collective fracability index (FI) results of L2 zone for all models. 103

LIST OF FIGURES

FIGURES

Figure 2.1. Amount and Share of Primary Energy Consumption by Source, World, in 2020 and 2050. (Nalley & Larose, 2021). 7
Figure 2.2. U.S. Primary Energy Consumption by Energy Source, 2021 (EIA, 2022). 8
Figure 2.3. Schematic of Conventional & Unconventional Reservoirs (Sahai, 2022). 9
Figure 2.4 World Resource Pyramid of Reservoirs (Lee & Kim, 2016). 10
Figure 2.5. Delineation of Conventional and Unconventional Resources Based on Fluid Mobility (Sahai, 2022). 11
Figure 2.6 Cross Plot Between the Production and Reservoir Quality Overlaid with Completion Efficiency (C_Efficiency) (Zee Ma, 2016). 14
Figure 2.7. Radar Plots for Ranking Reservoir and Completion Qualities of Shale Reservoirs with 6-Level Scores (0–5 From Low to High). (a) Parameter Ranking; (b) Parameter Ranking and Analog Comparison (Zee Ma, 2016) 15
Figure 2.8. Lower 48 States Shale Oil and Gas Plays in The U.S. (EIA, 2016). 16
Figure 2.9. Map of Basins with Assessed Shale Oil and Shale Gas Formations (EIA, 2013). 18
Figure 2.10. EIA AEO2021 Reference Case Forecast of Cumulative U.S. a-) Oil b-) Natural Gas Production by Source, 2020-2050 (Hughes, 2021). 19
Figure 2.11. Overview of Turkey's Energy System by Fuel and Sector, 2018/19 (IEA, 2021). 20
Figure 2.12. Energy Production by Source, Turkey, 2000-2019 (IEA, 2021). 21
Figure 2.13. Total Primary Energy Supply by Source, Turkey, 2000-2019 (IEA, 2021). 21
Figure 2.14. Distribution of primary energy consumption by source (MENR, 2022). 21
Figure 2.15. Major Shale Basins of Turkey (EIA, 2015). 22

Figure 2.16. The Extent of the Dadaş Shale within the Boundaries of SE Anatolian Basin (EIA, 2015). 23
Figure 2.17. Dadaş Shale Prospective Area, SE Anatolian Basin, Turkey (EIA, 2015). 24
Figure 2.18. The Regional Stratigraphy of SE Anatolia Basin (Aydemir, 2011). ... 26
Figure 2.19. Stratigraphic Column of the Dadaş Formation (Inan & Kavak, 2019). 27
Figure 2.20 Regional Thickness Map of Dadaş-I Member (Hosgor & Yilmaz, 2022). 30
Figure 2.21 Lithofacies of Dadaş-I Member (from Çalıktepe-2 well) (Kara & Isik, 2021). 31
Figure 2.22 Microfacies pictures of L2, L3, and L4 (Kara & Isik, 2021). 32
Figure 3.1. Anderson's stress regime classification: a) normal faulting; b) strike-slip faulting; c) reverse (thrust) faulting (Nacht et al., 2010). 38
Figure 3.2. Fracture configurations from a horizontal well: a) multiple transverse fractures and b) a longitudinal fracture (H. Y. Wang, 2016). 41
Figure 3.3. Stress map showing the faulting regime and the orientation of maximum horizontal stress around the Diyarbakir region (CASMO - World Stress Map, 2016; Heidbach et al., 2016). 42
Figure 3.4. The representation of an interaction between hydraulic fracture (HF) and natural fracture (NF) with an indicated differential horizontal stress (Δσ) and approach angle (θ) (Yildirim, 2022). 43
Figure 3.5. Influences of differential horizontal stress and approaching angle on fracture propagation. 'Connection' indicates that hydraulic fractures and natural fractures are interconnected, and natural fractures are ultimately extended by the intersected hydraulic fractures. 'Crossing' indicates that natural fractures are crossed by hydraulic fractures without inter-connection (Dou et al., 2022). 44
Figure 3.6. Eaton's method for pore pressure gradient calculation in Dadaş shales. 46

Figure 3.7. Graphical representation of a stress state at failure by Mohr-Coulomb criterion (Modified after: Thiercelin & Roegiers, 2000) 47
Figure 3.8 Selected Expressions of Brittleness (Jin et al., 2014). 50
Figure 3.9 The brittle and ductile behavior of material from stress vs. strain plot (Salah et al., 2019) 51
Figure 3.10 Modes of fracture initiation and propagation. a) Opening (Mode-I), b) Sliding-shear (Mode-II), c) Tearing-shear (mode-III) (Guo et al., 2017). 53
Figure 3.11. The schematic representation of hydraulic fracture (HF) propagation based on net pressure. The hydraulic fracture grows when the net pressure (i.e. Pn = Pf - Pc) is positive. The fracture shrinks in the region where the net pressure is negative. The resistance to fracture growth is fracture toughness (Bai, 2016). 55
Figure 3.12. Empirical correlations relating shale content, Vsh, to gamma ray shale index, Ish (Bassiouni, 1994). 58
Figure 4.1. Brittleness Indexes of Some Representative Gas Shales. (Yuan et al., 2017) 61
Figure 4.2. a) Brittleness Index Map Obtained from Elastic Properties b) Minimum Horizontal Stress Map for Calcite-rich Shale Formation. (Ardila et al., 2019). 61
Figure 4.3. The schematics showing (a) smaller fracture length (L) and width (w) due to higher min. horizontal stress (σ_h)*, (b) greater fracture length (L) and width (w) due to lower min. horizontal stress* (σ_h) *from a hydraulic fracturing stimulation (Bai, 2016)* 64
Figure 7.1 The digitalization of gamma-ray log from reference (Kara & Isik, 2021). 72
Figure 7.2 The digitalization of density log from reference (Kara & Isik, 2021). . 72
Figure 7.3 The digitalization of sonic log from reference (Kara & Isik, 2021). 73
Figure 7.4 An example of digitizing quality index for the digitalization part. 73
Figure 7.5 Profiles of Young's modulus and Poisson's ratio with respect to the profile of Gamma-ray log regarding Dadaş-I member. 75
Figure 7.6 Profiles of fracture toughness and normalized fracture toughness regarding Dadaş-I member. 76

Figure 7.7 Profiles of horizontal geostresses and differential horizontal stress regarding Dadaş-I member. 77
Figure 7.8 A ternary diagram shows the comparison of Dadaş shale mineralogy (indicated by triangles) with some major North American "shale" plays (indicated by circles) and one European-origin Derbyshire shale (indicated by red stars) (Modified after Yildirim, 2019). 81
Figure 7.9 A graph showing the mechanical elasticity comparison between Dadaş shale and some major North American shales (Drawn by using the data of Dobson & Houseworth, 2014). 83
Figure 7.10 Dry Shale Gas Production of the U.S. Shale Formations from 2007 to 2023 (EIA, 2023c). 83
Figure 7.11 The comparison of FI and BImech for some shale formations in the U.S. and for Dadaş shale (all zones)(Drawn by using the data of references listed above). 86
Figure 7.12 Distribution of normalized YM (EN) and PR (vN) for L2 zone. 89
Figure 7.13 Distribution of mode-I (K_{IC}) and mode-II (K_{IIC}) fracture toughness for L2 zone. 90
Figure 7.14 Distribution of normalized Kıc & Kııc for L2 zone. 90
Figure 7.15 Distributions of MinHS (σ_h) and DHS ($\Delta\sigma$) index for L2 zone. 91
Figure 7.16 Distribution graph of the PDF for Rickman et al.'s model. 92
Figure 7.17 Distribution graph of the CDF for Rickman et al.'s model. 92
Figure 7.18 Distribution graph of the PDF for Yuan et al.'s model. 93
Figure 7.19 Distribution graph of the CDF for Yuan et al.'s model. 93
Figure 7.20 Distribution graph of the PDF for Dou et al.'s model. 94
Figure 7.21 Distribution graph of the CDF for Dou et al.'s model. 94
Figure 7.22 Distribution graph of the PDF for Proposed model. 95
Figure 7.23 Distribution graph of the CDF for Proposed model. 95
Figure 7.24 Tornado chart of L2 zone for Rickman et al.'s model. 97
Figure 7.25 Spider chart of L2 zone for Rickman et al.'s model. 97
Figure 7.26 Tornado chart of L2 zone for Yuan et al.'s model. 98

Figure 7.27 Spider chart of L2 zone for Yuan et al.'s model. 98
Figure 7.28 Tornado chart of L2 zone for Dou et al.'s model. 99
Figure 7.29 Spider chart of L2 zone for Dou et al.'s model. 100
Figure 7.30 Tornado chart of L2 zone for Proposed model. 101
Figure 7.31 Spider chart of L2 zone for Proposed model. 101

LIST OF ABBREVIATIONS

ABBREVIATIONS

AHP	Analytical Hierarchy Process
BI	Brittleness Index
CBM	Coalbed Methane
CDF	Cumulative Distribution Function
DHS	Differential Horizontal Stress
EIA	Energy Information Administration
Eq.	Equation
FI	Fracability Index
GIP	Gas In Place
HC	Hydrocarbon
hF	Hydraulic Fracture
HF	Hydraulic Fracturing
HI	Hydrogen Index
IEA	International Energy Agency
L	Lithofacies
MEM	Mechanical Earth Model
MENR	Ministry of Energy and Natural Resources
nF	Natural Fracture
NF	Normal Faulting

OIP	Oil In Place
PDF	Probability Density Function
PP	Pore Pressure
PR	Poisson's Ratio
RF	Reverse Faulting
SE	Southeast
SRV	Stimulated Reservoir Volume
SS	Strike-Slip Faulting
TPC	Turkish Petroleum Corporation (TPAO)
TPES	Total Primary Energy Supply
U.K.	United Kingdom
U.S.	United States
WSM	World Stress Map
XRD	X-Ray Diffraction
YM	Young's Modulus

LIST OF SYMBOLS

SYMBOLS

a	Crack Length
^{o}API	American Petroleum Institute Gravity
bbl	Barrel
Bcf	Billion Cubic Feet
BI_{mech}	Mechanical Brittleness Index
BI_{min}	Mineralogical Brittleness Index
C_O	Cohesion
DT or Δt_C	Compressional Travel Time
E	Young's Modulus
E_{DYN}	Dynamic Young's Modulus
E_N	Normalized Young's Modulus
E_S	Static Young's Modulus
FI	Fracability Index
GCUR	Hilchie Index
GPa	Giga Pascal
GR	Observed Gamma Ray
H	Depth of Interest
I_{SH}	Shale-content Index of the Rock
k	Rock Permeability

$K_I^{(+)}$	Positive Fracture Toughness
$K_I^{(-)}$.	Negative Fracture Toughness
K_{IC}	Mode-I Fracture Toughness
K_{IC_N}	Normalized Mode-I Fracture Toughness
K_{IIC}	Mode-II Fracture Toughness
K_{IIC_N}	Normalized Mode-II Fracture Toughness
K_k	Stress Intensity Factor
kPa	Kilo Pascal
mD	Milli Darcy
mi^2	Square Mile
MM	Million
MMM	Billion
MPa	Mega Pascal
nD	Nano Darcy
P_C	Closure Pressure
P_F	Fluid Pressure
P_{HYD}	Hydrostatic Pressure
$P_{HYD, grad}$	Hydrostatic Pressure Gradient
P_N	Net Pressure
P_{norm}	Normalized Value of Parameter
P_P	Pore Pressure

$P_{P, grad}$	Pore Pressure Gradient
P_W	Injection Well Pressure
q	Flow Rate
R_O	Vitrinite Reflectance
Sw	Water Saturation
Tcf	Trillion Cubic Feet
Tcm	Trillion Cubic Meter
T_O	Tensile Strength
TOC	Total Organic Carbon
UCS	Unconfined Compressive Strength
V_P	Compressional Wave (P-Wave) Velocity
V_S	Shear Wave (S-Wave) Velocity
V_{SH}	Shale Content of the Rock
X	Value of the Parameter
X_{max}	Maximum value of Parameter
X_{min}	Minimum value of Parameter.
μ	Fluid Viscosity
λ	Fluid Mobility (k/μ)
ν	Poisson's Ratio
ν_{DYN}	Dynamic Poisson's Ratio
ν_N	Normalized Poisson's Ratio

ρ	Bulk Density of Rock (Shale)
$\tilde{\rho}$	Average Bulk Density of Overburden Rock
σ_A	Given Load
σ_h	Minimum Horizontal Stress
σ_h^G	Minimum Horizontal Stress Gradient
σ_H	Maximum Horizontal Stress
σ_N	Normal Stress
σ_V	Vertical (Overburden) Stress
$\sigma_{V,\ grad}$	Vertical (Overburden) Stress Gradient
τ	Shear Stress
α	Biot's Constant
ε_h	Tectonic Strain along Minimum Horizontal Stress
ε_H	Tectonic Strain along Maximum Horizontal Stress
$\Delta\sigma$	Differential Horizontal Stress
θ	Approaching Angle of Hydraulic Fracture
ϕ	Porosity
Δt	Observed Sonic Log Transit Time
Δt_n	Normal Compaction Trendline in Sonic Log
φ	Internal Friction Angle
μ_i	Coefficient of Internal Friction
β	Angle for which the Failure Criterion is Fulfilled

CHAPTER 1

INTRODUCTION

Although a significant part of oil and gas is still being produced from conventional reservoirs, the production potential of unconventional reservoirs has become a groundbreaking agenda in the petroleum industry since the beginning of the 21st century. Unconventional reservoirs, especially shale oil/gas reservoirs, have been regarded as alternative oil and natural gas resources not only in the United States but also in many parts of the world. The development of shale oil/gas reservoirs is even more vital for energy-dependent countries such as Turkey.

In an unconventional shale reservoir system, the source rock, the reservoir rock, and the caprock are all represented by the same shale formation. Shale reservoirs have poor natural productivity due to their extremely heterogeneous structures with ultra-low permeability. Therefore, an overwhelming majority of shale oil/gas wells require horizontal drilling technologies combined with multi-stage hydraulic fracturing. Accordingly, hydraulic fracturing (HF) of horizontal wells has been commonly used worldwide for the last 25 years to increase the stimulated reservoir volume (SRV) in order to form conductive paths for oil/gas production (**Zee Ma, 2016**).

The HF is one of the main stimulation techniques in the unconventional shale industry to put ultra-low permeable shale formations into production and increase the ultimate hydrocarbon (HC) recovery from these formations. The first step in HF operation is to carefully select the best layers and spots based on a specific set of criteria. The selection of ideal reservoir zones for high HC production by HF can be achieved by elaborately examining and then applying two categories of factors (reservoir quality and completion quality), which characterize shale reservoirs. Reservoir quality is related to petrophysical and geochemical properties such as kerogen, total organic carbon (TOC), thermal maturity, lithology, porosity,

permeability, pore pressure, and fluid saturation. On the other hand, completion quality is mainly affected by geomechanical parameters, which include mineralogy, in-situ stress regime, Young's modulus (YM), Poisson ratio (PR), brittleness, fracture toughness (K_C), the presence and characteristics of natural fractures (nFs), unconfined compressive strength (UCS), tensile strength (T_O), internal friction angle (φ), and cohesion (C_O) (**Zee Ma, 2016**). The selection process of HF candidates is pivotal in achieving complex fracture networks and in expanding SRV. However, without performing in-depth analyses of the fundamental properties of shales, optimizing the HF treatment is unlikely. (**Zendehboudi & Bahadori, 2017a**).

The production potential of shale reservoirs is determined by geochemical and petrophysical factors, whereas the primary and sustained productivity of shale reservoirs is strongly dependent on geomechanical properties. The fracability, which is stated as the most critical parameter in unconventional reservoir geomechanics, can be defined in its simplest form as the degree of a formation's ability to be fractured effectively. Fracability is closely linked to completion quality and fracability is mainly used to calculate the easiness of creating a discrete, complex fracture network system in a formation. In unconventional resources, consequently, the evaluation of fracability plays a crucial role in regard to characterizing sweet spots and optimizing HF operations. (**Huang et al., 2021**).

One of the most critical factors utilized to evaluate the fracability of a rock is brittleness. Brittleness can be defined as the amount of energy immediately before the rock's failure. When stressed, a rock is brittle if it fails with minimum or no plastic deformation. From the geomechanics perspective, brittleness is the point at which the elastic strain controlling the deformation of the rock exceeds the strength of the formation, so the rock fractures (**Salah et al., 2019**). Since brittle rocks are more likely to be naturally fractured, tending to respond positively to HF, a rock with higher brittleness is considered an excellent fracturing candidate. Therefore, the brittleness index (BI) has been widely used in the past years (such as **(Rickman et al., 2008**)) as a single parameter to represent sweet spots in HF operations of unconventional shale reservoirs (**Jin et al., 2014**). However, this viewpoint is found

to be inadequate according to the technological developments applied in the following studies, which have shown that BI alone precisely does not explain easily-fracable spots of unconventional shale formations (**Jin et al., 2014**). More clearly, Jin et al. (**2014**), Bai (**2016**), and Salah et al. (**2019**) states that since brittle formations may have greater strength than ductile formation, it is not certain that brittle formations can be easily fractured compared to ductile formations, and even brittle zones may behave as fracture barrier. Moreover, Yuan et al. (**2017**) and Ardila et al. (**2019**) verified that the selection of fracable zones only based on high BI was in contradiction with the results of stimulation efficiency and production performance. For these reasons, new concepts, particularly the "fracability" and the "fracability index" (FI), have been introduced to overcome the shortcomings of BI over the past several years. Fracability is defined as the effective fracturing capability of oil & gas reservoirs to develop fracture networks (**Salah et al., 2019**). Accordingly, the fracability index (FI) can be regarded as a theoretical benchmark to mathematically calculate the easiness of rocks to be fractured. The latest FI models consider other parameters, such as fracture toughness, minimum horizontal stress, and differential horizontal stress, as well as BI, and integrate these new parameters with BI. Yuan et al. (**2013**), Jin et al. (**2014**), and Salah et al. (**2019**) combined BI with fracture toughness to estimate the fracability of a rock. Additionally, Yuan et al. (**2017**), Yasin et al. (**2018**), and Iyare et al. (**2022**) built fracability assessment models based on BI, fracture toughness, and minimum horizontal stress index. More recently, Dou et al. (**2022**) proposed an extensive FI equation integrating differential horizontal stress with BI, fracture toughness, and minimum horizontal stress. As a matter of fact, all these studies suggest that the formation with higher FI is a good fracturing candidate because it has higher brittleness (does not continue absorbing energy after applied stress reaching rock strength) and lower fracture toughness (fracture propagation consumes less internal work). Besides, such formation is surrounded by relatively lower minimum horizontal stress (less external energy by closure stress) and resides in horizontal stresses with relatively lower anisotropy (better interaction between hydraulic fractures and natural fractures). On the other hand, the formation

with a relatively lower FI can be considered a fracture barrier. Hence, it should be avoided to perforate zones of fracture barriers while performing HF in shale reservoirs (**Jin et al., 2014**). Based on findings and fracability models explained above, a new fracability model including brittleness index, fracture toughnesses, minimum horizontal stress, and differential horizontal stress was proposed to more comprehensively evaluate the fracture tendency degree of shale reservoirs.

In conclusion, for an optimized production from unconventional shale reservoirs through HF, the FI is understood to be the most critical parameter in screening the best HF candidates as sweet spots and locating the position of fracture barriers. From this point forth, this study principally aims to investigate the fracability of Dadaş Shale obtained from geomechanical rock properties through the digitization of open-source well-log data. Accordingly, using two evaluation methods (deterministic and stochastic methods) the tendency of Dadaş formation to the HF process will be examined, and the effects of geomechanical properties on formation fracability will be evaluated. In this context, four different FI models (Rickman et al.'s model (2008), Yuan et al.'s model (2017), Dou et al.'s model (2022), and newly proposed model (2023)) will be deterministically implemented to validate the proven success of the Marcellus shale in the HF topic. Then these models will be analyzed by comparing FI results obtained from the Marcellus shale with FI results in Dadaş shale. Furthermore, for comparative analysis, the FI of Dadaş Shale and of some major productive shale formations in the U.S. will be estimated by Proposed model, and then FI results will be examined according to changing BI values. In stochastic evaluation, probabilistic risk analysis will be performed by Monte Carlo simulation to obtain various probability distributions (probability density function and cumulative distribution functions) of fracability as an outcome regarding changing input data. Subsequently, for all studied fracability models, the effect of fracability components as input data on output data (FI) will be assessed by sensitivity analysis using tornado chart and spider chart. Finally, deterministic and stochastic FI results of Dadaş shale will be compared for each model.

This study is expected to contribute to the existing knowledge about unconventional shale reservoirs in Turkey, call attention to geomechanics, an area generally ignored in the petroleum industry, and bring it to the forefront deservedly. In the near future, the results and findings obtained from this study can be used to build a geomechanical background to evaluate the fracability of unconventional shale reservoirs in Turkey.

CHAPTER 2

BACKGROUND INFORMATION

2.1 General Energy Perspective of the World

Fossil fuels, namely oil, gas, and coal, have been overwhelmingly meeting the energy needs of our civilization for decades. The consumption of renewable energy resources grew in the first quarter of this century, and the share of renewables in worldwide energy consumption is expected to grow by 2050 (**Nalley & Larose, 2021**) (***Figure 2.1***). Whereas renewables paint a promising picture regarding energy sustainability and environmental sensitivity for the future, nowadays, these resources are notably behind non-renewable fossil fuels from technical and economic aspects.

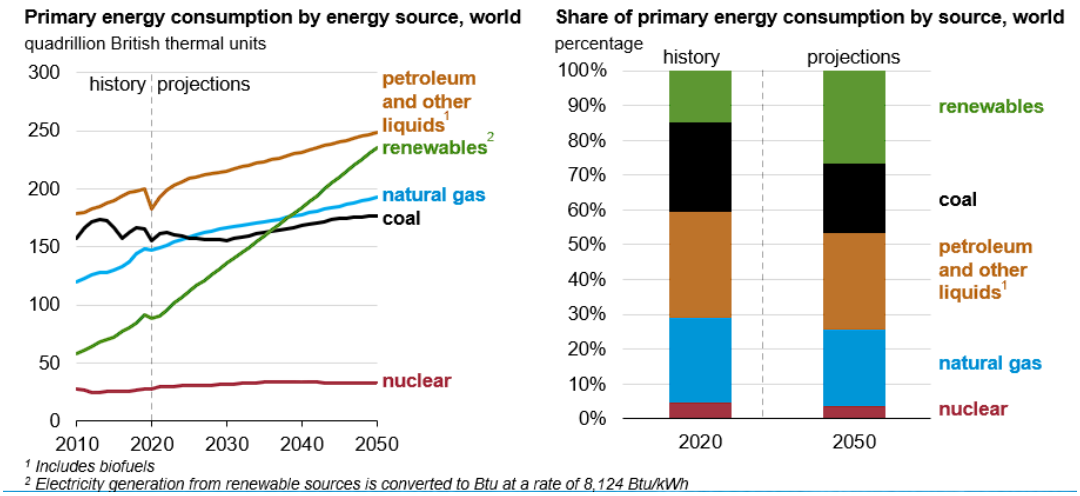

Figure 2.1. Amount and Share of Primary Energy Consumption by Source, World, in 2020 and 2050. (Nalley & Larose, 2021).

To illustrate, the primary energy consumption of the United States (U.S.), the biggest consumer country, was dominated by fossil fuels in 2021, with an approximate share of 80% (***Figure 2.2***). Moreover, Energy Information Administration (EIA) projections indicate that fossil fuels will continue their superiority and importance

for at least up to 2050, which is quite a long period. On the other hand, global energy consumption is increasing ceaselessly due to growth in population and economics (**Nalley & Larose, 2021**), and the hydrocarbon (HC) production from conventional reservoirs alone is insufficient to meet the growing energy demand (**Lee & Kim, 2016**). In response to this, at the beginning of the 2000s in North America, unconventional oil and gas reservoirs emerged as alternative energy resources to meet the deficit of conventional reservoirs.

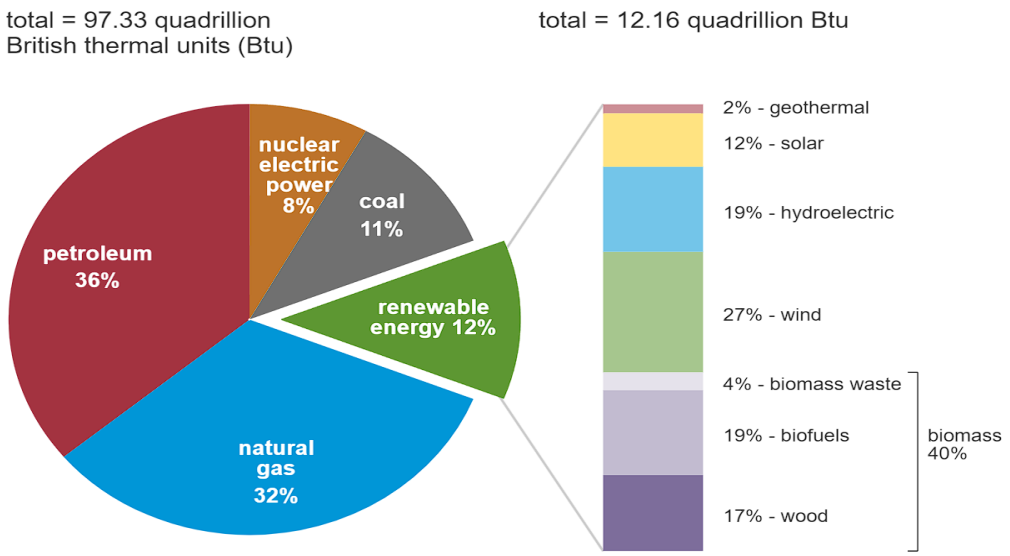

Figure 2.2. U.S. Primary Energy Consumption by Energy Source, 2021 (EIA, 2022).

The first large-scale success that occurred in Barnett Shale (in 2000-2001) paved the way for production from other unconventional shale reservoirs, such as Bakken, Eagle Ford, Fayetteville, Haynesville, Marcellus, Montney, Niobrara, Wolfcamp, and Woodford (**Zee Ma, 2016)**. Successful production histories of these unconventional resources, especially shale gas and oil reservoirs, have led to a shale revolution in the petroleum industry such that the U.S. has become the top producer country in the world both in yearly oil and yearly gas production (**Worldometer, 2023**). From this viewpoint, it can be said that shale reservoirs rewrote the world's energy equation, and nowadays, they are still regarded as a ground-breaking agenda in the energy sector.

2.2 Conventional Reservoirs versus Unconventional Reservoirs

Analyzing and classifying various hydrocarbon (HC) resources based on reservoir quality is needed to highlight the distinction between conventional and unconventional reservoirs. Conventional HC reservoirs typically possess porous and permeable formations but are sealed by an impermeable layer that acts as a barrier to prevent HC flow beyond the reservoir. Conventional underground systems contain migration pathways between source rocks and reservoirs, and the migration enables the movement of HCs accumulated in source rocks to reservoir rocks. Conventional formations have suitable rock characteristics for a simple fluid flow that obeys Darcy's law, and they generally do not require large-scale stimulation for HC production (**Sahai, 2022; Zee Ma, 2016**) (***Figure 2.3***).

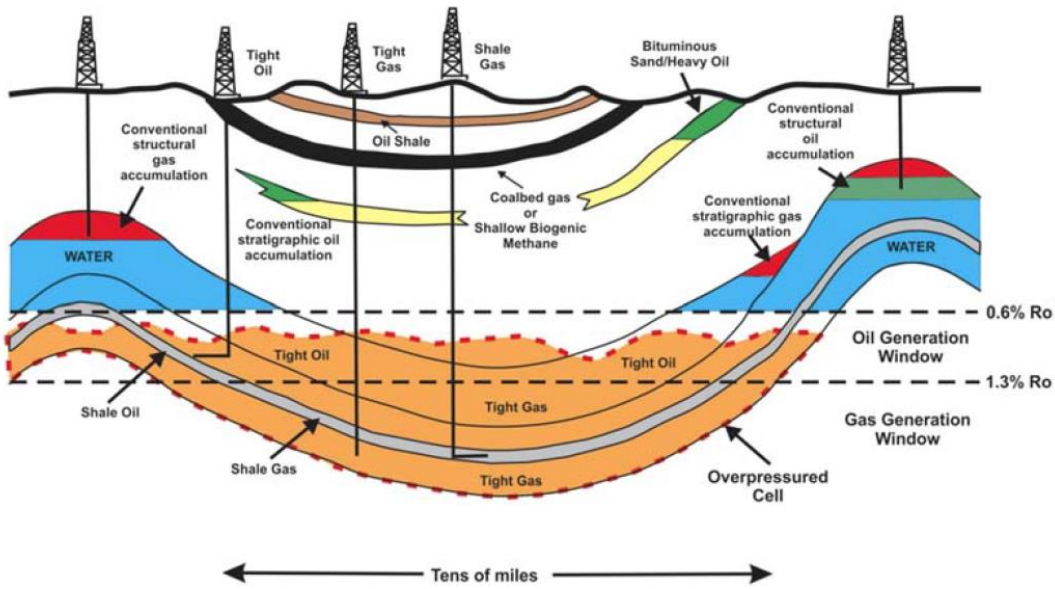

Figure 2.3. Schematic of Conventional & Unconventional Reservoirs (Sahai, 2022).

By contrast, unconventional HC systems are generally self-sourced and self-sealed reservoirs with permeability in low-to-ultralow scale and porosity in low (to medium) scale. In these systems, migration is unnecessary, and traps do not affect oil and gas accumulation (**Sahai, 2022**) (***Figure 2.3***). Unconventional reservoirs consist of tight formations, have lower reservoir quality, do not follow Darcy's law commonly, and are more abundant on the earth.

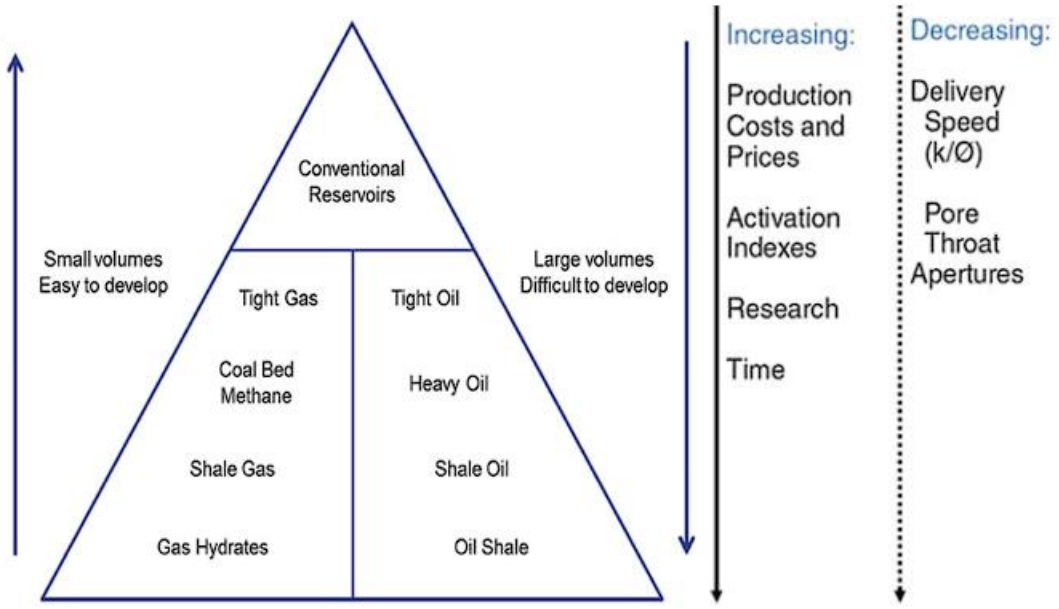

Figure 2.4 World Resource Pyramid of Reservoirs (Lee & Kim, 2016).

The world resource pyramid can represent the qualitative differences between conventional and unconventional resources, as shown in ***Figure 2.4***. Unconventional resources represent a great majority of the resource triangle (pyramid); however, they are challenging to be developed mainly due to the lower quality of formations, geological conditions, and the corresponding production costs. The difference between conventional and unconventional resources can be delineated more quantitatively based on rock permeability (k) and fluid viscosity (μ) (***Figure 2.5***). Increasing the HC fluid mobility (λ, [k/μ]) with advanced drilling and stimulation technologies is critical for achieving commercial oil and gas production.

It is not always easy to quantitatively distinguish a reservoir into a specific category, but reservoirs with permeability below 0.1 mD (milli Darcy) are mostly considered to be unconventional (**Zee Ma, 2016**). Accordingly, the unconventional reservoirs include tight oil/ gas sands, shale oil/gas, oil shale and coalbed methane (CBM). From this point on, further parts of the study are purposely allocated to shale oil and shale gas reservoirs.

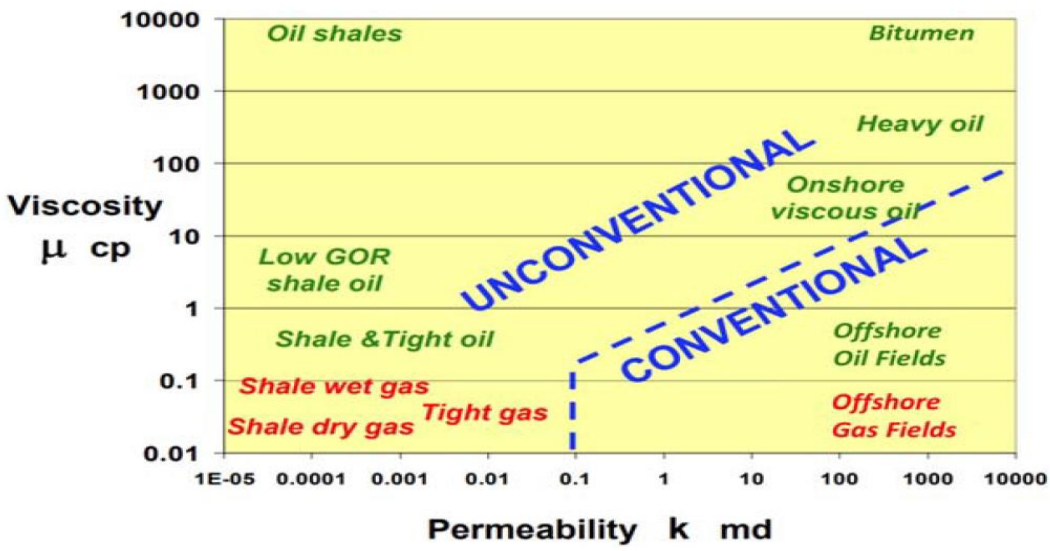

Figure 2.5. Delineation of Conventional and Unconventional Resources Based on Fluid Mobility (Sahai, 2022).

2.3 Geological Characterization of Shale Reservoirs

Organic-rich shales are the most abundant type of sedimentary rocks, which have a very fine-grained and laminated structure, including predominantly silt and clay minerals. In most conventional reservoirs, shales are considered source rocks and/or seal rocks as they are rich in organic matter and have impermeable structures. Shale formations are self-contained systems such that source rock, reservoir rock, and cap rock are all represented by a shale formation, which makes shales classified as unconventional hydrocarbon (HC) reservoirs (**Suriamin & Ko, 2022; Zee Ma, 2016**). Shale reservoirs have poor natural productivity due to their unusual heterogeneous and changeable structures with very low permeability. Therefore, the overwhelming majority of shale reservoirs need combined technologies of horizontal drilling and multi-stage hydraulic fracturing in their development. Multistage hydraulic fracturing of horizontal wells has been commonly used over the last two decades to form highly conductive paths for HC migration and increase shale reservoirs' stimulated volume. The ultimate goal in developing shale reservoirs is to find the sweet spots by applying the above-mentioned technologies.

As in other unconventional resources, the development of shale formations necessitates a multi-disciplinary workflow integrating all available information from geological, geochemical, geomechanical, and petrophysical areas (**Zendehboudi & Bahadori, 2017b**) for handling high uncertainty and risk, characterizing and rating critical parameters, optimizing fracture design, and thereby increasing production (**Zee Ma, 2016**). The critical or desired values (***Table 2.1***) of parameters combined from various sciences should be considered in evaluating shale reservoirs.

High HC production cannot be specified by one unique geological factor, but two categories of factors can be used to reflect the main characteristics of shale reservoirs. The first category is reservoir quality, symbolizing HC potential, HC amount in place, and HC deliverability. The critical variables in reservoir quality are kerogen, total organic carbon (TOC), thermal maturity, lithology, porosity, permeability, pore pressure, and fluid saturation (**Labani & Rezaee, 2015; Zee Ma, 2016**).

The second category is completion quality, which shows the hydraulic fracturing (HF) potential or the ability to create and maintain fracture surface area and complex fracture systems. Completion quality is mainly affected by geomechanical parameters, which include mineralogy, in-situ stress regime, Young's modulus (YM), Poisson ratio (PR), brittleness, fracture toughness (K_C), the presence and characteristics of natural fractures (nFs), unconfined compressive strength (UCS), tensile strength (T_O), internal friction angle (φ), and cohesion (C_O) (**Addis et al., 2016; Zee Ma, 2016**). Completion quality is closely linked to ***fracability***, which represents easy and efficient stimulation of rock by HF to determine the sweet spots. Accordingly, the fracability index (FI) can come together all the above-mentioned geomechanical factors in various combinations by an integrative equation.

Completion effort stands for various methods and tools used in the optimization of completion design. In the completion effort, it is essential to analyze HF factors such as lateral length, proppant tonnage, and stage count. Completion effort and completion quality constitute completion efficiency (**Zee Ma, 2016**).

Table 2.1 Important Parameters in Evaluating Shale Reservoirs (Zee Ma, 2016).

Parameter	Critical or Desired Values	Data Sources
TOC	> 2% (weight)	Leco TOC, Rock-Eval
Thermal Maturity	Oil window: $0.5 < R_O < 1.3$, Gas window: $1.3 < R_O < 2.6$	Vitrinite reflectance, Rock-Eval
Mineralogy	Clay < 40%, Quartz or Carbonate > 40%	X-ray diffraction, Spectroscopy, Log-based
Av. Porosity	> 4%	Core, Logs
Av. Water Saturation	< 45%	Core, Capillary pressure, Log-based
Av. Permeability	> 100 nD (nanoDarcy)	Mercury injection capillary pressure, Nuclear magnetic resonance, Gas expansion
Oil or gas in-place	Gas: free and adsorbed gas >100 Bcf/section	Log-based, Integrated evaluation
Natural Fracture	Moderate to dense, and contained in the target zone	Seismic, Image log
Wettability	Oil-prone wetting of kerogen	Special core analysis
Hydrocarbon Type	Oil or thermogenic gas	Geochemistry, Rock-Eval
Pressure	Overpressure is preferable	Log-based, Seismic
Reservoir Temp.	> 110 ˚C (230 ˚F)	Drill Stem Test
Stress	< 13.80 MPa (2000 psi)	Logs, Image log, Seismic
Young's Modulus	> 20.68 GPa (3 MM psi)	Acoustic logs, Cores
Poisson's Ratio	< 0.25	Acoustic logs, Cores

Reservoir quality and completion efficiency (completion quality + completion effort) are multi-dimensional elements derived from physical quantities. Production in shale reservoirs is mostly positively correlated with reservoir quality and completion efficiency, yet the reservoir quality has to reach a certain level for the completion to be efficient (***Figure 2.6***). For rocks with a very low reservoir quality, production is low regardless of the completion efficiency, whereas for moderate to high reservoir-quality rocks, completion efficiency is the decisive element in production. On the contrary, positive correlations between production and variables of reservoir & completion qualities may not always be high; even inversed correlations and uncorrelated variables may be frequently observed (**Zee Ma, 2016**).

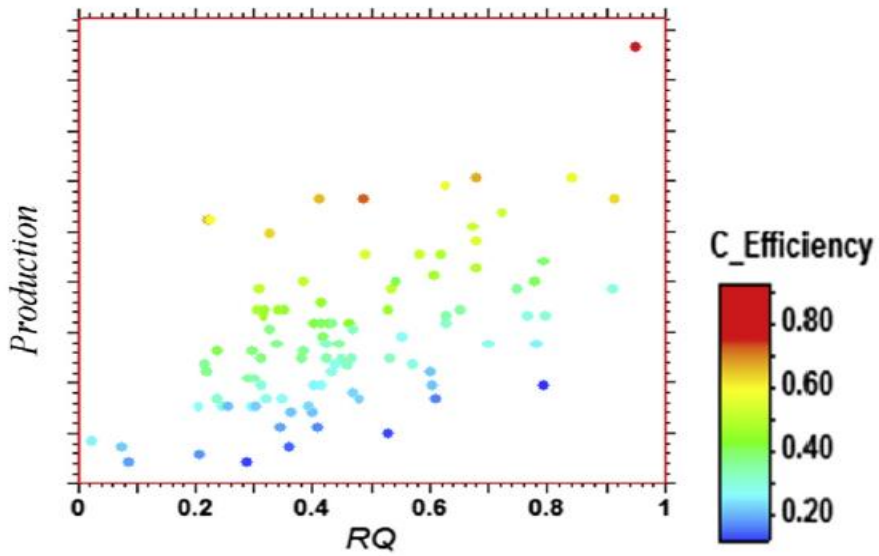

Figure 2.6 Cross Plot Between the Production and Reservoir Quality Overlaid with Completion Efficiency (C_Efficiency) (Zee Ma, 2016).

Radar charts can provide convenience for better observing and analyzing reservoir and completion qualities (***Figure 2.7a***). As more variables are presented in the chart, the ranking becomes more complex, but analysis of more variables enables more sound judgments. Radar plots can also help to compare analogue reservoirs and identify the strengths and weaknesses of the studied reservoir (**Zee Ma, 2016**) (***Figure 2.7b***).

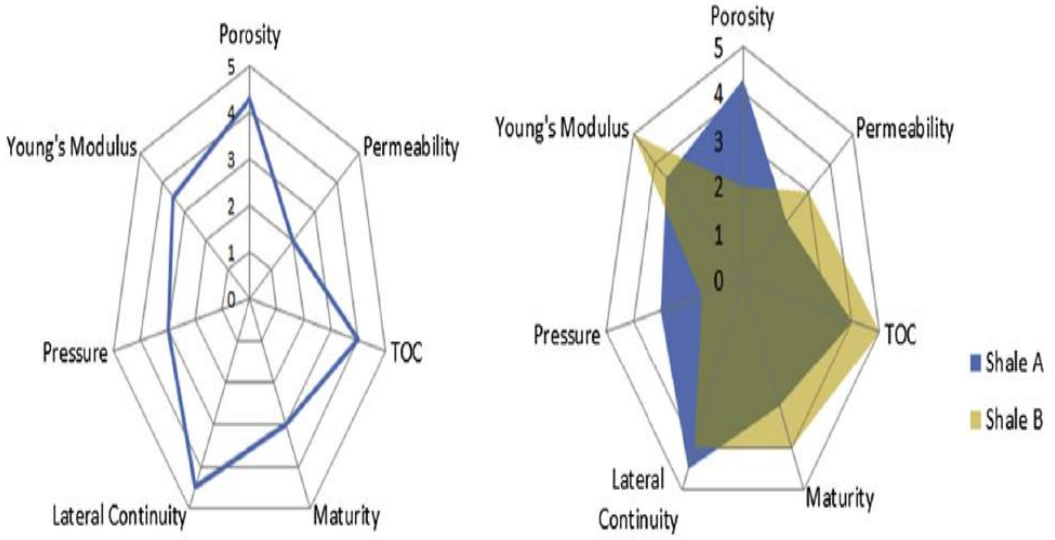

a) b)

Figure 2.7. Radar Plots for Ranking Reservoir and Completion Qualities of Shale Reservoirs with 6-Level Scores (0–5 From Low to High). (a) Parameter Ranking; (b) Parameter Ranking and Analog Comparison (Zee Ma, 2016)

2.4 Unconventional Shale Reservoirs in the World

Although the development of some unconventional resources, such as tight gas sands, oil sands, and heavy oils, dates back to old times, the origin of the large-scale production of oil and gas from shale formations is not far away from the present. At the beginning of the 21st century, the success story of Barnett Shale regarding the commercial quantities of oil and gas production triggered development studies of other shale plays in the United States (U.S.), from the Fayetteville to Haynesville, Woodford to Eagle Ford, Marcellus to Bakken (***Figure 2.8***). Subsequently, hydrocarbon (HC) production from shales has spread across the country in the U.S., and this period, known as the ***shale revolution***, made unconventional resources, especially shales, a focal point and shifted the route of the petroleum industry.

Not surprisingly, this epic-like success story in the U.S. has attracted a great deal of attention in the last few years from many countries that primarily have the important potential for unconventional resources. Research institutions, universities, and

exploration companies have developed cooperation at an international level and have intensified their scientific studies on finding and exploiting unconventional resources (**Baiyegunhi et al., 2022**). To illustrate, Baiyegunhi et al. (**2022**) revealed that the number of publications and citations to shale gas research showed a massive increase from 2010 to 2020 and that the top five countries are China, the U.S., Canada, the United Kingdom (U.K.), and Australia in terms of the number of publications. The leading country among these countries is China; accordingly, it is not a coincidence that the top five institutions with the highest number of articles are all from universities in China. Shale gas reservoirs even drew considerable interest in many Middle Eastern countries, where conventional reservoirs are among the world's most prolific producers (**Zee Ma, 2016**).

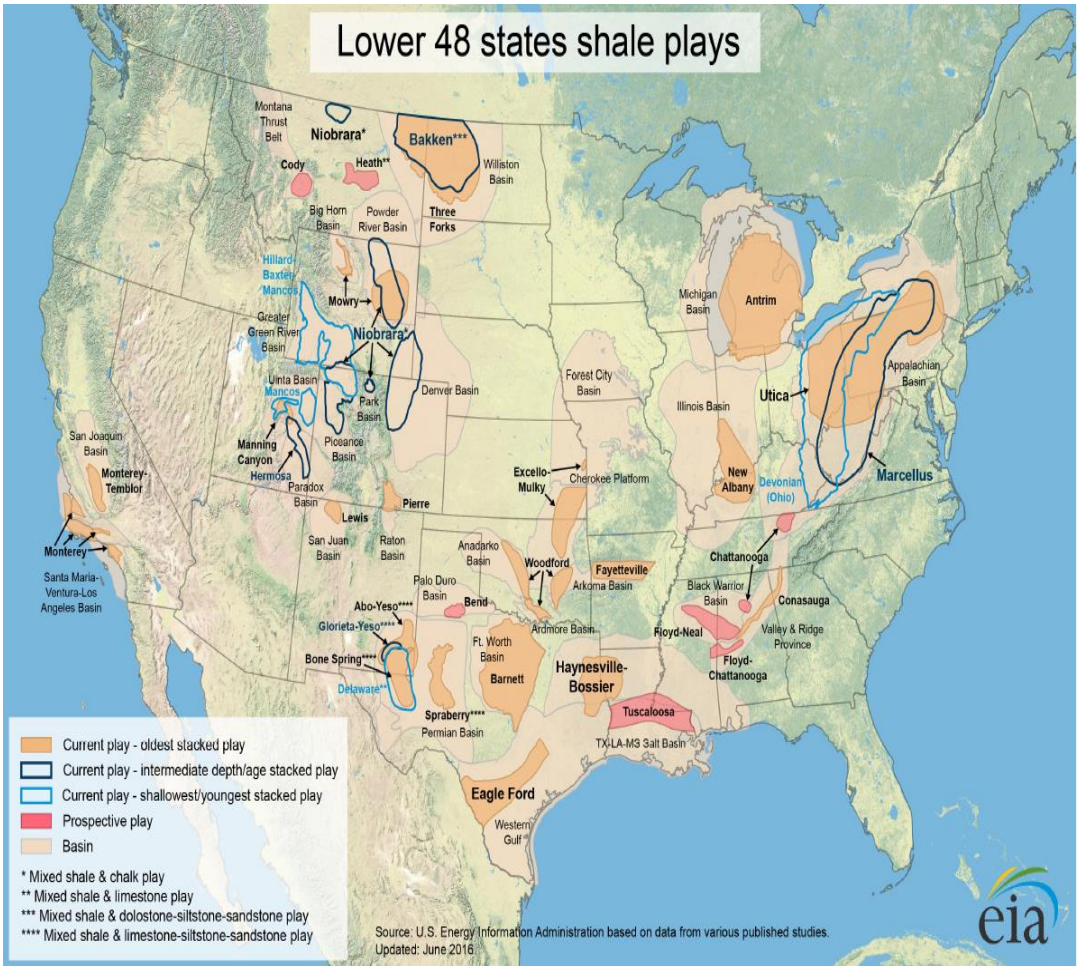

Figure 2.8. Lower 48 States Shale Oil and Gas Plays in The U.S. (EIA, 2016).

Figure 2.9 shows the distribution map of globally assessed shale oil and shale gas formations with and without resource estimates. Countries can be reviewed into two groups that shale development may be intriguing. Countries like the U.S., Canada, Russia, Mexico, China, Australia, and Argentina belong to the first group where their technically recoverable shale estimates are considered significant (***Table 2.2***), and these countries have well-developed oil and gas production infrastructure (**Gholinezhad et al., 2018**). The U.S. is by far the best shale gas producer country in the world. In recent years, Canada also became a leading producer, and in the rest of the world, apart from Argentina and China, no country produces shale gas at a considerable amount. The second group comprises countries like France, Poland, Turkey, Ukraine, South Africa, Morocco, and Chile. This group largely depends on crude oil and natural gas imports and has at least substantial shale resources relative to their current consumption; however, their sedimentary basins are not well-defined (**Gholinezhad et al., 2018**). There are still many difficulties on the road to producing HCs from unconventional resources in the second-group countries that are still in their infancy stage. Currently, the development of shale resources comes with some risks or uncertain results. Due to unknown factors, these adverse conditions have grown over time and could vary with geographical locations. The experiences gained from the shale revolution, as well as through the analysis of methodological and technical information, may be adopted as an inspirational starting point by the countries in the second group to develop their unconventional resources. Furthermore, better use of existing technologies and developing new technologies can lead to appreciable results in minimizing energy dependency (**Gholinezhad et al., 2018; Zee Ma, 2016**).

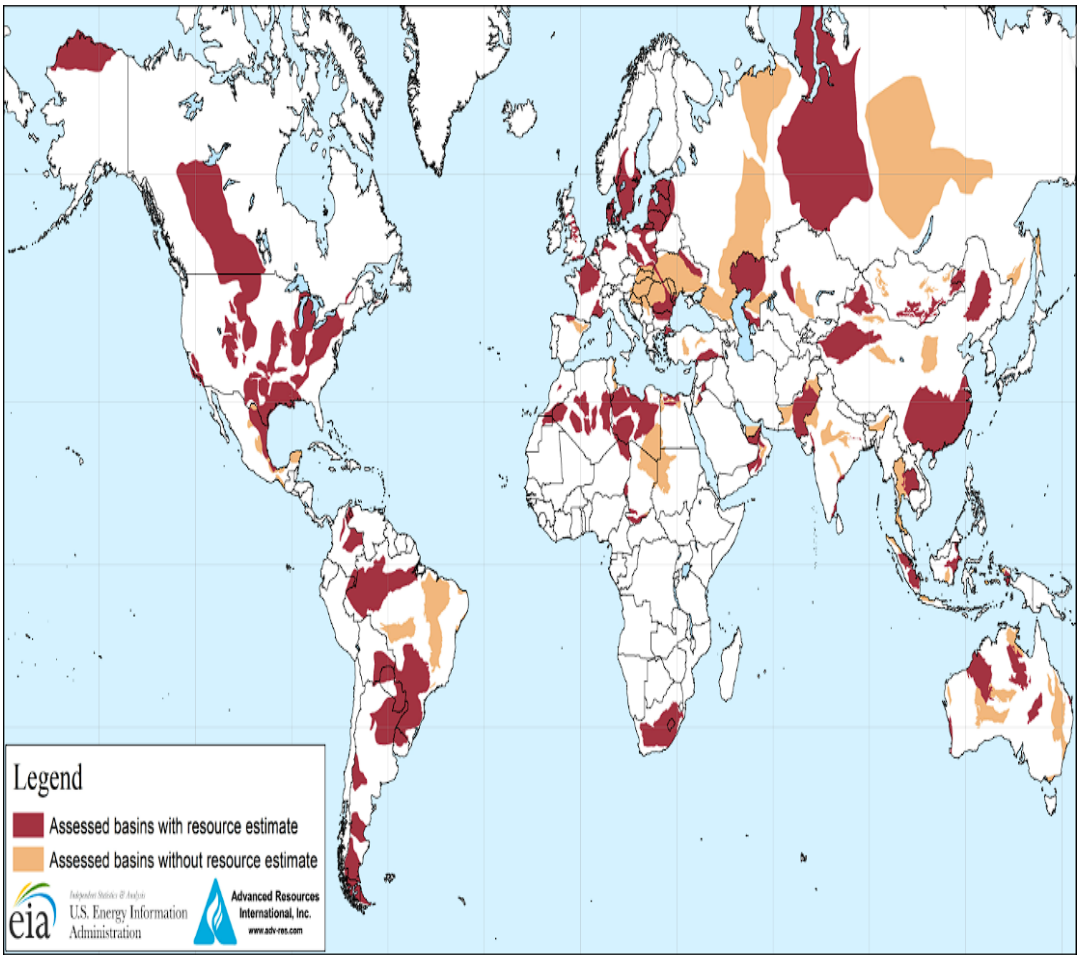

Figure 2.9. Map of Basins with Assessed Shale Oil and Shale Gas Formations (EIA, 2013).

As the world economy and population grow, the high potential of unconventional resources is gaining more prominence; in the near future, this trend may not change quickly. To give an example, the Energy Information Administration (EIA) (**2023a**) estimates that about 2.84 MMM (billion) barrels of crude oil, equal to about 66% of total U.S. crude oil production in 2022, were produced directly from unconventional oil resources. Additionally, in 2022, dry natural gas production in the U.S. from shale formations was about 28.5 trillion cubic feet (tcf), equal to about 80% of total U.S. dry natural gas production in that year (**EIA, 2023b**). Furthermore, Hughes' study (**2021**) highlights that 69% of U.S. oil production and 88% of U.S. gas production (***Figure 2.10***) will come from unconventional plays over the period from 2020 to 2050 based on the EIA's reference case forecast projections in Annual Energy Outlook (2021).

Table 2.2 Top 10 Countries with Technically Recoverable Shale Resources (EIA, 2013).

Rank	Country	Shale Oil (billion barrels)	Country	Shale Gas (trillion cubic feet)
1	Russia	75	China	1115
2	The U.S.	58	Argentina	802
3	China	32	Algeria	707
4	Argentina	27	U.S.[1]	665
5	Libya	26	Canada	573
6	Australia	18	Mexico	545
7	Venezuela	13	Australia	437
8	Mexico	13	South Africa	390
9	Pakistan	9	Russia	285
10	Canada	9	Brazil	245
World Total		345	World Total	7299

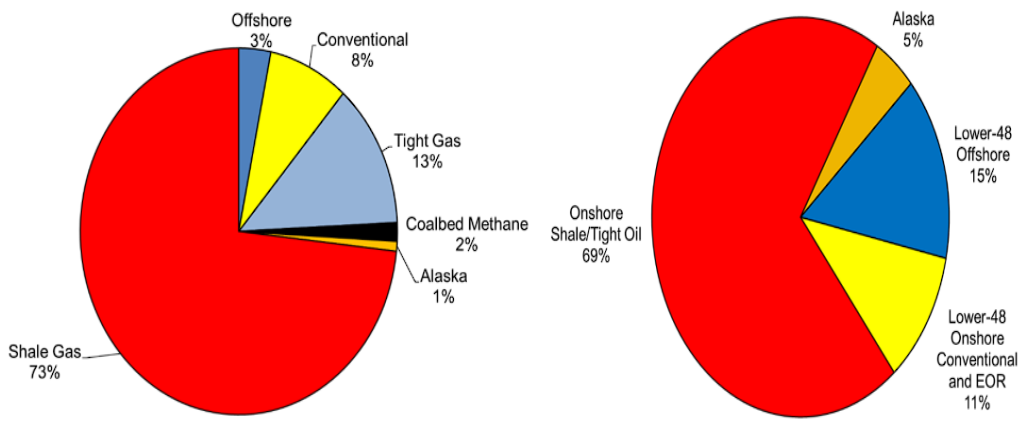

a) b)

Figure 2.10. EIA AEO2021 Reference Case Forecast of Cumulative U.S. a-) Oil b-) Natural Gas Production by Source, 2020-2050 (Hughes, 2021).

2.5 Overview of Energy Distribution in Turkey

According to the 2021 Energy Policy Review report for Turkey **(International Energy Agency (IEA), 2021**), the energy system in Turkey is mainly determined by fossil fuels. The share of fossil fuels corresponds to 83% of the total primary energy supply (TPES) and 73% of total final consumption (***Figure 2.11***). The remaining part of the supply chain and consumption distribution is composed of various renewable sources, which include geothermal, hydro, bioenergy, solar, and wind. Domestic energy production increased rapidly, with a growth of almost 60% from 2014 to 2019, driven mainly by renewables and coal (***Figure 2.12***). Domestic production occupied 30% of TPES in 2019, and all types of renewable energy were produced within the country. Despite the rapid growth in domestic production with the growing share of renewable energy in the energy distribution over the last two decades (***Figure 2.13***), Turkey's energy relies primarily on fossil fuels, supplied chiefly from abroad (**IEA, 2021**). More clearly, more than 90% of oil and gas and 60% of coal are imported, and fossil fuels will continue to dominate the energy market of Turkey, according to the Turkey Ministry of Energy and Natural Resources (MENR) (***Figure 2.14***).

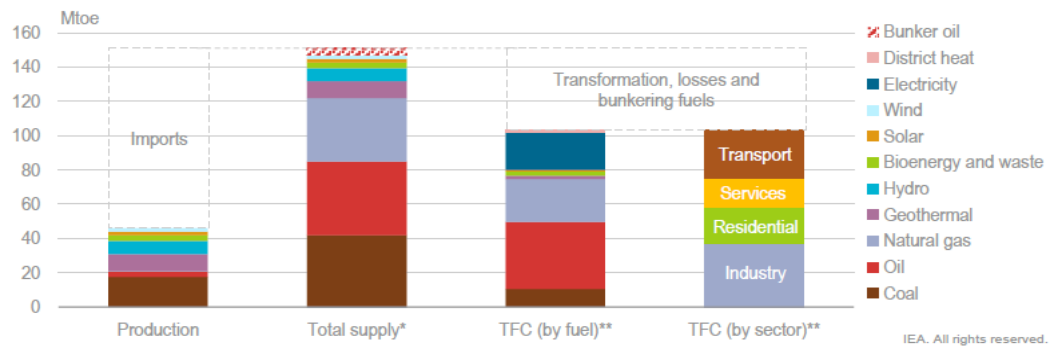

Figure 2.11. Overview of Turkey's Energy System by Fuel and Sector, 2018/19 (IEA, 2021).

** Total supply includes total primary energy supply plus international bunker fuels.*

*** TFC data are from 2018.*

Notes: Mtoe = million tonnes of oil equivalent. TFC = total final consumption. Production and total supply data for 2019 are provisional.

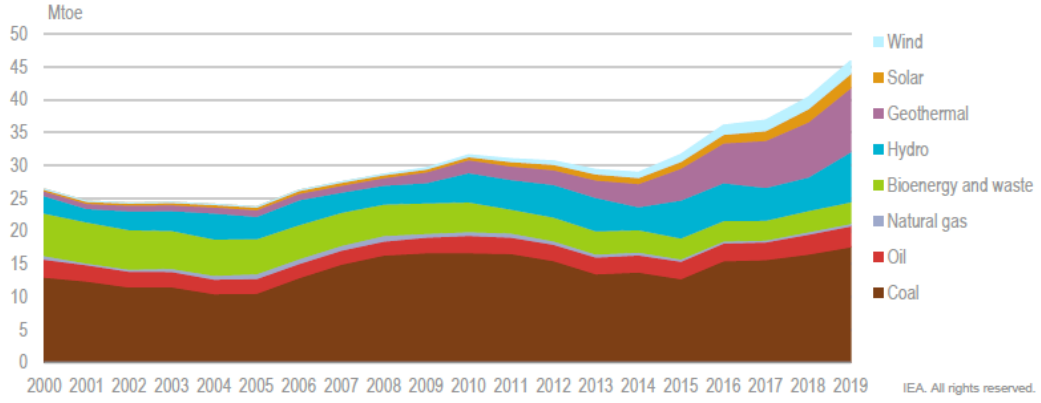

Figure 2.12. Energy Production by Source, Turkey, 2000-2019 (IEA, 2021).

Notes: Mtoe = million tonnes of oil equivalent.

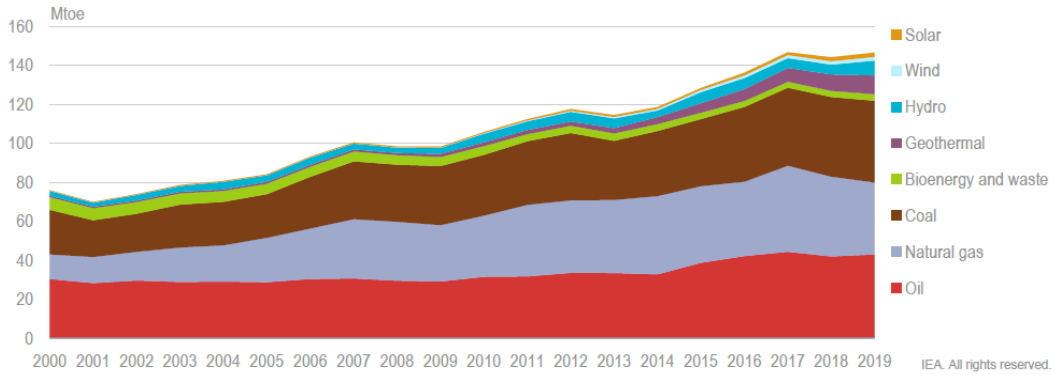

Figure 2.13. Total Primary Energy Supply by Source, Turkey, 2000-2019 (IEA, 2021).

Notes: Mtoe = Million Tonnes of Oil Equivalent. Supply Data For 2019 are Provisional. Electricity Imports and Exports Are Not Shown in the Chart.

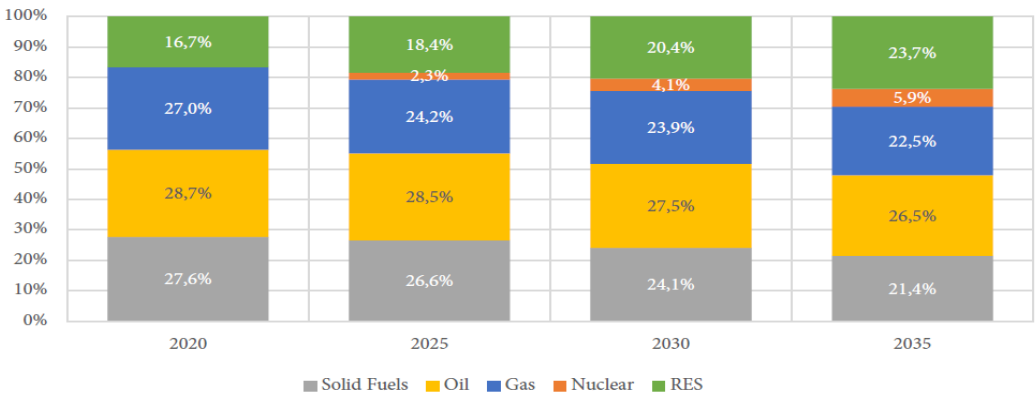

Figure 2.14. Distribution of primary energy consumption by source (MENR, 2022).

2.6 Major Shale Basins in Turkey

Given that the share of domestic oil and gas production in consumption is ultra-low, Turkey must expand its domestic exploration and production activities and diversify the energy supply chain accordingly. In this respect, Turkey is trying to restructure its energy system to manage energy demand growth, reduce huge import dependency on the oil and gas supply, and lower energy prices. As a part of reducing import dependency policy, Turkish Petroleum Corporation (Türkiye Petrolleri Anonim Ortaklığı, TPAO), a state-owned petroleum company, is conducting exploration studies in cooperation with several local and international firms to determine the potential of unconventional shale oil and gas resources (**IEA, 2021**). Initial shale exploration studies showed that Turkey has considerable potential in many basins across the country (**EIA, 2015**) (***Figure 2.15***). Shale exploration and development activities have focused on prospective basins, the Thrace Basin, and the Southeast (SE) Anatolian Basin. Horizontal drilling and hydraulic fracturing operations have been performed by TPAO and its partners in the SE Anatolian region since 2014 and in the Thrace region since 2015 (**TPAO, 2023**). Turkey also has under-explored basins, such as the Sivas and Salt Lake basins, which may contain shale resources; however, their shale resource potential has not been assessed because of limited reservoir data (**EIA, 2015**).

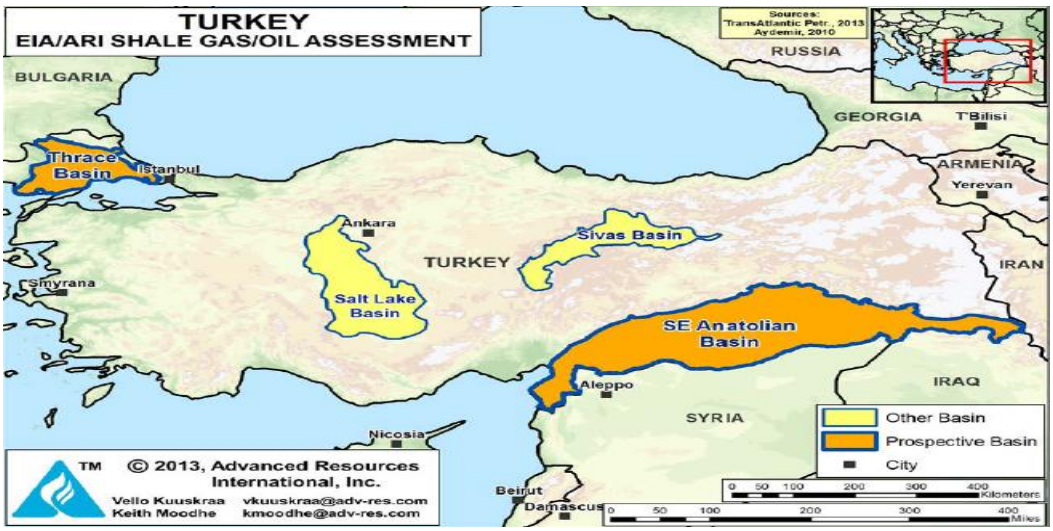

Figure 2.15. Major Shale Basins of Turkey (EIA, 2015).

2.7 Dadaş Shale in the Southeast Anatolia Basin

Southeast (SE) Anatolian Basin occupies nearly 32,000-mi^2 ($\approx$ 83,000-km^2) area in the Asian part of Turkey (***Figure 2.16***), which contains the most productive reservoirs of the country for hydrocarbon (HC) extraction, mostly oil. Silurian-aged, black, organic-rich Dadaş Shale resides in the north-central portion of the SE Basin and covers around one-eighth of the basin area ($\approx$ 10,500-km^2). The larger part of the Dadaş Shale ($\approx$ 9,200-km^2) is comprised of shale oil, and the remaining smaller part ($\approx$ 1,300-km^2) is of shale gas (***Figure 2.17***). According to the Energy Information Administration (EIA) (**2015**) predictions, the gas-in-place (GIP) amount for shale gas resources is approximately 130 trillion cubic feet (tcf) ($\approx$ 3.70 trillion cubic meter [tcm]), 17 tcf ($\approx$ 0.5 tcm) of which is the technically recoverable amount, whereas 5% (4.57 billion barrels $\approx$ 0.75 billion m^3) of shale oil resources (91.3 billion barrels $\approx$ 14.5 billion m^3) is stated as the technically recoverable amount (***Table 2.3***).

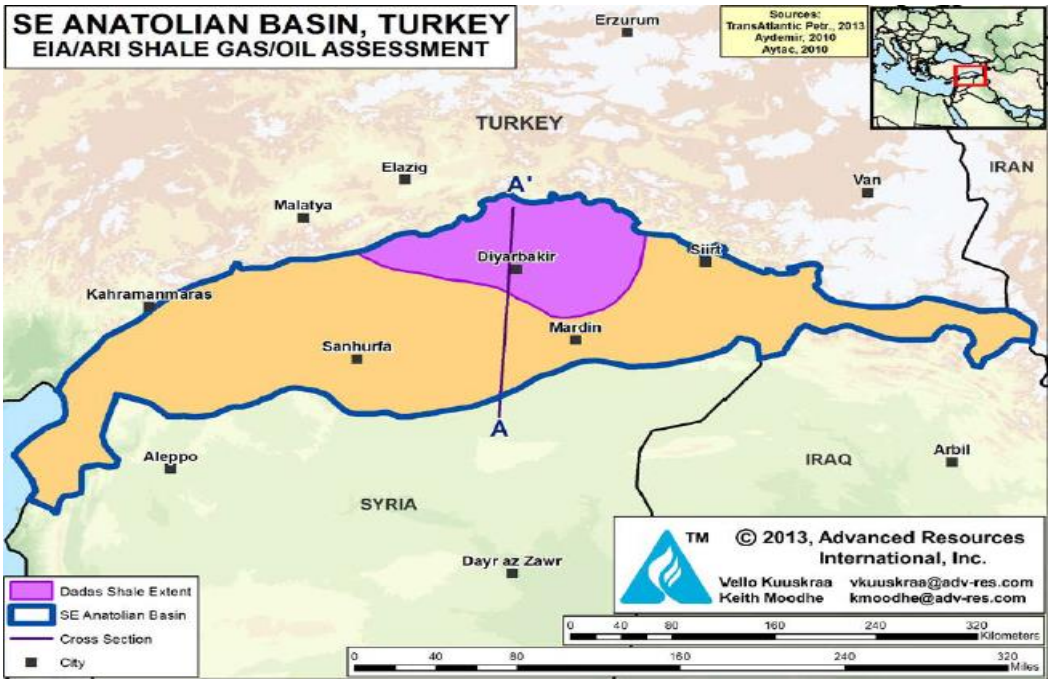

Figure 2.16. The Extent of the Dadaş Shale within the Boundaries of SE Anatolian Basin (EIA, 2015).

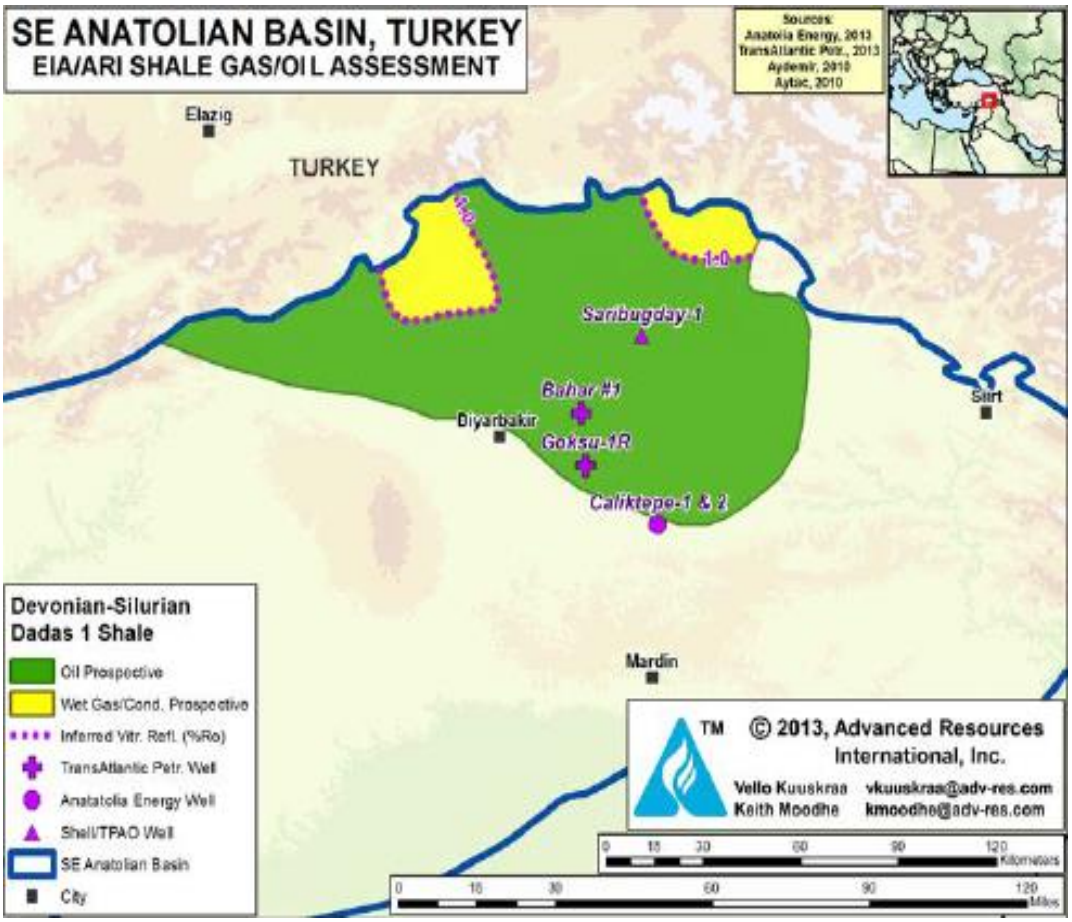

Figure 2.17. Dadaş Shale Prospective Area, SE Anatolian Basin, Turkey (EIA, 2015).

Table 2.3 Shale Gas & Oil Properties of Dadaş Formation (EIA, 2015).

Basic Data	**Basin/Gross Area**		SE Anatolian (32100 mi^2)	
	Shale Formation		Dadas	
	Geological Age		Silurian-Devonian	
	Depositional Environment		Marine	
Physical Extent	**Prospective Area (mi^2)**		3540	500
	Thickness (ft)	**Organically Rich**	394	377
		Net	216	207
	Depth (ft)	**Interval**	6000-11500	5500-13000
		Average	9000	9500
Reservoir Properties	**Reservoir Pressure**		Mod. Overpress.	Mod. Overpress.
	Average TOC (wt. %)		3.6 %	3.6 %
	Thermal Maturity (% Ro)		0.85%	1.15%
	Clay Content		Med./High	Med./High
Resource	**Gas Phase**		Assoc. Gas	Wet Gas
	GIP Concentration (Bcf/mi^2)		48.2	91.4
	Risked GIP (Tcf)		102.4	27.4
	Risked Recoverable (Tcf)		10.2	6.9
Resource	**Oil Phase**		Oil	Condensate
	OIP Concentration (MMbbl/mi^2)		41.0	14.2
	Risked OIP (MMMbbl)		87.1	4.2
	Risked Recoverable (MMMbbl)		4.36	0.21

As seen in ***Figure 2.18***, the Dadaş Formation, surrounded from above by the Hazro Formation and from below the Bedinan Formation, is composed of three units from bottom to top: Dadaş-I, Dadaş-II, and Dadaş-III. Dadaş-I, the basal unit of formation, comprises organic-rich brownish-gray-colored bituminous shales interbedded by limestone and banded by siltstone. The Dadaş-II member contains marine-organic rich shales and limestones and is the thickest unit of formation. The Dadaş-III member is at the uppermost, which embodies various lithologies such as shales, sandstones, limestones, dolostones, and marls **(Aydemir, 2011; Inan & Kavak, 2019; Ozturk et al., 2016**).

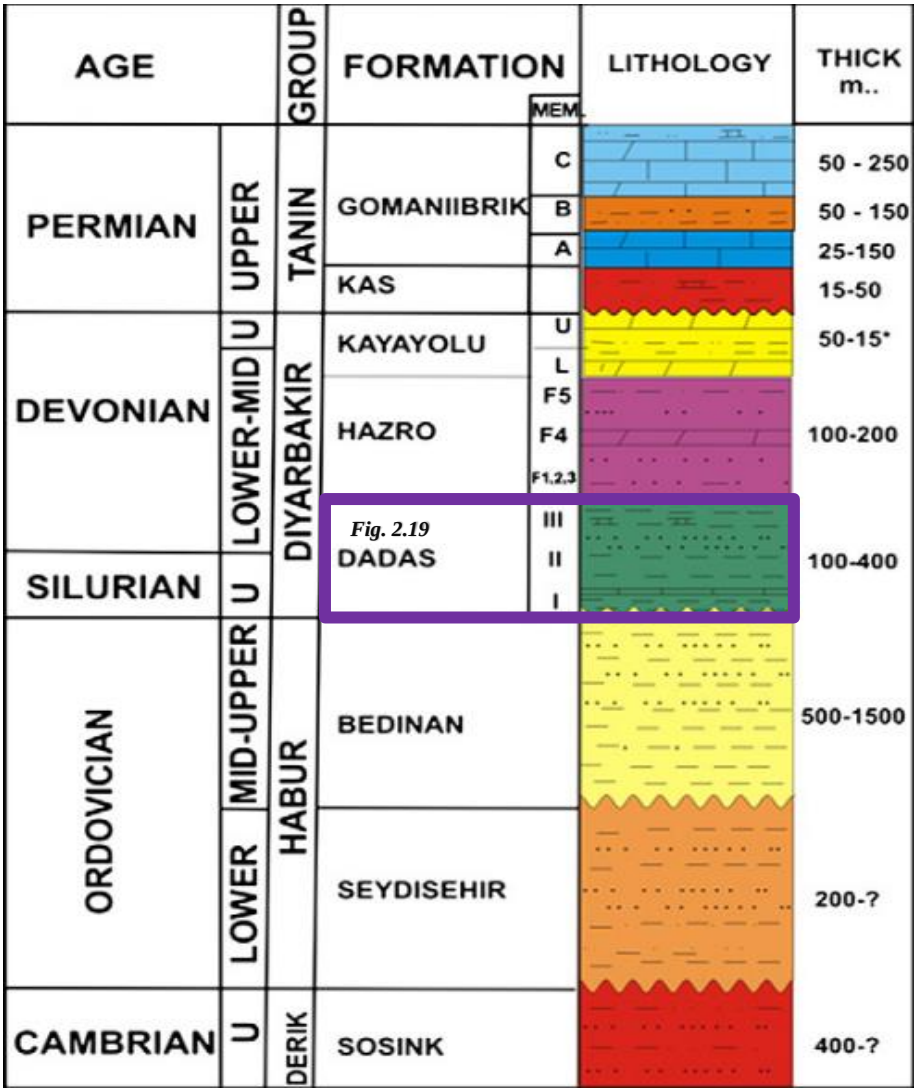

Figure 2.18. The Regional Stratigraphy of SE Anatolia Basin (Aydemir, 2011).

The detailed stratigraphic illustration of Dadaş members is represented in ***Figure 2.19***. Among all members, only the Dadaş-I member has presented a productive source rock characteristic for many conventional reservoirs in the Southeastern Anatolia region (**Kara & Isik, 2021; Sen & Kozlu, 2020**). More importantly, Dadaş-I is the most promising member for unconventional shale recovery and exploitation. The geochemical analyses, such as hydrogen index (HI) versus total organic carbon (TOC) curve, kerogen type, and the range of vitrinite reflectance (R_o, %), obtained from core samples show that Dadaş-I shale is both in oil window and gas window but mostly oil-origin (**Kara & Isik, 2021; Merey, 2019; Merey et al., 2021**)

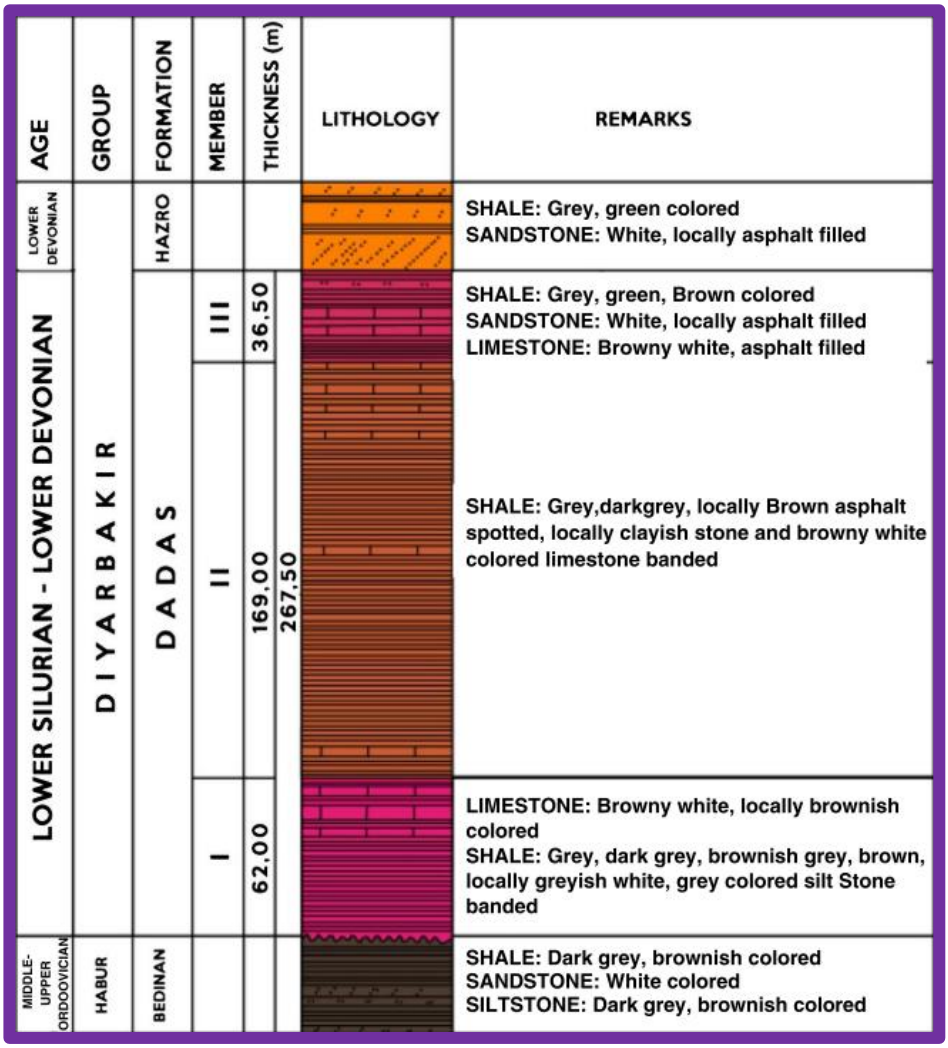

Figure 2.19. Stratigraphic Column of the Dadaş Formation (Inan & Kavak, 2019).

The Dadaş Formation has become the central point of unconventional shale research since the beginning of the 2010s. Between 2012 and 2014, three exploration wells, namely the Bahar-1, Çatak-1, Çalıktepe-2 wells, and one re-entry, Goksu-1R, well were drilled (**Hosgor & Yilmaz, 2022**), and later on, a fair amount of gas and light oil was extracted from Goksu-1 and Bahar-1 wells during the well testing period (**Merey, 2019**). In 2014, Konacik-1 well was drilled 500m horizontally, and then 42 ^{o}API high-gravity shale oil was obtained by hydraulic fracturing (HF). In 2019, in the drilling of the Gozalan-1/K/M well, the horizontal section was completed at a more distant point (approximately 1000m) than the Konacik-1 well (**TPAO, 2023**). More exploration wells should be drilled to collect more coring data and well logging data, and more studies regarding horizontal drilling and HF designs should be carried out to evaluate the commercial HC extraction from Dadaş shales. Additionally, many researchers (**Aydemir, 2011; Hosgor & Yilmaz, 2022; Inan & Kavak, 2019; Kara & Isik, 2021; Merey, 2019; Merey et al., 2021; Ozturk et al., 2016; Sen & Kozlu, 2020; Topcu, 2013; Tugan, 2017**) have emphasized the Dadaş Formation, and more specifically, Dadaş-I section of the Dadaş Formation as the primary target due to its favorable geological and petrophysical properties (***Table 2.4***).

Figure 2.20 shows the thickness distribution of various wells drilled within the Dadaş-I unit. High-quality, 50.9 ^{o}API light-sweet shale oil was obtained from Çalıktepe-2 well (**Merey, 2019**), one of the distinguished wells that can produce oil from Dadaş-I. The Çalıktepe-2 well, denoted by the number 37 on the map (***Figure 2.20***), in the south of the basin is the area of interest in this thesis study and serves as the stand-alone data source for the upcoming chapters accordingly.

Table 2.4 The geological & petrophysical properties of Dadaş I shale gas/oil reservoirs (Merey, 2019).

Property	Explanation/Value
Age	Devonian-Silurian
Depth, m	1676 to 3962 (Average: 2500)
Gross Thickness, m	30-400
Net Thickness, m	15 to 198 (Average: 50)
Kerogen Type	Type-II/Type-III (mainly marine shales)
TOC, %	0.4-18 (Average: 5.5)
Ro, %	0.5-1.5 (Average: 0.7-0.8)
Clay Content, %	34-49 (Average: 40)
Quartz Content, %	18-39 (Average: 25)
Porosity, %	0.5-10 (Average: 6.8)
Permeability, mD	4×10^{-4}-1.0 (Average: 0.1)
Water Saturation, %	5-20 (Average: 8.15)
Pressure, kPa/m	Normal to moderately over-pressurized, 9.73-15.83 (Average: 11)
Natural Fractures	Medium

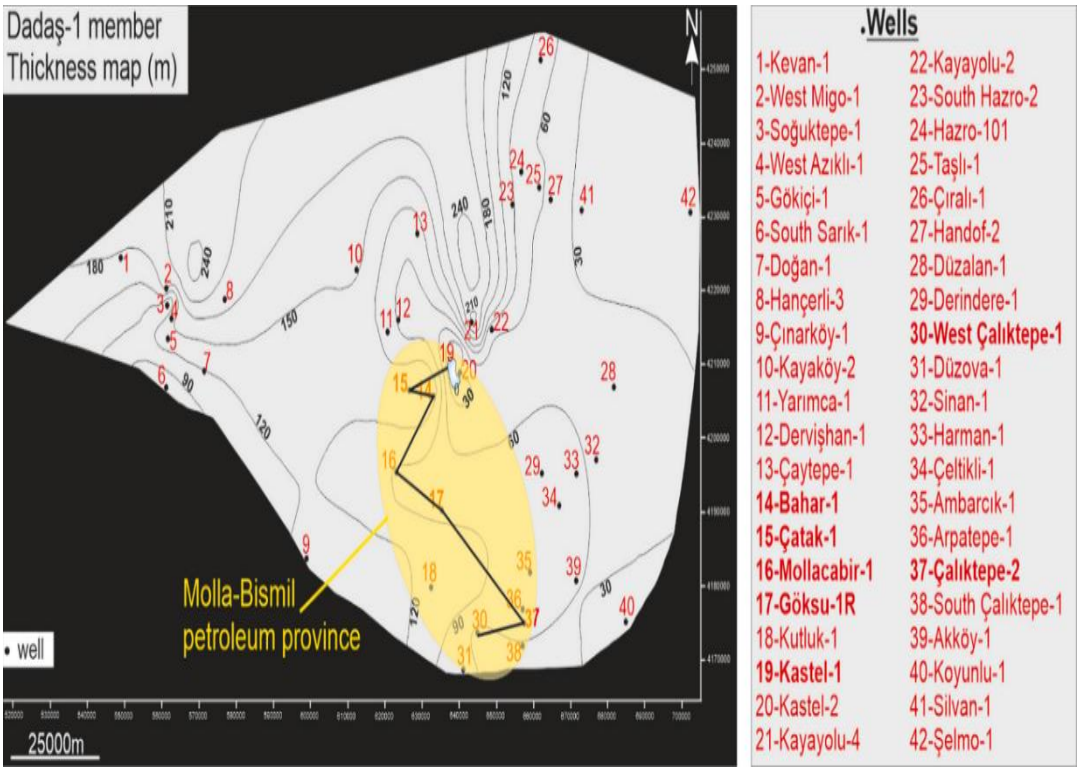

Figure 2.20 Regional Thickness Map of Dadaş-I Member (Hosgor & Yilmaz, 2022).

Kara & Isik (**2021**) divided the Dadaş-I unit into four lithofacies (L1, L2, L3, and L4 from bottom to top) based on differences in their lithological, geochemical, and petrophysical properties (***Figure 2.21***). The top and bottom depths of subunits (lithofacies) in Çalıktepe-2 well are distinguished in ***Figure 2.21***. Lithofacies-1 (L1) is at the bottom of Dadaş-I and made up of dark gray-to-black colored massive shales interbedded with siltstone, sandstone, and limestone. L1 is the thinnest section in Dadaş-I member, and its hydrocarbon potential is stated to be unattractive for unconventional shale production. On the other hand, Lithofacies-2 (L2) is mainly composed of bituminous, brownish-black, organic-rich shales (***Figure 2.22*a**). The petrophysical and geochemical properties of L2 (***Table 2.5***) highly support the unconventional HC potential, and roughly 75% of the HCs generated from Dadaş belong to this section.

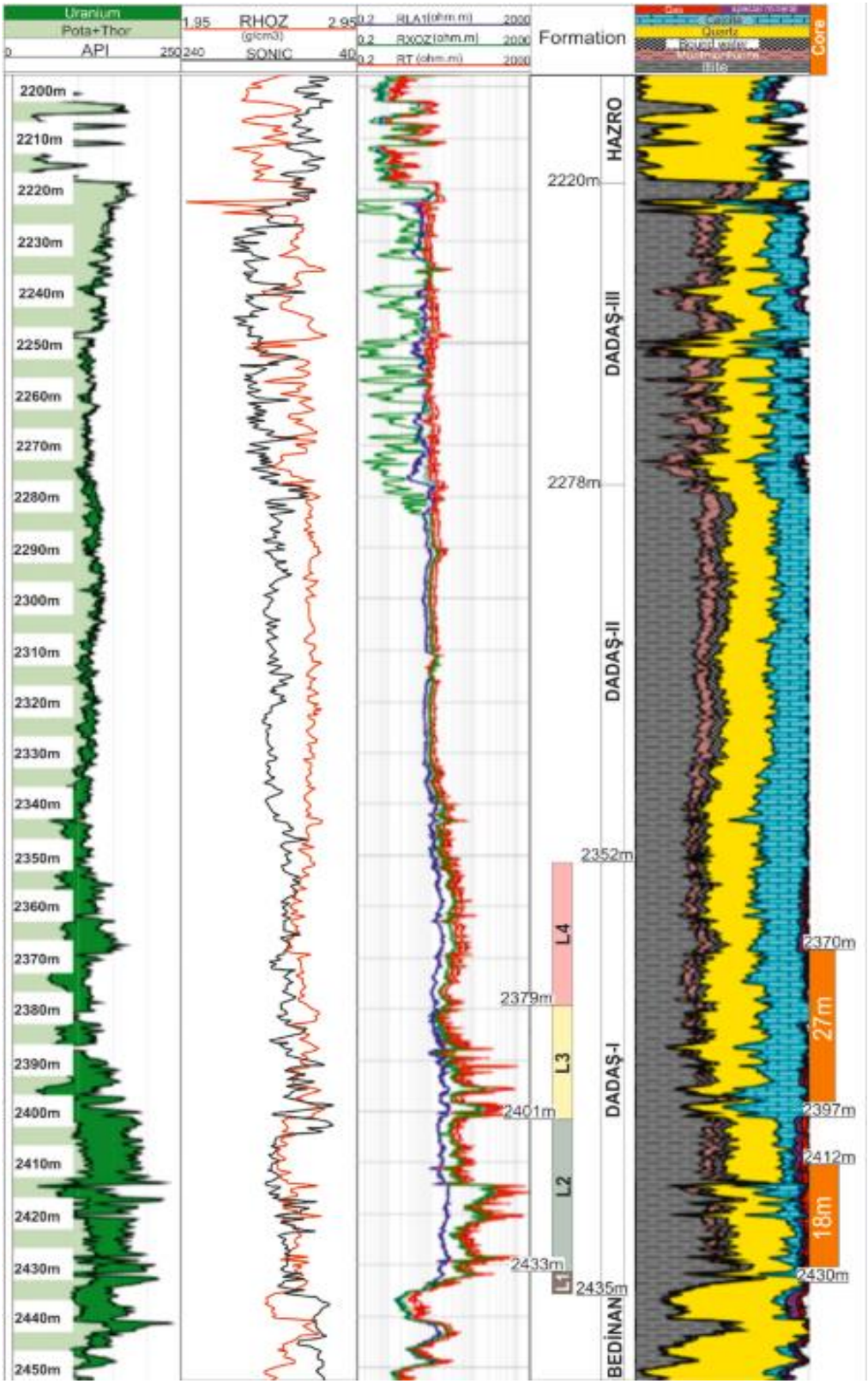

Figure 2.21 Lithofacies of Dadaş-I Member (from Çalıktepe-2 well) (Kara & Isik, 2021).

Lithofacies-3 (L3) is represented by organic-rich, brownish-black shales interlayered by thin dolomitic limestones (***Figure 2.22*b**). Due to high carbonate presence (up to 50%), L3 lacks source rock and unconventional reservoir potential considerably. Lithofacies-4 (L4) consists of brownish-dark gray-black colored silty and organic-rich shales with laminated carbonate intrusions (***Figure 2.22*c**), and it is the second most HC-prone zone in Dadaş-I member **(Kara & Isik, 2021**) (***Table 2.5***).

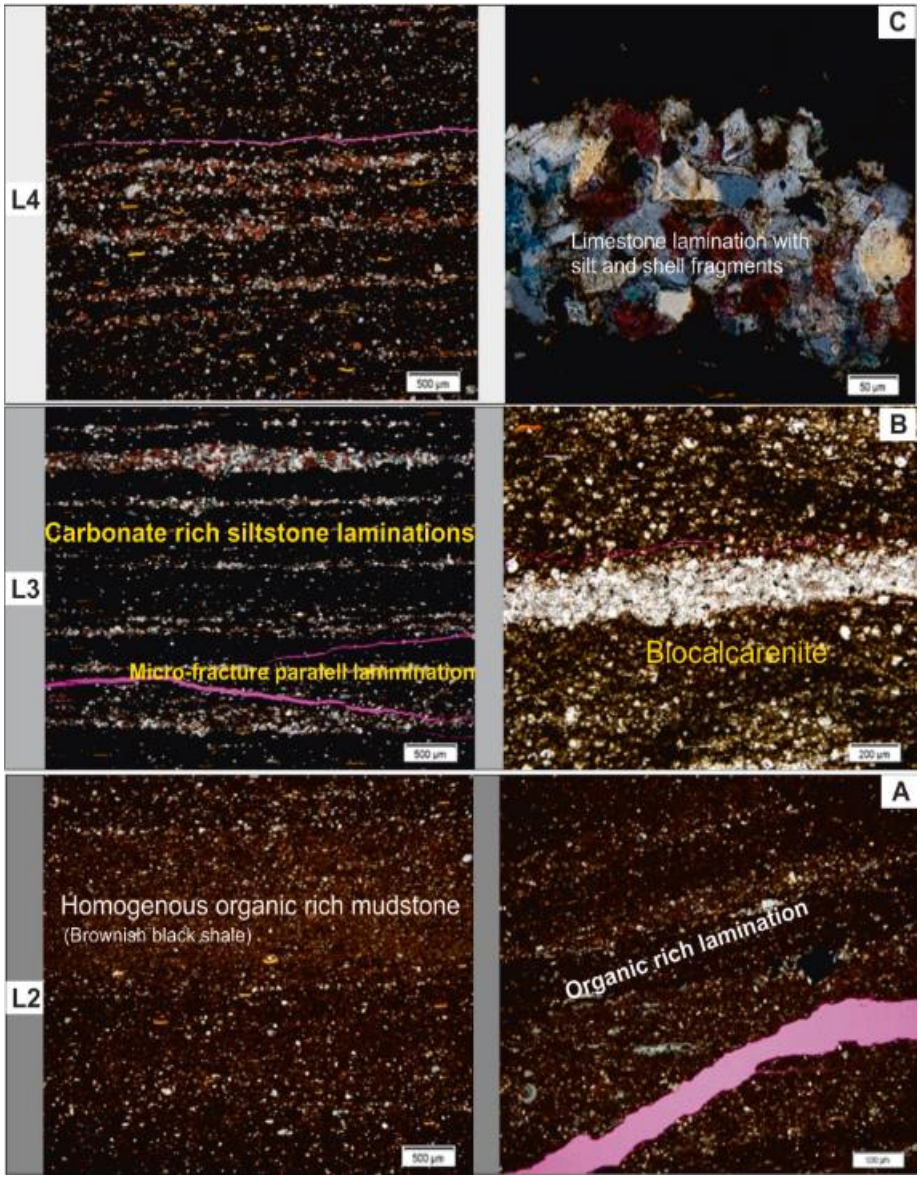

Figure 2.22 Microfacies pictures of L2, L3, and L4 (Kara & Isik, 2021).

Table 2.5 Reservoir Parameters of Dadaş Units and Dadaş-I Subunits Obtained from Log Analyses in Çalıktepe-2 well (Kara & Isik, 2021).

*Note: (f: Faulty contact), * Rounded to a nearest whole number.*

Unit	**Depth (m)**	**Gross Pay (m)**	**Net Pay* (m)**	**Por. (avg) (%)**	**Sw (avg) (%)**	**Perm. (avg) (nD)**	**TOC (avg) (%)**	**Cum. OIP (MMbbls/ km^2)**
Dadaş-III	2220f	58	0	3.12	100	0	1.06	0
Dadaş-II	2278	74	0	4.00	98	0.2	1.03	0.20
Dadaş-I (L4)	2352	27	26	6.00	50	130	1.69	4.21
Dadaş-I (L3)	2379	22	14	3.60	73	50	1.79	1.67
Dadaş-I (L2)	2401	32	31	7.60	28	423	2.69	8.76
Dadaş-I (L1)	2433	3	1	1.80	96	0	2.70	0

CHAPTER 3

THEORETICAL FRAMEWORK

3.1 The Role of Geomechanics in Hydraulic Fracturing for Unconventional Shale Reservoirs

Geomechanics, a branch of mechanics, is the theoretical and applied science of the mechanical behavior of rocks, which deals with elastic, plastic, strength, and deformation properties of subsurface formations that result from in-situ stress changes throughout field exploration and development stages. Rock mechanics has been serving as a significant area in the petroleum industry for many years since the mechanical properties of a rock affect completion, stimulation, and production processes in several ways (**Addis et al., 2016; Thiercelin & Roegiers, 2000**). The main roles of the geomechanics in the development of unconventional shale reservoirs by hydraulic fracturing (HF) are the characterization of mechanical parameters as screening criteria in the identification of sweet spots, and the evaluation of these mechanical parameters as input data in the analysis of fractures and fracture networks in numerical modeling studies.

3.2 Mechanical Earth Model

A mechanical earth model (MEM) is a mathematical quantification and graphical representation of the geomechanical behavior of subsurface formations, fields, or basins. For this purpose, the MEM works as a data repository to predict and measure the mechanical rock properties. This tool can be useful to increase the efficiency of a geomechanical analysis and minimize the risk of geomechanical problems faced during drilling, production, stimulation operations, and enhanced oil and gas recovery studies.

The MEM method is rather spread within the geomechanics community and having been applied to thousands of wells throughout the world. MEM has become more important in recent years due to increased fracturing operations in shale reservoirs (**Afsari et al., 2009; Berard & Prioul, 2016; Higgins-Borchardt et al., 2016**).

The MEM may both reflect a snapshot of a single event at a specific time and a time-lapse record of events, or it may track the situation of parameters as the reservoir conditions change. The MEM contains depth profiles of elastic or elasto-plastic rock parameters, principal stresses, rock failure properties, pore pressure gradient, fracture pressure gradient, and rock strength parameters. Fundamental parameters can be obtained from various measurement sources such as seismic data, well-log data, image data, mud logs, cutting data, and coring data. Other geomechanical parameters can be derived from generally accepted equations or empirical correlations. Depending on the intended application and the available data, models may be simple or complex, of high- or low-resolution, within the scale of small or big intervals, 1,2, or 3-dimensional (**Afsari et al., 2009; Berard & Prioul, 2016; Higgins-Borchardt et al., 2016**).

3.3 Geomechanical Properties

Most of the unconventional reservoirs have anisotropy in various ways due to their layered and heterogeneous structures. However, in this study, due to the inadequacy of data, the geomechanical parameters were derived under the assumptions below for the sake of simplification.

Assumptions

- Dadaş Formation is isotropic and homogenous,
- Dadaş Formation behaves linearly and elastically
- There is a clearly and directly (linear and unique) defined relationship between stress and strain, which is known as Hooke's Law.

According to these assumptions, a 1-D MEM was constructed to quantify and reflect geomechanical properties of Dadaş shale based on well-log (Gamma Ray log, Sonic log, Density log) data and coring data, obtained from Çalıktepe-2 well studied in Kara & Isik's research (**2021**). The following subsections provide theoretical information about these geomechanical properties that can be used to evaluate the fracability of Dadaş-I section.

3.3.1 Young's Modulus & Poisson's Ratio

Young's modulus (YM, E) is a measure of the stiffness of an elastic material, and it is defined as the ratio of axial stress to axial strain. Poisson's ratio (PR, ν) is a measure of the deformation (strain) of an elastic material, and it is defined as the strain in the unloaded direction (lateral strain) divided by the strain in the loaded direction (axial strain). For hydraulic fracturing (HF) operations, YM (E) reflects the ability of a rock after being ruptured to keep fractures open and to resist the proppant embedment along the fracture surface (**Huang et al., 2021**); PR (ν) indicates the deformation tendency of a rock to be fractured as ductile way, under applied stress (**Fernandez Rojas et al., 2016**). Thus, generally shales with low YM (E) (< 20 GPa) and high PR (ν) (> 0.25) tend to be ductile, whereas rocks with high YM (> 20 GPa and low PR (< 0.25) tend to be brittle.

Dynamic YM and dynamic PR can be obtained from Fjær et al.'s (**2008**) equations below related to acoustic sonic log and density log:

$$\boldsymbol{E_{DYN}} = \frac{\rho V_S^2(3V_P^2-4V_S^2)}{(V_P^2-V_S^2)} \quad \textbf{(3.1)}$$

$$\boldsymbol{\nu_{DYN}} = \frac{(V_P^2 - 2\,V_S^2)}{2(V_P^2-V_S^2)} \quad \textbf{(3.2)}$$

where E_{DYN}: Dynamic Young's modulus (GPa); ν_{DYN}: Dynamic Poisson's ratio (dimensionless); ρ: Bulk density of shale (g/cm^3); V_P: Compressional wave (P-wave) velocity (km/s); V_S: Shear wave (S-wave) velocity (km/s).

V_P is obtained from the reciprocal of sonic log reading (compressional travel time [DT=Δt_C], μs/ft), and V_S can be calculated from the Brocher's (**2005**) regression fit, which is valid for rocks in the earth's crust including shale as follows, respectively:

$$\boldsymbol{V_P\left({}^{ft}/_{\mu s}\right) = {}^{1}/_{DT} = {}^{1}/_{\Delta t_C}} \quad \text{.....(3.3)}$$

$$\boldsymbol{V_S = 0.7858 - 1.2344V_P + 0.7949V_P^2 - 0.1238V_P^3 + 0.0064V_P^4,}$$
$$\boldsymbol{where\ 1.5 < Vp < 8} \quad \text{.....(3.4)}$$

3.3.2 Geological Principal Stresses

The tectonic stress field, one of the main components of any geomechanical study, has a significant effect on the HF of unconventional shale reservoirs. Based on Anderson's faulting theory (**Zoback, 2007a**), stress fields (or regimes) are described in terms of the orders of magnitude between the vertical (or overburden, σ_V) stress and two mutually perpendicular horizontal stresses (minimum horizontal stress, σ_h, and maximum horizontal stress, σ_H) (***Figure 3.1***).

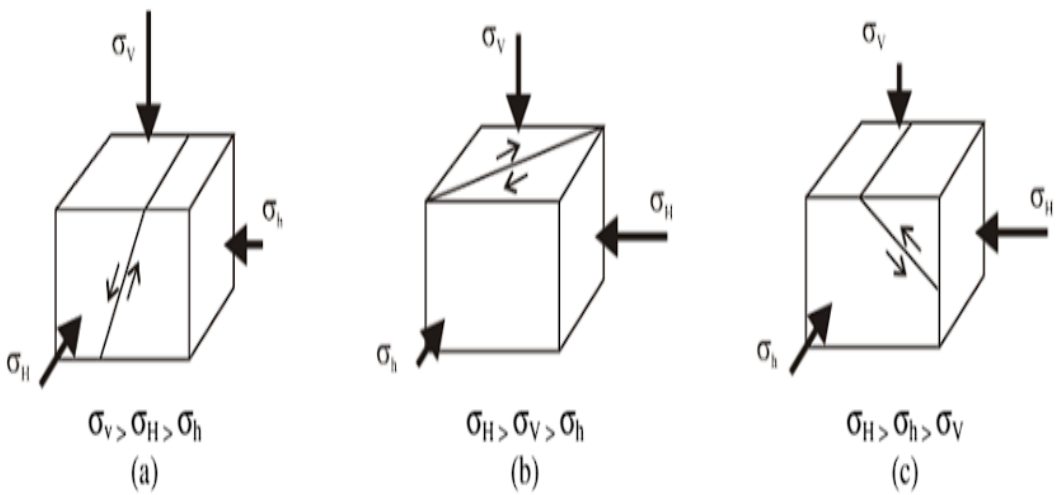

Figure 3.1. Anderson's stress regime classification: a) normal faulting; b) strike-slip faulting; c) reverse (thrust) faulting (Nacht et al., 2010).

3.3.2.1 Vertical Stress

Vertical stress (σ_V) is the stress applied to subsurface rock due to the weight of overlying rocks above it. By the integration of rock densities above the depth of interest, the vertical stress can be calculated (**Zoback, 2007a**):

$$\boldsymbol{\sigma_V = \int_0^H \frac{\rho}{144} dh \approx \frac{\bar{\rho}\, H}{144}} \quad \text{.....(3.5)}$$

3.3.2.2 where σ_v: Vertical stress (psi); $\bar{\rho}$: Average bulk density of overburden rocks (lb/ft^3); H: Depth of interest (ft).Minimum and Maximum Horizontal Stresses

Horizontal stress anisotropy due to rock heterogeneity and tectonic factors leads to a noteworthy difference between the two horizontal principal stresses. In a tectonically active region, minimum and maximum horizontal stresses can be distinguished with the consideration of resulting tectonic stresses, as represented in Eqs. (**3.6 and 3.7**) below (**Higgins-Borchardt et al., 2016)**:

$$\boldsymbol{\sigma_h = \frac{\nu}{1-\nu}(\sigma_V - \alpha P_P) + \alpha P_P + \frac{E_S}{1-\nu^2}(\epsilon_h + \nu \epsilon_H)} \quad \text{.....(3.6)}$$

$$\boldsymbol{\sigma_H = \frac{\nu}{1-\nu}(\sigma_V - \alpha P_P) + \alpha P_P + \frac{E_S}{1-\nu^2}(\epsilon_H + \nu \epsilon_h)} \quad \text{.....(3.7)}$$

where $\boldsymbol{\epsilon_h = \frac{\nu\, \sigma_V}{E_S}\left(\frac{\nu}{1-\nu}\right)}$, and $\boldsymbol{\epsilon_H = \frac{\nu\, \sigma_V}{E_S}\left(1 - \frac{\nu^2}{1-\nu}\right)}$ .....**(3.8, 3.9)**

σ_h and σ_H: Minimum and maximum horizontal stress (psi), respectively; ν: Poisson's ratio (dimensionless); σ_V: Vertical stress (psi); α: Biot's constant (dimensionless); P_P: Pore Pressure (psi); E_S: Static Young's modulus (psi); ϵ_h *and* ϵ_H: Tectonic strains along minimum and maximum horizontal stress directions (dimensionless), respectively.

The last terms on the right-hand side of both equations (**3.6 and 3.7**) refer to the resulting tectonic stresses in each horizontal principal direction, respectively. For the tectonic stress part, the static YM can be derived from an empirical correlation for shales developed by Horsrud (**2001**):

$$\boldsymbol{E_S = 0,076 * V_P^{3,23}} \quad \textbf{(3.10)}$$

where E_S: Static Young's modulus (psi), and Vp: P-wave velocity (km/s).

Static YM is a constant number and normally, it is derived from the stress-strain rock deformation behavior measured in core samples when the circumstances allow (**Addis et al., 2016**). On the other hand, dynamic YM is variable, and it can be obtained from compressional and shear sonic logs (**Addis et al., 2016**).

For most HF applications, the direction and magnitude of minimum horizontal stress (σ_h) are more important than those of maximum horizontal stress (σ_H) as the far-field fracture geometry is only affected by the profile of the minimum horizontal stress (σ_h). The orientation and magnitude of minimum horizontal stress (σ_H) have a direct influence on the trajectory of horizontal wells and the propagation of hydraulic fractures (**Guo et al., 2017**).

In normal faulting (NF) and strike-slip (SS) faulting regions, horizontal wells are mostly drilled parallel to minimum horizontal stress (σ_h) direction (perpendicular to maximum horizontal stress [σ_H] direction), as a result of which vertical (transverse) fractures (***Figure 3.2a***) are created that will propagate perpendicular to the minimum horizontal stress (σ_h) direction (parallel to maximum horizontal stress [σ_H] direction). The fracture initiation and propagation are maintained as long as the fracture fluid pressure is larger than the minimum principal stress (σ_h). For this reason, unless a reverse faulting (RF) regime is encountered, the minimum principal stress (σ_h) is also named as the "closure stress" below which the fracture will close eventually **(Guo et al., 2017**).

In a reverse fault (RF) environment, on the other hand, horizontal (longitudinal) fractures (***Figure 3.2*b**) are generated. Reservoir fluid is recovered in the vertical direction in case of horizontal fractures, which stimulate reservoir rocks less effectively compared to vertical fractures (**Guo et al., 2017**).

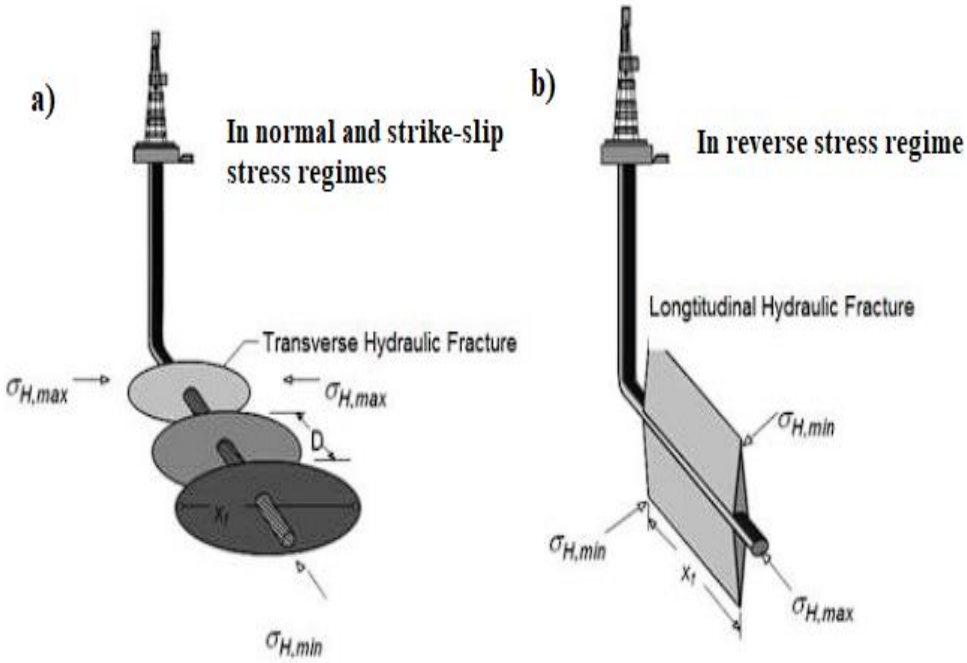

Figure 3.2. Fracture configurations from a horizontal well: a) multiple transverse fractures and b) a longitudinal fracture (H. Y. Wang, 2016).

The World Stress Map (WSM) is a useful tool to estimate the tectonic stress regime and the orientation of maximum horizontal stress (σ_H) in any specific geological region. By analyzing the WSM data (***Figure 3.3***) with Merey et al.'s study (**2021**), it was observed in the Diyarbakir region that the stress regime is dominated by the strike-slip (SS) faulting system, but the reverse faulting (RF) system is also considerably observed. Additionally, it was found that the orientation of maximum horizontal stress (σ_H) for Dadaş shales is almost along the North-South direction.

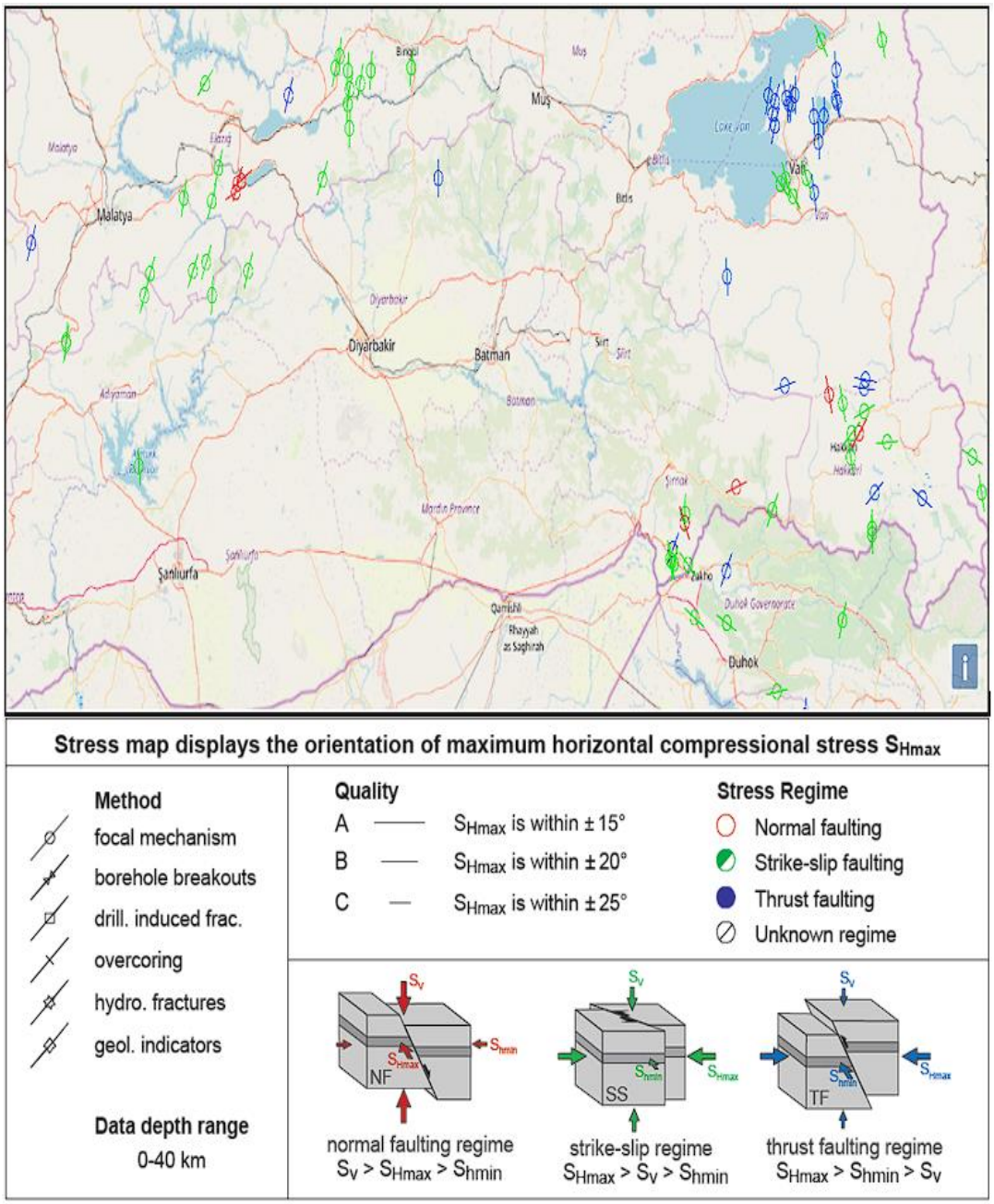

Figure 3.3. Stress map showing the faulting regime and the orientation of maximum horizontal stress around the Diyarbakir region (CASMO - World Stress Map, 2016; Heidbach et al., 2016).

3.3.2.3 Differential Horizontal Stress

Differential horizontal stress (DHS, Δσ) refers to the difference between the maximum and minimum horizontal principal stress ($\Delta\sigma = \sigma_H - \sigma_h$). Stress difference in company with approaching angle (θ) are the main controlling factors of interactions between hydraulic fracture (hFs) and natural fractures (nFs) (***Figure 3.4***).

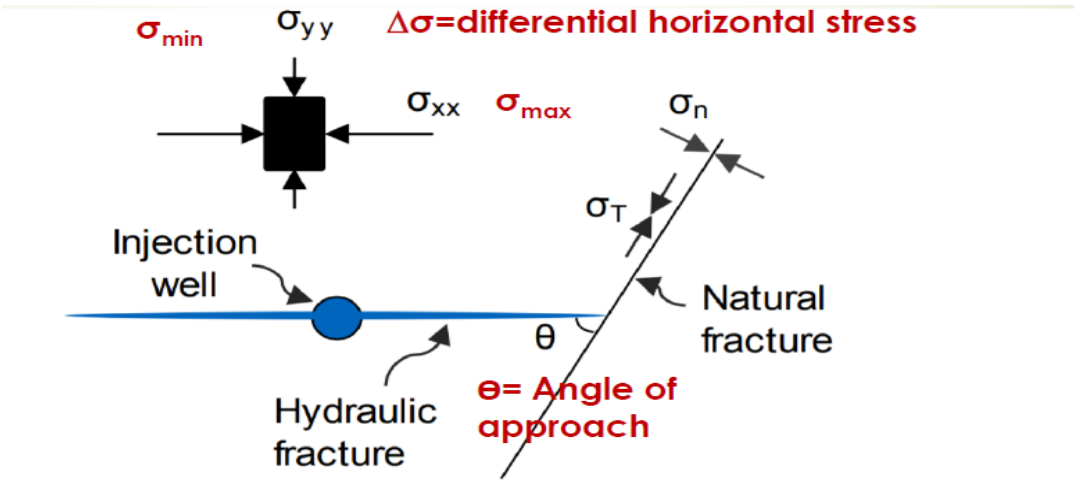

Figure 3.4. The representation of an interaction between hydraulic fracture (HF) and natural fracture (NF) with an indicated differential horizontal stress (Δσ) and approach angle (θ) (Yildirim, 2022).

The former studies (**Blanton, 1982, 1986; P. Chen et al., 2014; P. Chen & Rahman, 2015; Dong et al., 2015; Dou et al., 2022; Lihong et al., 2019**) indicated that the hFs tend to extend along nFs in relatively low DHS (Δσ) and low approaching angle (θ) conditions. Under these conditions, the chance for dilation and/or re-activation interaction mechanisms (connection in ***Figure 3.5***) to occur increases, which, in turn, means complex fracture networks and larger stimulated reservoir volumes (SRVs). When a hF approaches a nF at larger differential stresses at a constant angle, it extends across the nF. In this case, the direct crossing or crossing with offset interaction scenarios occur quite likely, and generally, a simple major fracture can be observed instead of a fracture network.

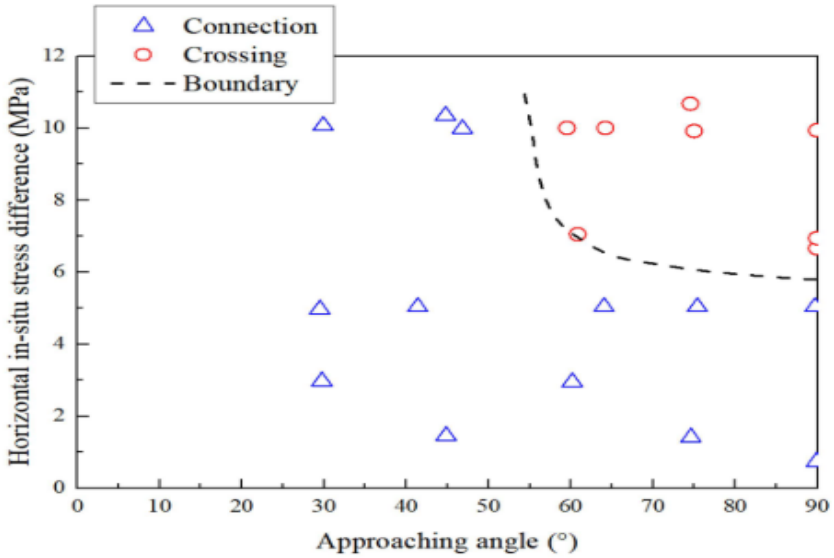

Figure 3.5. Influences of differential horizontal stress and approaching angle on fracture propagation. 'Connection' indicates that hydraulic fractures and natural fractures are interconnected, and natural fractures are ultimately extended by the intersected hydraulic fractures. 'Crossing' indicates that natural fractures are crossed by hydraulic fractures without inter-connection (Dou et al., 2022).

The influences of DHS and approaching angle on hF-nF interactions can be estimated by Lihong et al.'s (**2019**) equation:

$$\boldsymbol{F_N = 1 - \frac{\Delta\sigma\ x\ \sin^2\theta}{(\Delta\sigma\ x\ \sin^2\theta)_{max}}} \quad \text{.....(3.11)}$$

Here, F_n: Influencing factor of the openness of nFs (dimensionless); σ_H *and* σ_h: Maximum and minimum horizontal stress (MPa), respectively; θ: Approaching angle (angle between a hF surface and a nF surface, (°)).

It is not easy to quantitatively evaluate the effect of approaching angles without performing a lab experiment or a numerical simulation study. An alternative equation can be derived by excluding the approaching angle (θ) in Eq. **3.11** to measure the effect of DHS on the hF-nF interaction as follows:

$$\boldsymbol{\Delta\sigma_{Index} = 1 - \frac{\Delta\sigma}{\Delta\sigma_{max}}} \quad \text{.....(3.12)}$$

where, $\Delta\sigma_{Index}$: Normalized DHS index (dimensionless); $\Delta\sigma$ *and* $\Delta\sigma_{max}$: Actual and maximum DHS (MPa), respectively.

3.3.3 Biot's Coefficient

Biot's poro-elastic constant reflects the ability of the fluid for transmission of pore pressure into rock grains. If absolute porosity values are known, a rough prediction of Biot's constant can be obtained using Eq. **3.13** (**Belyadi et al., 2017**)

$$\boldsymbol{\alpha = 0.64 + 0.854\, x\, \phi} \quad \text{.....(3.13)}$$

where ϕ: Absolute porosity, fraction.

3.3.4 Pore Pressure

Pore pressure (PP, P_P) is the pressure of fluid in the pore space of an underground rock. PP has a deep impact on the in-situ stress state, hydrocarbon (HC) flow rate and production, and borehole stability in all formations. PP corresponds to hydrostatic water pressure in a normally-pressured environment, but in under-pressured regions such as coal bed methane (CBM) reservoirs PP is smaller than hydrostatic pressure (P_{HYD}), and in over-pressured regions such as shale reservoirs PP is greater than hydrostatic pressure (P_{HYD}).

It is not simple to measure the PP in unconventional reservoirs due to operational and technical difficulties in impermeable formations. Among many PP estimation methods, Eaton's method (**1975**) and Bower's method (**1995**) have widely used for many years in the petroleum industry (**Ahmad & Rezaee, 2015**). However, it is more practical to use Eaton's method in case of the limited data source. Eaton's method empirically correlates the sonic transit time (Δt) profile with the pore pressure gradient (Pp,grad), through a calculation of the effective stress acting on the rock (**Ahmad & Rezaee, 2015; Higgins-Borchardt et al., 2016**). For instance, the pore pressure gradient (Pp,grad) at Caliktepe-2 well drilled within Dadaş-I shale may be predicted by Eaton's method, as shown in Eq. **3.14**.

$$\boldsymbol{P_{P,grad} = \sigma_{V,grad} - \left(\sigma_{V,grad} - P_{hyd,grad}\right) * \left({\Delta t_n}/{\Delta t}\right)^3} \quad \text{.....(3.14)}$$

where $P_{P,grad}$: Pore pressure gradient (psi/ft); $\sigma_{V,grad}$: Vertical stress gradient (psi/ft); $P_{hyd,grad}$: Hydrostatic pressure gradient (psi/ft); Δt_n: Normal compaction trendline in sonic log (µs/ft); Δt: Observed sonic log transit time (µs/ft).

Δt_n and Δt values are estimated by Eaton's Method from the semi-log curve of sonic transit time and depth (***Figure 3.6***).

$\Delta t_n \approx 85$ µs/ft and $\Delta t \approx 120$ µs/ft (at the depth of middle of the abnormal pressure region)

$\sigma_{V,grad}$ is calculated as 1.112 psi/ft (**Eq. 3.5**), and $P_{hyd,grad}$ is taken as 0.433 psi/ft, which yields the pore pressure gradient as:

$$P_{P,grad} = 1.112 - (1.112 - 0.433)\left({}^{85}/_{120}\right)^3 = 0.871 \text{ psi/ft}$$

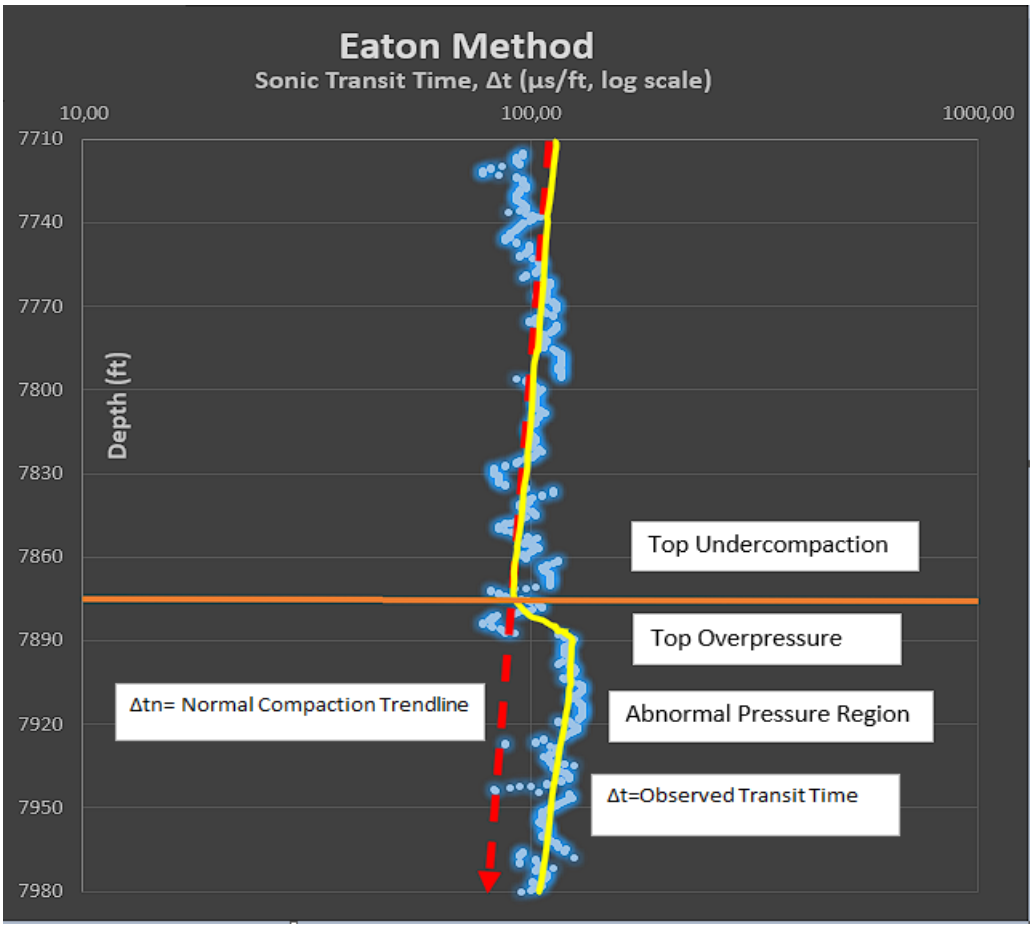

Figure 3.6. Eaton's method for pore pressure gradient calculation in Dadaş shales.

3.3.5 Strength Parameters

Rock strength can be defined as the stress level of rock that is required to resist permanent deformation. From a mechanical perspective, the key rock strength parameters contain unconfined compressive strength (UCS), cohesion (C_0), and internal friction angle (φ). These strength parameters can be represented by the Mohr-Coulomb failure system (***Figure 3.7***), the most commonly employed triaxial criterion in geomechanical studies (**Rasouli, 2015**). The Mohr-Coulomb criterion is based on the assumption that shear stress (τ) is a linear function of normal stress, as described in Eq. **3.15** (**Thiercelin & Roegiers, 2000**)

$$\boldsymbol{\tau = C_O + \sigma_N \tan \varphi} \quad \text{.....} \textbf{(3.15)}$$

Here, τ: Shear stress; σ_N: Normal stress; C_O: Cohesion; φ: Internal friction angle.

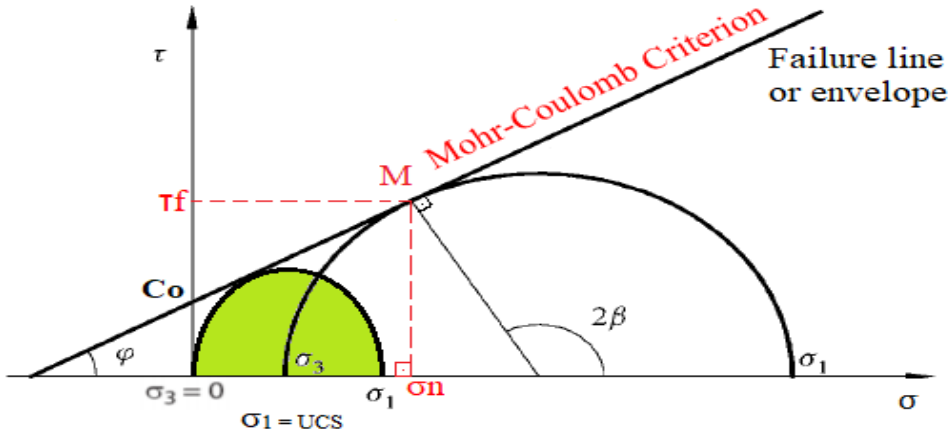

Figure 3.7. Graphical representation of a stress state at failure by Mohr-Coulomb criterion (Modified after: Thiercelin & Roegiers, 2000)

In the τ-σ plane, the failure line distinguishes the safe region from the failure region and intersects the τ-axis at the point, which is called cohesion (inherent shear strength) (**Thiercelin & Roegiers, 2000**).

The internal friction angle (φ) between the failure line and σ-axis, is the slope of the Mohr-Coulomb system, and it is linked to the coefficient of internal friction (μ_i) by:

$$\boldsymbol{\mu_i = \tan \varphi} \quad \text{.....} \textbf{(3.16)}$$

Figure 3.7 shows the point M (σ_N, τ_F) that the Mohr circle contacts with the failure line. At this contact point, the shear stress and the normal stress are (**Zoback, 2007b**)

$$\boldsymbol{\tau = 0.5(\sigma_1 - \sigma_3)\, sin\, 2\beta} \quad \text{.....} \textbf{(3.17)}$$

$$\boldsymbol{\sigma_n = 0.5(\sigma_1 + \sigma_3) + 0.5(\sigma_1 - \sigma_3) \cos 2\beta} \quad \text{.....} \textbf{(3.18)}$$

where, σ_1 *and* σ_3: The maximum and minimum principal stress, respectively.

β is the angle for which the failure criterion is fulfilled, and it is related to the internal friction angle by (**Thiercelin & Roegiers, 2000**)

$$\boldsymbol{\beta = {}^{\pi}/_{4} + {}^{\varphi}/_{2}} \quad \text{.....} \textbf{(3.19)}$$

After inserting equations **3.17** and **3.18** into criterion expression **(3.15)** and replacing β by φ, the alternative form of Eq. **3.15** in terms of principal stresses can be obtained by a set of trigonometric operations as follows:

$$\boldsymbol{(\sigma_1 - \sigma_3) = (\sigma_1 + \sigma_3) \sin \varphi + 2C_O \cos \varphi} \quad \text{.....} \textbf{(3.20)}$$

When another Mohr circle is constructed by a green-shaded area (***Figure 3.7***) where σ_1= UCS, and σ_3= 0, UCS can be derived from the equation above:

$$\boldsymbol{UCS = \frac{2C_O \cos \varphi}{1 - sin\, \varphi}} \quad \text{.....} \textbf{(3.21)}$$

From this viewpoint, UCS can be described as the ultimate strength of the rock, when it is compressed uniaxially under zero confining pressure (**Zoback, 2007b**).

UCS can be estimated from log data using empirical relations listed in ***Table 3.1***, when lab measurements on core samples are not available. Among all UCS correlations, the globally applicable correlation related to compressive transit time can be utilized to estimate the UCS of shales.

$$UCS = 195.75\,(304.8/\Delta t)^{2.6} \quad \text{.....(3.22)}$$

UCS: Unconfined compressive stress (psi); Δt: Compressional transit time (µs/ft).

Since cohesion is not measured physically (**Zoback, 2007b**), it can be estimated from the re-written form of Eq. **3.21**.

$$C_O = \frac{UCS\,(1-\sin\varphi)}{2\cos\varphi} \quad \text{.....(3.23)}$$

Lal (**1999**) developed a relation for friction angle in shales as a function of compressional sonic transit time:

$$\varphi = sin^{-1}\frac{\left(\left[\frac{304878}{\Delta t}\right]-1000\right)}{\left(\left[\frac{304878}{\Delta t}\right]+1000\right)} \quad \text{.....(3.24)}$$

where φ: Internal friction angle (degree); Δt: Compressional transit time (µs/ft).

Table 3.1 Empirical relationships between unconfined compressive strength (UCS) and other physical properties in shale (Chang et al., 2006).

UCS (MPa)	Region Where Developed	General Comments
$0.77\,(304.8/\Delta t)^{2.93}$	North Sea	Mostly high porosity Tertiary shales
$0.43\,(304.8/\Delta t)^{3.2}$	Gulf of Mexico	Pliocene and younger
$1.35\,(304.8/\Delta t)^{2.6}$	Globally	-
$0.5\,(304.8/\Delta t)^{3}$	Gulf of Mexico	-
$10\,(304.8/\Delta t - 1)$	North Sea	Mostly high porosity Tertiary shales
$7.97\,E^{0.91}$	North Sea	Mostly high porosity Tertiary shales
$7.22\,E^{0.712}$	-	Strong and compacted shales
$1.001\,\phi^{-1.143}$	-	Low porosity (ϕ<0.1) high strength (~79 MPa) shales
$2.922\,\phi^{-0.96}$	North Sea	Mostly high porosity Tertiary shales
$0.286\,\phi^{-1.762}$	-	High porosity (ϕ>0.27) shales

3.3.6 Brittleness and Brittleness Index

Brittleness has no a unique expression, and historically, brittleness has been defined in several ways by many scholars from various disciplines. In ***Figure 3.8***, expressions of most commonly used brittleness types are summarized by Jin et al. (**2014**). Brittleness can be described as the ability of a rock to resist permanent deformation reflecting material failure under the effect of applied external forces.

Formula	Variable Declaration	Test Method	Reference
$B_1 = (H_m - H)/K$	H and H_m are macro- and microhardness; K is bulk modulus.	Hardness test	Honda and Sanada (1956)
$B_2 = q\sigma_c$	q is percent of debris (<0.6 mm diameter); σ_c is compressive strength.	Proto impact test	Protodyakonov (1962)
$B_3 = \varepsilon_{ux} \times 100\%$	ε_{ux} is unrecoverable axial strain.	Stress/strain test	Andreev (1995)
$B_4 = (\varepsilon_p - \varepsilon_r)/\varepsilon_p$	ε_p is peak of strain; ε_r is residual strain.		Hajiabdolmajid and Kaiser (2003)
$B_5 = \tau_p - \tau_r/\tau_p$	τ_p and τ_r are peak and residual of shear strengths.		Bishop (1967)
$B_6 = \varepsilon_r/\varepsilon_t$	ε_r and ε_t are recoverable and total strains.		Hucka and Das (1974)
$B_7 = W_r/W_t$	W_r and W_t are recoverable and total strain energies.		
$B_8 = \sigma_c/\sigma_t$	σ_c and σ_t are compressive and tensile strength.	Uniaxial compressive strength and Brazilian test	Hucka and Das (1974)
$B_9 = (\sigma_c - \sigma_t)/(\sigma_t + \sigma_c)$			Altindag (2003)
$B_{10} = (\sigma_c\sigma_t)/2$			
$B_{11} = (\sigma_c\sigma_t)^{0.5}/2$			
$B_{12} = H/K_{IC}$	H is hardness; K_{IC} is fracture toughness.	Hardness and fracture-toughness test	Lawn and Marshall (1979)
$B_{13} = c/d$	c is crack length, d is indent size for Vickers indents at a specified load; empirically related to H/K_{IC}.	Indentation test	Sehgal et al. (1995)
$B_{14} = P_{inc}/P_{dec}$	P_{inc} and P_{dec} are average increment and decrement of forces.		Copur et al. (2003)
$B_{15} = F_{max}/P$	F_{max} is the maximum applied force on the specimen; P is the corresponding penetration.		Yagiz (2009)
$B_{16} = H \times E/K_{IC}^2$	H is hardness, E is Young's modulus, and K_{IC} is fracture toughness.	Hardness, stress/strain, and fracture-toughness test	Quinn and Quinn (1997)
$B_{17} = 45° + \varphi/2$	φ is the internal-friction angle.	Mohr circle or logging data	Hucka and Das (1974)
$B_{18} = \mathrm{Sin}\varphi$			
$B_{19} = (E_n + v_n)/2$	E_n and v_n are normalized dynamic Young's modulus and dynamic Poisson's ratio	Density and sonic-logging data	Modified from Rickman et al. (2008)
$B_{20} = (W_{qtz})/W_{Tot}$	W_{qtz} is the weight of quartz; W_{Tot} is total mineral weight.	Mineralogical logging or XRD in the laboratory	Jarvie et al. (2007)
$B_{21} = (W_{qtz} + W_{dol})/W_{Tot}$	W_{qtz} and W_{dol} are weights of quartz and dolomite; W_{Tot} is total mineral weight.		Wang and Gale (2009)
$B_{22} = (W_{QFM} + W_{Carb})/W_{Tot}$	W_{QFM} is the weight of quartz, feldspar, and mica; W_{Carb} is the weight of carbonate minerals consisting of dolomite, calcite, and other carbonate components. W_{Tot} is total mineral weight.		Jin et al. (2014)

Figure 3.8 Selected Expressions of Brittleness (Jin et al., 2014).

As shown in ***Figure 3.9***, ductile rocks can hold permanent deformation (plastic strain) for a long period of time without losing the ability to resist load. On the contrary, brittle rocks have much shorter plastic deformation, and their ability to resist load decreases with plastic strain. Therefore, brittle shales are more likely to be naturally fractured, tending to response to hydraulic fracturing (HF) positively. Accordingly, a brittleness index (BI) can be used to differentiate brittle shales from ductile shales in unconventional reservoirs. Brittleness has been regarded for many years as the only criterion for whether shale reservoirs are easy to be effectively fractured. However, it is not certain that brittle formations can be easily fractured compared to ductile formations, since brittle formations may have greater strength than ductile formation, and brittle zones may behave as fracture barrier. From this fact, the rock fracability term was introduced to correct the shortcomings of rock brittleness (**Bai, 2016; Jin et al., 2014; Salah et al., 2019**).

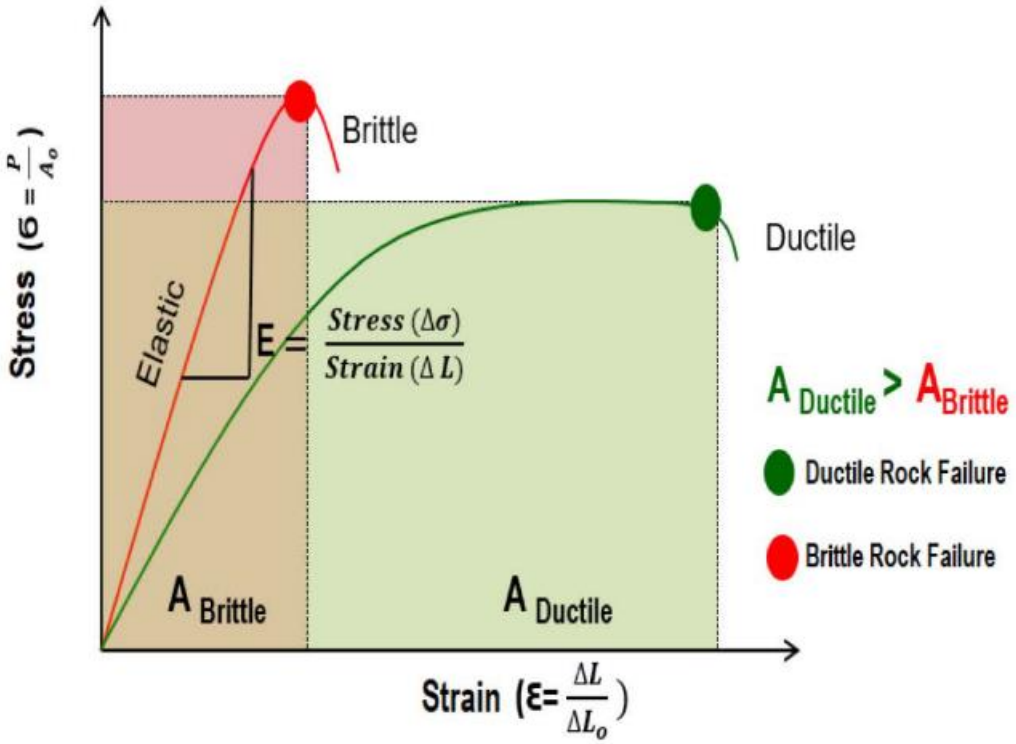

Figure 3.9 The brittle and ductile behavior of material from stress vs. strain plot (Salah et al., 2019)

The BI is calculated predominantly from the mineralogic method or the mechanical method. From a mineralogical aspect, as the amount of non-brittle minerals (clay minerals) decreases and the amount of brittle minerals (quartz minerals and carbonates) increases in a rock, the rock tends to show brittle behavior. From a mechanical aspect, generally shales with high Young's modulus (YM, E) and low Poisson's ratio (PR, ν) tend to be brittle. On the other hand, according to Yuan et al. (**2017**) and Yasin et al. (**2018**), brittleness is more related to the mechanical characteristic of a rock rather than the mineralogical characteristic of a rock. Thus, it is more reasonable to utilize mechanical brittleness in fracability evaluation. YM and PR are two mechanical parameters that shape the tendency of shale brittleness. Yet, YM and PR should be normalized because they are not in the same unit.

Normalization for the positive factor and the negative factor, respectively:

$$\boldsymbol{P_{norm}} = \frac{\boldsymbol{X - X_{min}}}{\boldsymbol{X_{max} - X_{min}}}, \text{ and } \boldsymbol{P_{norm}} = \frac{\boldsymbol{X_{max} - X}}{\boldsymbol{X_{max} - X_{min}}} \quad \textbf{(3.25, 3.26)}$$

P_{norm} is the normalized value of a parameter; X is the value of the parameter; X_{max} is the maximum value of the parameter, X_{min} is the minimum value of the parameter.

Rickman et al. (**2008**) proposed the mechanical BI as a function of Young's modulus and Poisson's ratio as follows:

$$\boldsymbol{BI_{mech} = 0.5E_N + 0.5\nu_N} \quad \textbf{(3.27)}$$

$$\boldsymbol{E_N = \frac{E - E_{min}}{E_{max} - E_{min}}} \quad \textbf{(3.28)}$$

$$\boldsymbol{\nu_N = \frac{\nu_{max} - \nu}{\nu_{max} - \nu_{min}}} \quad \textbf{(3.29)}$$

where BI_{mech}: Normalized mechanical brittleness index (dimensionless); E_N : Normalized Young's modulus (dimensionless); ν_N : Normalized Poisson's ratio (dimensionless); E: Young's modulus (GPa or psi); ν: Poisson's ratio (dimensionless); E_{max} and E_{min}: Maximum and minimum Young's modulus of a formation (GPa or psi); ν_{max} and ν_{min}: Maximum and minimum Poisson's ration of formation (dimensionless).

3.3.7 Fracture Toughness

Rock failure can be estimated by the generation (or initiation) and propagation of fractures inside the rock. This requires knowledge about the stress around fracture tips and the energetic conditions that lead to the generation and propagation of fractures. Fractures are assumed to be planar structures, which grow by the generation of new surfaces at their tips (**Salah et al., 2019**). In fracture mechanics literature, the initiation and propagation modes of fractures are classified into three distinct groups (***Figure 3.10***); opening or tensile mode (Mode-I), sliding-shear or in-plane shear mode (Mode-II), and tearing-shear or anti-plane shear mode (Mode-III). Tensile fractures occur when the displacements are perpendicular to the fracture plane, sliding-shear fractures occurs when the displacements are parallel to the fracture plane and perpendicular to the fracture front, and tearing-shear fractures occur when the displacements are both parallel to the fracture plane and the fracture front (**Anderson, 2005; Salah et al., 2019**).

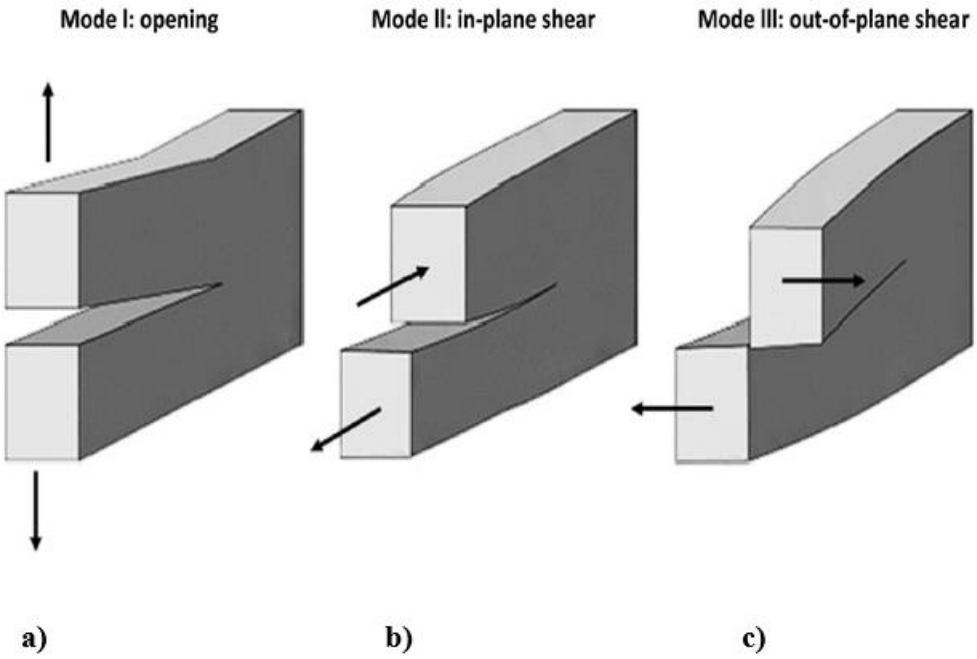

Figure 3.10 Modes of fracture initiation and propagation. a) Opening (Mode-I), b) Sliding-shear (Mode-II), c) Tearing-shear (mode-III) (Guo et al., 2017).

Based on Irwin's fracture mechanics theory (**1957**), the stress and deformation field around the tip of a crack can be expressed by the stress intensity factor. Stress intensity factor is the grade of stress concentration at the tip of a crack, and it is given by

$$\boldsymbol{K_k = \sigma_A \sqrt{\pi \, x \, a}} \quad \textbf{(3.30)}$$

where K_k: Stress intensity factor (MPa x $m^{1/2}$), σ_A: Given load (MPa); a: Crack length (m). The subscript k in K_k stands for the fracture mode.

The critical value of the stress intensity factor initiating the crack (or fracture) generation is called fracture toughness. In other words, fracture toughness is the consumption rate of fracture energy required to create new crack surfaces. Fracture toughness is a basic rock property used to explain the ability of the rock to resist hydraulic fracturing and propagation of pre-existing cracks (**Salah et al., 2019**). During hydraulic fracturing (HF), the fracture can be generated only when the net pressure (the difference between the fluid pressure and the closure pressure) overcomes the fracture toughness. As depicted schematically in ***Figure 3.11***, the fracture will grow when the positive net pressure (the fluid pressure > the closure pressure) is created that exceeds the fracture toughness $K_I^{(+)}$. In case of the negative net pressure (the fluid pressure < the closure stress) and toughness $K_I^{(-)}$ resulting from the fluid lag in the fracture tip area, the fracture will shrink (**Bai, 2016**).

The fracture growth modes in HF operations are mostly Mode-I, Mode-II, or a combination of Mode-I and Mode-II (mixed mode). In contrast, Mode-III fractures are rarely encountered, so they could be neglected in geo-mechanical evaluations (**Yuan et al., 2017**). The Mode-I fracture toughness (K_{Ic}) quantifies the ability of a rock to withstand crack initiation and propagation due to tensile stress (**Bai, 2016**). To this end, the lower Mode-I fracture toughness (K_{Ic}) would generate longer and extensile hydraulic fractures, which, in turn, would lead to a larger stimulated reservoir volume (SRV) (**He et al., 2019**). The Mode-II fracture toughness (K_{IIc}), on the other hand, represents the ability of a rock to resist shear fracture growth (**Yuan et al., 2017**). Accordingly, the smaller Mode-II fracture toughness (K_{IIc})

values would result in more shear interactions between hydraulic fractures (hFs) and natural fractures (nFs), which, in turn, would lead to more efficient SRV with improved fracture conductivity (**He et al., 2019**). Besides, fracture toughness can also be presented by its normalized version in the fracability evaluation. In this case, normalized fracture toughness is positively correlated with fracability index as opposed to direct fracture toughness (**Huang et al., 2021; Jin et al., 2014**). Normalization process for fracture toughness is carried out over the negative-factor normalization equation below:

$$\boldsymbol{K_{C_N}} = \frac{\boldsymbol{K_{C,max} - Kc}}{\boldsymbol{K_{C,max} - K_{C,min}}} \quad \textbf{(3.31)}$$

K_{C_N} is the normalized value of fracture toughness; K_C is the value of fracture toughness; $K_{C,max}$ is the maximum value of fracture toughness, $K_{C,min}$ is the minimum value of fracture toughness.

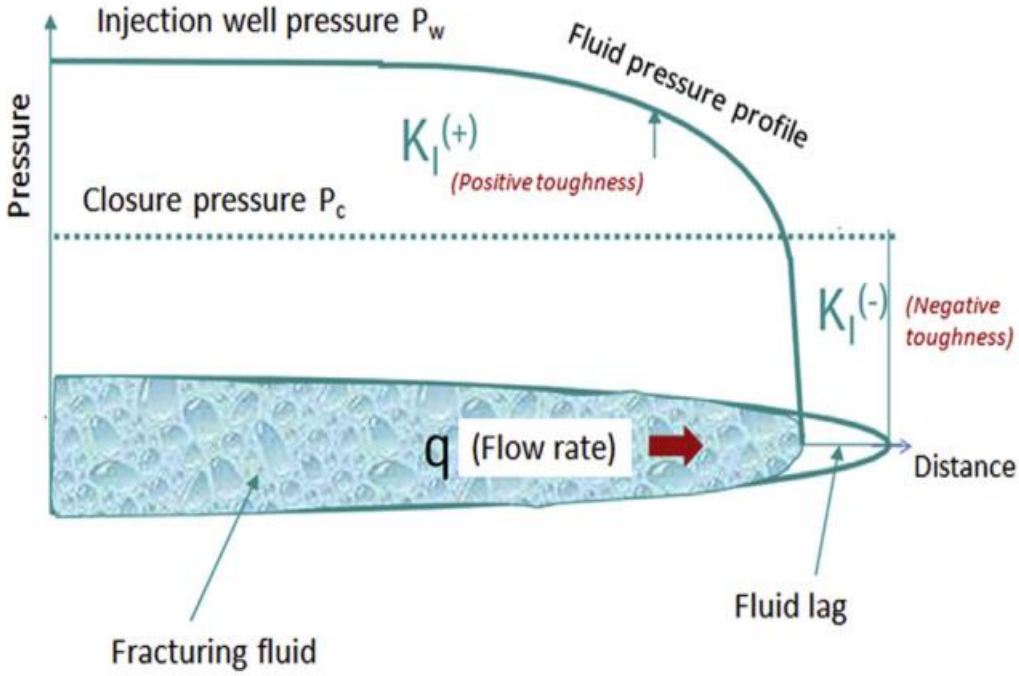

Figure 3.11. The schematic representation of hydraulic fracture (HF) propagation based on net pressure. The hydraulic fracture grows when the net pressure (i.e. Pn = Pf - Pc) is positive. The fracture shrinks in the region where the net pressure is negative. The resistance to fracture growth is fracture toughness (Bai, 2016).

Although the most accurate way to estimate the fracture toughness is laboratory tests, due to the technical and economic infeasibility of core sampling from unconventional reservoirs and performing corresponding mechanical experiments on them, scholars alternatively developed empirical correlations between fracture toughness and other reservoir properties of rock (**Yuan et al., 2017**).

For unconventional reservoirs, fracture toughness can be obtained by prediction models listed in ***Table 3.2***. In Chen et al.'s model and Yuan et al.'s model, K_{IC} and K_{IIC} can be directly predicted as immediate functions of the conventional well-logging data, without the need of calculating mechanical parameters of rocks (as in Jin et al.'s model). These two methods, therefore, can effectively eliminate the errors that may occur in the intermediate processes while calculating the mechanical properties with logging data (**Yuan et al., 2017**).

Table 3.2 Fracture Toughness Prediction Models for Unconventional Reservoirs.

Prediction Model	**Units**	**Lithology**	**Reference**
$K_{IC} = 0.0059T_O^3 + 0.00923T_O^2 + 0.517T_O - 0.3322$	T_O (MPa)	Tight Sandstone	(Jin et al., 2001)
$K_{IIC} = 0.1744T_O - 0.2381$	T_O (MPa)		(Jin et al., 2011)
$K_{IC} = 0.317\rho + \frac{0.0457}{Vsh} + 0.213\ln(DT) - 0.504$	ρ (g/cm^3) DT (μs/m) Vsh (%)	Shale Oil Shale Gas	(Chen et al., 2015)
$K_{IIC} = 2.133\rho + \frac{0.0768}{Vsh} + 1.189\ln(DT) - 9.181$			
$K_{IC} = 0.450\rho - 0.151e^{Vsh} + 0.201\ln(DT) - 0.877$	ρ (g/cm^3) DT (μs/ft) Vsh	Shale Oil Shale Gas	(Yuan et al., 2017)
$K_{IIC} = 2.119\rho - 0.245e^{Vsh} + 1.152\ln(DT) - 8.378$			

From all reasons above, Yuan et al.'s (**2017**) correlation was applied to evaluate fracture toughnesses of Dadaş-I shale.

$$\boldsymbol{K_{IC} = 0.450\rho - 0.151e^{Vsh} + 0.201\ln(DT) - 0.877} \quad \text{.....(3.32)}$$

$$\boldsymbol{K_{IIC} = 2.119\rho - 0.245e^{Vsh} + 1.152\ln(DT) - 8.378} \quad \text{.....(3.33)}$$

$$\boldsymbol{V_{sh} = \frac{2^{GCUR\ x\ I_{SH}} - 1}{2^{GCUR} - 1}} \quad \text{.....(3.34)}$$

$$\boldsymbol{I_{SH} = \frac{GR - GR_{min}}{GR_{max} - GR_{min}}} \quad \text{.....(3.35)}$$

where K_{IC} *and* K_{IIC} : Mode-I and Mode-II fracture toughnesses (MPa x $m^{1/2}$), respectively; ρ: Density of shale (g/cm^3); V_{SH}: Shale content of the rock (dimensionless); DT: Acoustic travel time (µs/ft); GR: Observed gamma ray (API); GR_{min} and GR_{max}: Gamma-ray of clean sand and clean shale (API), respectively; I_{SH}: Shale-content index of the rock (dimensionless); GCUR: Dimensionless Hilchie index (**Hilchie, 1982**), which is related to geological age of the formation (3.7 for Mesozoic and Cenozoic formations, and 2 for Paleozoic formations).

Since Dadaş shale belongs to the Silurian-Devonian period (**EIA, 2015**), which is a part of the Paleozoic era within the geologic time-scale (**The Geological Society of America, 2022**), GCUR can be taken as 2 for Dadaş Formation. Thus, the shale content equation fundamentally corresponds to Larionov's empirical correlation (**Bassiouni, 1994**) for older rocks (***Figure 3.12***).

$$\boldsymbol{V_{sh} = 0.33(2^{2\ x\ I_{SH}} - 1)} \quad \text{.....(3.36)}$$

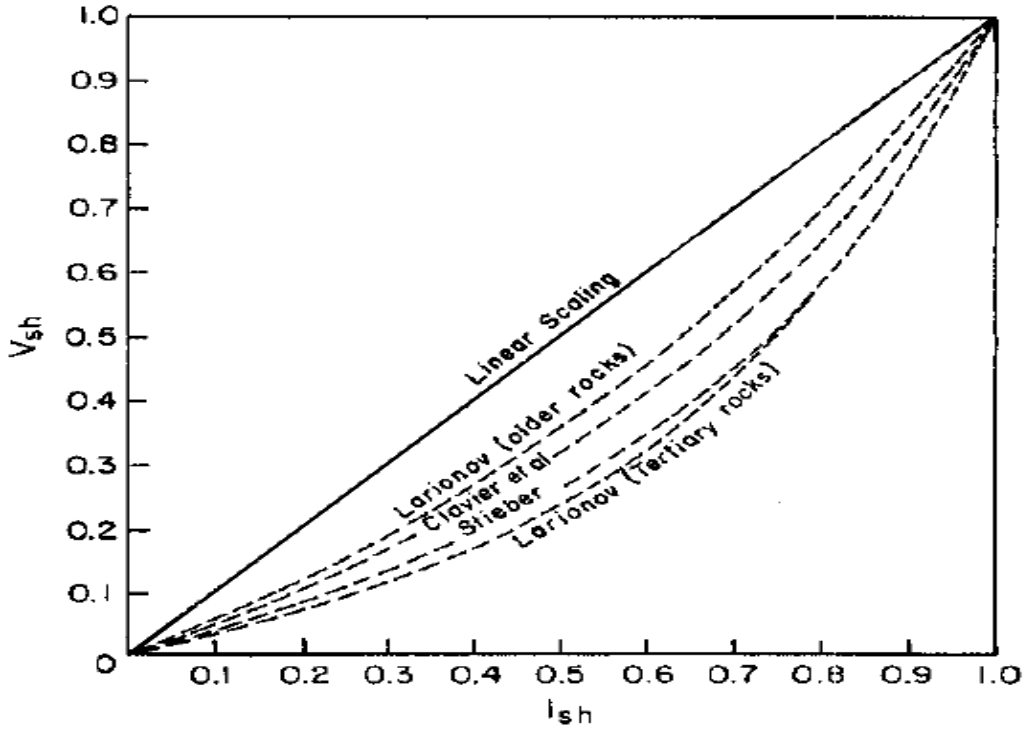

Figure 3.12. Empirical correlations relating shale content, Vsh, to gamma ray shale index, Ish (Bassiouni, 1994).

CHAPTER 4

LITERATURE REVIEW FOR FRACABILITY AND FRACABILITY INDEX

The production potential of shale reservoirs is determined by geochemical and petrophysical factors, whereas the primary and sustained productivity of shale reservoirs is strongly dependent on geomechanical properties. Fracability, the fundamental geomechanical property of an unconventional reservoir rock, is first defined by Chong et al. (**2010**) as the capability of reservoirs to be efficiently stimulated by hydraulic fracturing (HF) operation and creating a system of complex fracture networks. Accordingly, the fracability index (FI) term has emerged as a theoretical benchmark to calculate the easiness of rocks to be fractured. Since the FI strongly affects the identification of ideal reservoir zones, i.e., the sweet spots, and ultimate oil and gas recovery rate, the evaluation of geomechanical parameters plays a crucial role in characterizing HF performance in unconventional reservoirs.

One of the most critical parameters used to assess the fracability of rock is brittleness. Brittleness is utilized by numerous researchers in various scientific fields for different purposes; thus, it has no universally accepted definition or a particular measurement method (**Altindag, 2010**). Generally, brittleness refers to the property of a material that either fails with no plastic deformation or low plastic deformation under the action of external forces (**Huang et al., 2021**). From the geomechanical perspective, brittleness is the point at which the elastic strain controlling the deformation of rock exceeds the strength of the rock, which leads the rock to rupture (**Salah et al., 2019**). Jin et al. (**2014**) compiled a wide range of methods for measuring brittleness in rock mechanics quantitatively. Among all methods by researchers, the mineralogical brittleness index (BI_{min}), which is determined by the proportion of brittle mineral components in a rock, and the mechanical brittleness index (BI_{mech}), which is calculated by elastic rock properties, such as Young's

modulus (E) and Poisson's ratio (ν), are the two most commonly applied methods for brittleness evaluation.

On the other hand, the formation brittleness was confused with the fracability for many years, which resulted in evaluating the fracability of rocks and determining the potential sweet spots only based on the brittleness index (BI). In this context, many researchers have proposed that a formation with only high BI shows a tendency to be fractured easily (**Alzahabi et al., 2015; Dargahi & Rezaee, 2013; Fernandez Rojas et al., 2016; Grieser & Bray, 2007; Jahandideh & Jafarpour, 2014; Jarvie et al., 2007; Lu et al., 2021; Mews et al., 2019; Rickman et al., 2008; Sondergeld et al., 2010; Wang & Gale, 2009**).

Chong et al. (**2010**) summarized a considerable amount of stimulation success achieved in the United States (U.S.)' leading shale reservoirs from the 1990s to 2010s, where the efficiency of HF operations has been discussed based on the single-factor BI approach. However, Enderlin et al. (**2011**), Bruner & Smosna (**2011**), and Bai (**2016**) realized that some formations having high brittleness indexes (BIs) could not be easily fractured, and even they may act as a fracture barrier (**Jin et al., 2014**). To illustrate, Jin et al. (**2014**), Lili Sui et al. (**2015**), and Haoyue Sui et al. (**2019**) pointed out that higher energy is required to create fractures in the Barnett dolomite formation in comparison to Barnett shale, as the fractures cannot be initiated in dolomite by applying the fracturing pressure ranges applied in shale formations.

The analyses of field experiences in the U.S. and Colombia, performed by Yuan et al. (**2017**) and Ardila et al. (**2019**), indicated that the selection of sweet spots only based on high BI was in contradiction with the results of stimulation efficiency and production performance. Yuan et al. (**2017**) asserted that although Barnett-2 Shale has a much larger BI than Haynesville-1 Shale (***Figure 4.1***), in many cases, Haynesville-1 Shale has shown better stimulation efficiency compared to Barnett-2 Shale.

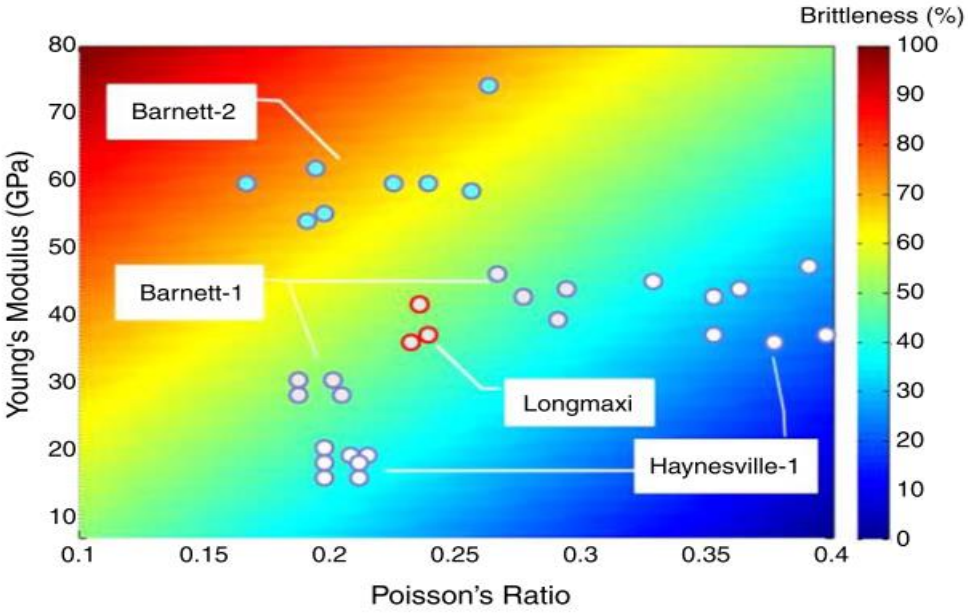

Figure 4.1. Brittleness Indexes of Some Representative Gas Shales. (Yuan et al., 2017)

Similarly, Ardila et al. (**2019**) presented the fallacy of using BI alone to select the best area for fracturing. The area of the polygon selected by using the BI alone (***Figure 4.2a***) is turned out to be undesirable when the minimum horizontal stress (σ_h) is included in the fracability evaluation (***Figure 4.2b***).

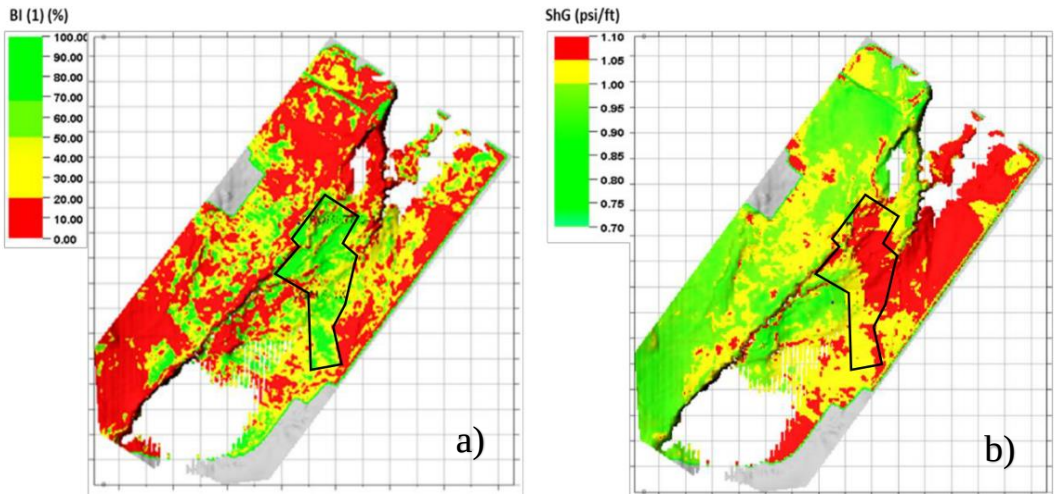

Figure 4.2. a) Brittleness Index Map Obtained from Elastic Properties b) Minimum Horizontal Stress Map for Calcite-rich Shale Formation. (Ardila et al., 2019)

Similarly, Wang et al. (**2015**), Bai (**2016**), and Iyare et al. (**2022**) put forward that brittleness is not equivalent to fracability and the BI alone is insufficient to accurately and comprehensively detect the sweet spots of shale reservoirs. All these studies show that current brittleness indices based on elasticity or mineralogy could not explain the strength and failure mechanism of the rock properly in many cases **(Ardila et al., 2019; Huang et al., 2021; Salah et al., 2019**).

Within this context, it is inferred that the conventional BI technique failed to select the optimum formation sections in well-stimulation treatments, which, in turn, indicates that fracability is a multivariable problem. To this end, although the BI may be adopted as one of the primary factors to designate the optimal formation intervals to be fractured, this parameter alone remains insufficient to characterize the exact fracturing mechanism of shale reservoirs. In light of all these clarifications, a significant amount of research has been performed to establish a more realistic correlation between the fracability and the other vital parameters in the HF process. To better describe the fracability, researchers have considered mainly the effects of fracture toughness (K_{IC}, KI_{IC}), minimum horizontal stress (σ_h), differential horizontal stress (DHS, $\Delta\sigma$), natural fracture (nF) density, interactions between natural fractures (nFs) and hydraulic fractures (hFs), and rock strength parameters such as unconfined compressive strength (UCS), cohesion (C_O), and internal friction angle (φ).

Based on theoretical analyses, laboratory experiments, field-scale HF operations, and numerical modeling research, fracture toughness is indicated to be as one of the key parameters in the assessment of FI. The ***'fracture toughness'*** term was first derived from the research conducted on metals and ceramics in material science (**Govindarajan et al., 2017**), which has been adopted as a property of an unconventional rock by researchers in the field of HF. A rock will be fractured when the stress intensity factor (K_k), which is a fracture mechanics element used to estimate the stress state around a crack tip, exceeds its critical value (**Salah et al., 2019**). This critical value of the stress intensity factor is called fracture toughness, defined as rock resistance to the initiation and/or propagation of hFs and the extension of existing nFs (**Huang et al., 2021; Salah et al., 2019**).

In a sense, formation toughness represents the consumption rate of fracture energy required to create new surfaces and complex networks (Salah et al., 2019). It follows that an efficient HF treatment requires a lower stress energy release rate, which, in turn, means that smaller fracture toughness values lead to smaller breakdown pressure values (**Bai, 2016; Jin et al., 2014**), corresponding to a higher FI (**Iyare et al., 2022**). Therefore, candidate intervals, i.e., the sweet spots, should have a lower fracture toughness (or higher normalized fracture toughness) and a relatively higher BI while selecting sweet spots.

The research using the BI and fracture toughness as key factors in the evaluation of fracability have gained prominence and drawn attention in recent years. To illustrate, Yuan et al. (**2013**), Jin et al. (**2014**), and Salah et al. (**2019**) implemented BI and fracture toughness in their fracability models developed for tight sandstone and shale reservoirs. Yuan et al. (**2013**) and Salah et al. (**2019**) used the mechanical brittleness index to calculate the fracability. On the other hand, the fracability equations proposed by Jin et al. (**2014**) and Salah et al. (**2019**) included the Mode-I fracture toughness (K_{IC}) but neglecting the Mode-II fracture toughness (K_{IIC}).

Over the years, the importance of the minimum horizontal stress (σ_h) for the degree of fracability has been studied in detail by many researchers. The minimum horizontal stress (σ_h) at relatively lower levels, which indicates smaller confining pressure and fracture closure pressure, is a conducive factor to the initiation and propagation of fractures (**Dou et al., 2022; Huang et al., 2021; Iyare et al., 2022; Yuan et al., 2017**). This leads to relatively wider and conductive fractures (***Figure 4.3***) as well as to higher stimulated reservoir volume (SRV) values, particularly after the proppant placement in the induced fracture network.

Yuan et al. (**2017**) developed a FI equation by taking the minimum horizontal stress (σ_h) in addition to the mechanical brittleness index (BI_{mech}) and Type-I & Type-II fracture toughness (K_{Ic}, K_{IIc}) into account, which was then verified by the actual results of field-scale HF operation. Moreover, the study proposed a way to estimate

the fracture toughness specific to shale reservoirs directly from the well-log data rather than using conventional estimations using the mechanical properties of rocks.

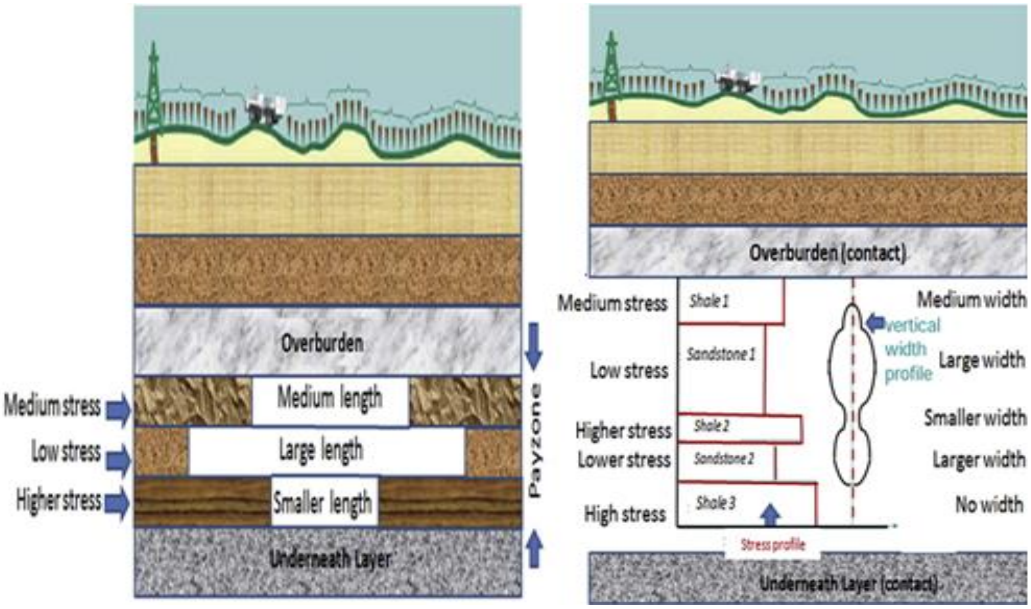

a) b)

Figure 4.3. The schematics showing (a) smaller fracture length (L) and width (w) due to higher min. horizontal stress (σ_h)*, (b) greater fracture length (L) and width (w) due to lower min. horizontal stress* (σ_h) *from a hydraulic fracturing stimulation (Bai, 2016)*

Similar to the study of Yuan et al. (**2017**), Yasin et al. (**2018**) built a fracability model for shale formations mainly based on brittleness index (BI), fracture toughness (K_{Ic}, K_{IIc}), and minimum horizontal stress (σ_h). In contrast to other studies, Yasin et al. (**2018**) assigned a mineralogy-based brittleness model by asserting that mechanical brittleness negatively correlates with the rock's total organic carbon (TOC) content. Ardila et al. (**2019**) highlighted the role of minimum horizontal stress (σ_h) for unconventional reservoirs in an effective HF, and exemplified the importance of minimum horizontal stress (σ_h) in fracability evaluation. The study results indicated that the intervals suggested by fracability indexes (FIs) without considering the effects of minimum horizontal stress (σ_h), which sometimes acts as a fracture barrier, might lead to erroneous interpretations.

By taking Yuan et al.'s study (**2017**) as a reference, Iyare et al. (**2022**) set a fracability assessment model using mechanics-based brittleness for a shale formation in Trinidad, which enabled to compare the fracability model using the mineral-based brittleness. The fracability model that implemented the mechanical brittleness, suggested generally lower FI values than those suggested by the fracability model including the mineralogical brittleness. In parallel with these fracability results, BI values obtained from the mechanical approach are generally noticed to be less than the BI values obtained from the mineralogical approach.

Zhang et al. (**2015**) incorporated the ratio of shear stress (τ) to the normal stress (σ_N) of natural fractures in fracability evaluation besides rock mechanical brittleness (BI_{mech}), mode-I fracture toughness (K_{IC}), and minimum horizontal stress (σ_h). The fracability model represents the shear deformation ability of natural fractures and lays emphasis more on the effects of in-situ stress.

Recently, Dou et al. (**2022**) brought an innovative approach to fracability literature by proposing a more inclusive equation including differential horizontal stress difference (DHS, $\Delta\sigma$) in addition to mechanical brittleness index (BI_{mech}), type-I fracture toughness (K_{IC}), and minimum horizontal stress (σ_h). In this study, the minimum horizontal stress (σ_h) was used to determine the conductivity and the size of SRV, which is also affected by type-I fracture toughness (K_{IC}); brittleness index (BI) and horizontal stress anisotropy were used to quantify the complexity of the induced fracture networks. This model has matched true enough with the production history of studied wells in tight sandstone reservoirs and can be integrated to enlighten fracability evaluation for other unconventional reservoirs.

Zhang et al. (**2022**) built a fracability model on mechanical brittleness index (BI_{mech}), fracture toughnesses (K_{Ic}, K_{IIc}), and differential horizontal stress coefficient (including differential horizontal stress ($\Delta\sigma$) and minimum horizontal stress (σ_h)). More importantly, the result of the study showed that the change in the FI may be closely related to the change in the water saturation rate.

From another aspect, Guo et al. (**2015**) combined the BI and mode-I fracture toughness (K_{IC}) with internal friction angle (φ) to express the complexity of the fracture network system in terms of shear strength. The results of the study suggested that brittleness is affected by the mechanical properties and the mineralogy of rock. In this context, researchers proposed an innovative idea about the BI, which brought both mechanical brittleness and mineralogical brittleness into the same fracability equation. However, the equation had the deficiency of reflecting the actual mechanism of fracture toughness due to the non-inclusion of Mode-II toughness (K_{IIC}).

Similarly, Haoyue Sui et al. (**2019**) researched to generate more complex fracture networks and emphasized the importance of rock quality designation. Accordingly, the research proposed a new fracability estimation method, which integrates the brittleness index (BI) and fracture toughnesses (K_{IC}, K_{IIC}) with the structural properties of rock, such as bedding orientation, the existence of joints and weak planes, fracture zones, and cavities.

Huang et al. (**2019**) proposed a mathematical fracability model using the analytical hierarchy process (AHP), which incorporates the brittleness index (BI), fracture toughnesses (K_{IC}, K_{IIC}), the presence of natural fractures (nFs), and the rock matrix cohesion (C_O) using certain weighting factors assigned to each parameter.

CHAPTER 5

STATEMENT OF PROBLEM

A significant amount of research has been conducted to correlate the hydraulic fracture (HF) performance in shale formations mainly by using the brittleness index (BI), which, in turn, is mostly derived either from mineralogical properties, mainly the amounts (wt. %) of clay, carbonate, and silica minerals in shale, or from rock mechanical parameters such as Young's Modulus (E) and Poisson ratio (ν). However, recent studies have indicated that there is not always a direct relationship between the BI and fracability of formation, and there might even be a reverse effect of BI on fracability. To illustrate, the main problem regarding Turkey's promising shale formations (e.g., Dadaş shale) is stated to be the higher clay percentage (>40%) (***Table 7.5***) as obtained by X-ray diffraction (XRD) mineralogical analysis, so the lower BI. However, when the mineralogical contents of some of the most productive shale formations in North America are analyzed comparatively by using the ternary diagram (***Figure 7.8***), the results propose similar ranges of brittleness indexes (BIs) with Dadaş shale, whereas the well-proven performance of HF in North American shales is observed to be high.

Similarly, Dadaş shale is found to show unattractive elastic properties (relatively lower Young's modulus and higher Poisson's ratio) in terms of mechanical brittleness index (***Table 7.6***). However, it can be observed from ***Figure 7.9***, some of the most productive shale formations in North America (having high HF performance) present a close mechanical tendency with Dadaş shale. To explain more specifically, Dadaş shale shows similarities at a reasonable level with Marcellus shale (the most productive shale gas formation in the world, ***Figure 7.10***) in terms of mineralogy and mechanical elasticity.

All these findings, indeed, imply that using a single parameter (brittleness index, BI) to define the overall fracability of formation would be misleading; thus, a more complex and multivariable parameter (fracability index, FI) is required. To this end, a field-scale study that considers the selection of ideal reservoir zones in HF operations from a different angle was applied for the better development of Turkey's domestic shale oil and gas resources.

CHAPTER 6

RESEARCH METHODOLOGY

As a starting point, the composite well-log data (gamma-ray log, density log, and compressional sonic log) of the Caliktepe-2 well as presented in ***Figure 2.21***, was manually digitized point by point using Neuralog software to form a dataset related to Dadaş shale. Next, a set of critical geomechanical parameters was estimated by fundamental equations and/or empirical correlations, which were previously explained in **Chapter 3.3**. To this end, the pore pressure gradient was estimated as an intermediate parameter from Eaton's method to calculate desired geomechanical properties. Besides, WSM was utilized to detect the active faulting regime around the Diyarbakir region and to determine the orientation of maximum horizontal stress. Additionally, fracture toughness (type-I & type-II) prediction models for unconventional reservoirs were compiled. In addition to all these, a bundle of geomechanics-based graphs related to fracability components was plotted to be canalized into the process of building the one-dimensional mechanical earth model (MEM) for Dadaş shale.

Apart from these efforts, the mineralogical and mechanical elasticity tendencies of the United States' (U.S.) major shale formations were reviewed. In this respect, it was reached that Dadaş shale has a tendency close enough to Marcellus shale, and Marcellus was taken as a reference for further studies.

In light of the works mentioned above, the fracability of Dadaş-I member was calculated by implementing four fracability index (FI) models (Rickman et al.'s model, Yuan et al.'s model, Dou et al.'s model, and a newly Proposed model in this study) deterministically and stochastically. Then, to validate the high hydraulic fracturing performance of Marcellus shale by studying fracability index models, the fracability of this formation was calculated deterministically as well. From this point, deterministic FI results of Marcellus shale were compared with those obtained from

Dadaş shale. Moreover, the FIs of Dadaş Shale and of some major productive shale formations in the U.S. (Marcellus, Barnett, Haynesville, Bakken, and Eagle Ford) were estimated by Proposed model, and then FI results was examined according to changing BI values.

Besides all these, a new mathematical fracability model modified from Dou et al.'s equation is proposed to identify favorable spots that may increase the hydraulic fracturing efficiency in Dadaş shale. The new model investigates the effects of differential horizontal stress (DHS, $\Delta\sigma$) and the type-II fracture toughness (K_{IIC}) in the fracability evaluation of shale reservoirs, which especially reside in strike-slip faulting environments. In this new model, mode-I and mode-II fracture toughness (K_{IC} & K_{IIC}) are assumed to equally impact fracability index as in Yuan et al.'s study.

Reasons for this assumption

- the limited data on the studied formation,
- high uncertainty of fracture modes due to heterogeneous structure of shale formations,
- no general opinion about the coefficients of fracture toughness in the fracability literature.

CHAPTER 7

RESULTS & DISCUSSIONS FOR DADAŞ SHALE CASE STUDY

In this study, the fracability of Dadaş shale is discussed within the scope of composite well-log data obtained from Çalıktepe-2 well (**Kara & Isik, 2021**) (***Figure 2.21***). To this end, firstly, gamma-ray log, density log, and compressional sonic log were elaborately digitized through Neuralog software as shown in , ***Figure 7.2***, and ***Figure 7.3,*** respectively. For the digitalization operation, the majority of logs are processed with a quality higher than 90%, and in most cases 95% (***Figure 7.4***). Then, necessary geomechanical parameters (listed in ***Table 7.1***) were obtained from digitized well-log data using the fundamental empirical correlations presented in ***Table 7.1***. Subsequently, four fracability models listed in ***Table 7.2*** were implemented deterministically (for L2, L3, and L4 zones) and stochastically (for only L2 zone) to estimate the fracability index (FI) of Dadaş-I (presented in ***Figure 2.21***) as a function of mechanical brittleness index (BI_{mech}), fracture toughness (K_{IC} & K_{IIC}), minimum horizontal stress gradient (σ_h^G), and differential horizontal stress (DHS, $\Delta\sigma$). The FI of L1 zone in Dadaş-I member was not evaluated in this study since that zone has very low net pay thickness and porosity, and its permeability and cumulative oil-in-place (OIP) potential is almost zero. Finally, profiles of fracability components (***Figure 7.5***, ***Figure 7.6,*** and ***Figure 7.7***) regarding Dadaş-I member were represented by geomechanical logs.

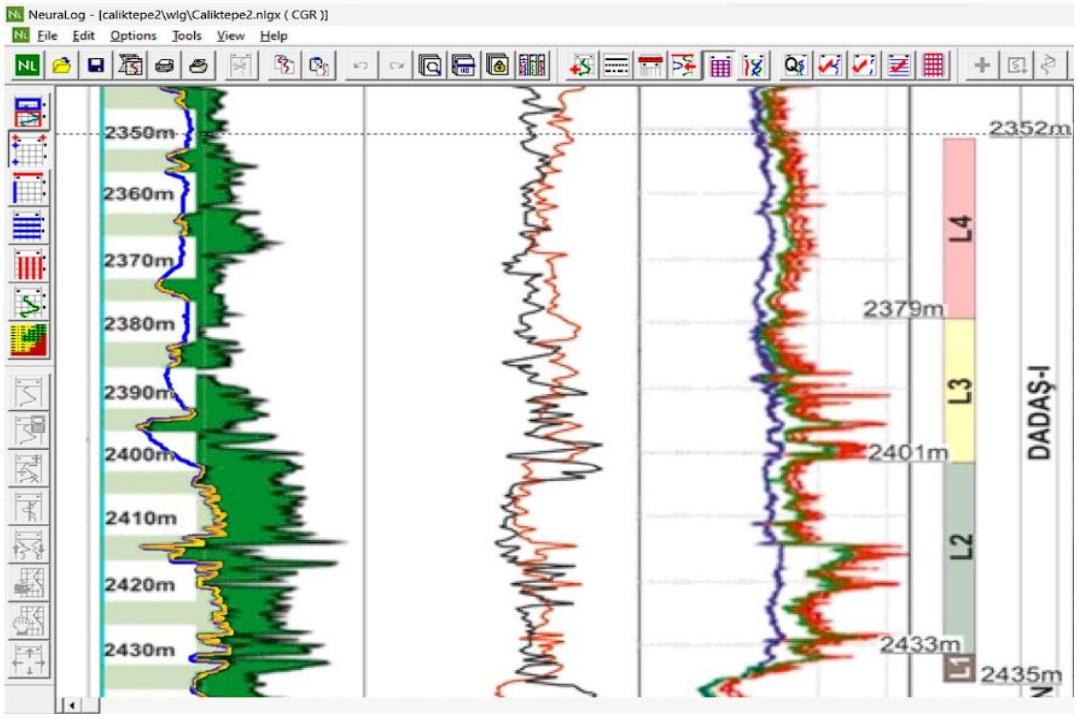

Figure 7.1 The digitalization of gamma-ray log from reference (Kara & Isik, 2021).

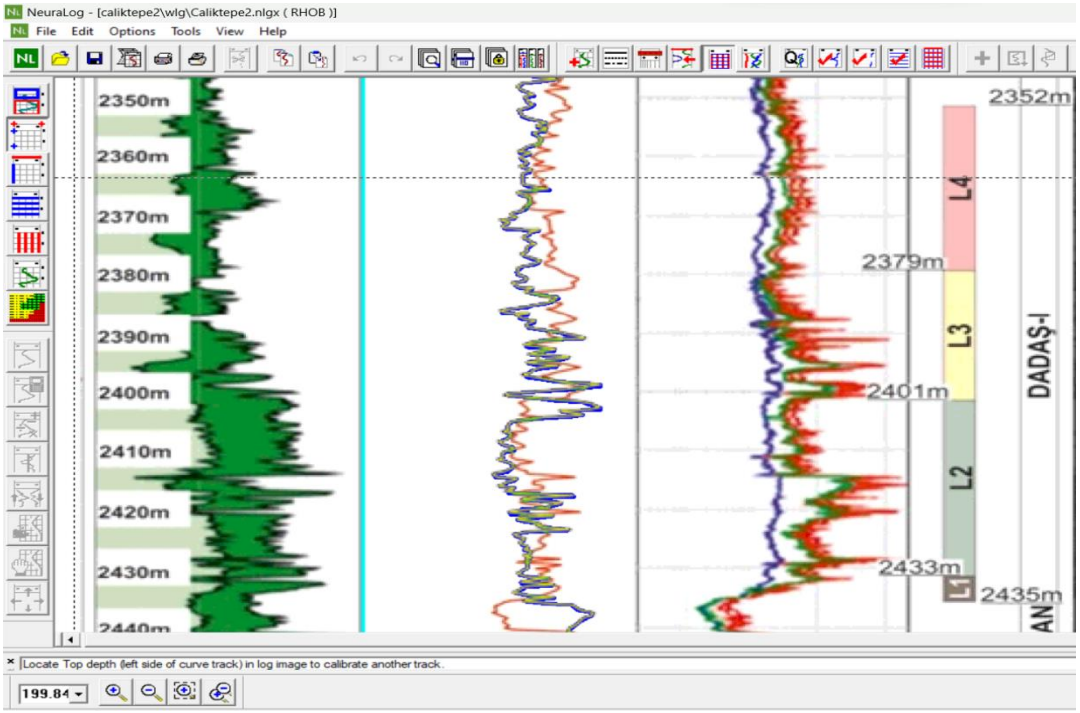

Figure 7.2 The digitalization of density log from reference (Kara & Isik, 2021).

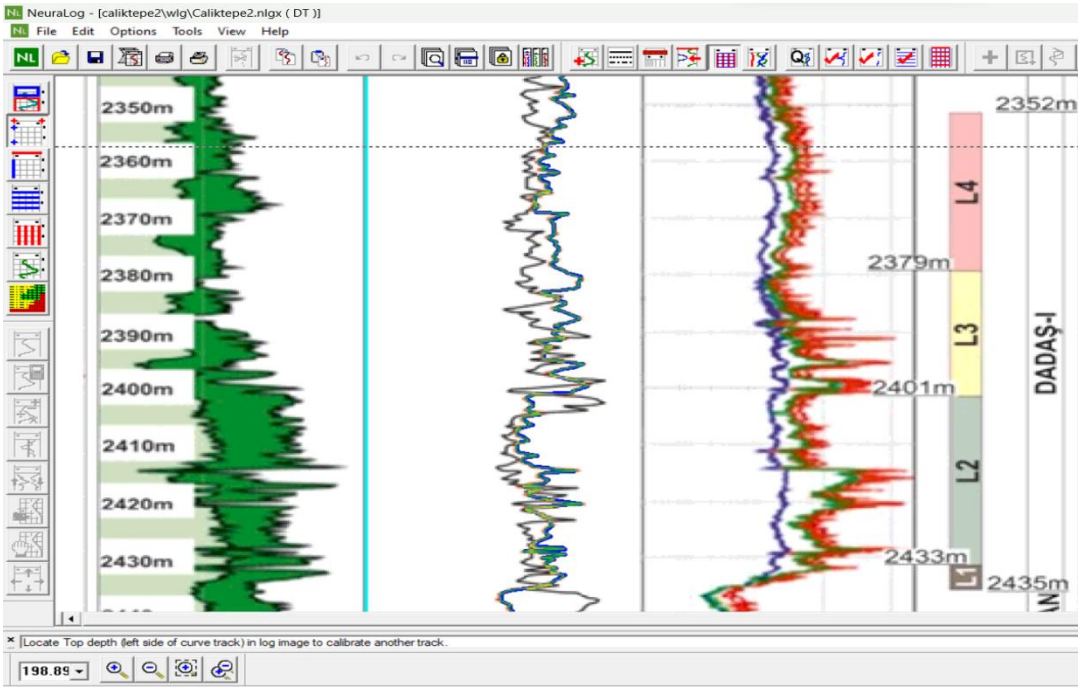

Figure 7.3 The digitalization of sonic log from reference (Kara & Isik, 2021).

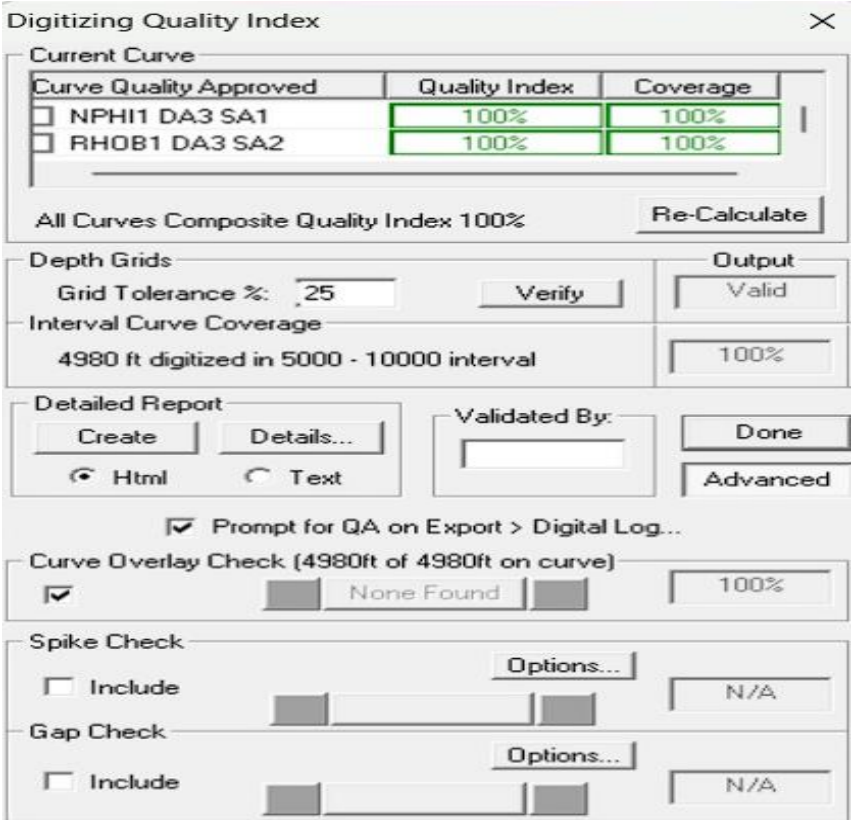

Figure 7.4 An example of digitizing quality index for the digitalization part.

Table 7.1 The list of geomechanical parameters used in the fracability evaluation.

Estimated Parameter	Equation/Correlation	Reference
Poisson's Ratio	$\nu = \frac{(V_P^2 - 2V_S^2)}{2(V_P^2 - V_S^2)}$	(Fjær et al., 2008)
Young's Modulus	$E = \frac{\rho V_S^2 (3V_P^2 - 4V_S^2)}{(V_P^2 - V_S^2)}$	
Static Young's Modulus	$E_S = 0{,}076 * V_P^{3{,}23}$	(Horsrud, 2001)
Biot's Constant	$\alpha = 0.64 + 0.854\, x\, \phi$	(Belyadi et al., 2017)
Pore Pressure Gradient	$P_{P,gr} = \sigma_{V,gr} - (\sigma_{V,gr} - P_{hyd,gr}) \left({}^{\Delta t_n}/_{\Delta t} \right)^3$	(Eaton, 1975)
Vertical Stress	$\sigma_V = \bar{\rho}\, H/144$	(Zoback, 2007a)
Max. Horizontal Stress	$\sigma_H = \frac{\nu}{1-\nu}(\sigma_V - \alpha P_P) + \alpha P_P + \frac{E_S}{1-\nu^2}(\epsilon_H + \nu\epsilon_h)$	(Higgins-Borchardt et al., 2016)
Min. Horizontal Stress	$\sigma_h = \frac{\nu}{1-\nu}(\sigma_V - \alpha P_P) + \alpha P_P + \frac{E_S}{1-\nu^2}(\epsilon_h + \nu\epsilon_H)$	
DHS Index	$\Delta\sigma_{Index} = 1 - ({}^{\Delta\sigma}/_{\Delta\sigma_{max}})$	(Dou et al., 2022)
Mechanical Brittleness Index	$BI = 0.5E_N + 0.5\nu_N$	(Rickman et al., 2008)
Mode-I Fracture Toughness	$K_{IC} = 0.450\rho - 0.151e^{Vsh} + 0.201\ln(DT) - 0.877$	(Yuan et al., 2017)
Mode-II Fracture Toughness	$K_{IIC} = 2.119\rho - 0.245e^{Vsh} + 1.152\ln(DT) - 8.378$	

Table 7.2 Selected fracability models for this study.

Fracability Model	Fracability Equation	FI Unit
Rickman et al.	$FI = BI_{mech} = 0.5E_N + 0.5\nu_N$	Unitless
Yuan et al.	$FI = \frac{BI}{0.5\ x\ K_{IC} + 0.5\ x\ K_{IIC}}\ x\ \frac{1}{\sigma_h^G}$	$MPa^{-2}.\ m^{0.5}$
Dou et al.	$FI = (0.33BI + 0.33K_{IC_N} + 0.34\Delta\sigma_{Index})/\ \sigma_h^G$	$MPa^{-1}.\ m$
Proposed Model	$FI = (0.33BI + 0.33[0.5K_{IC_N} + 0.5K_{IIC_N}] + 0.34\Delta\sigma_{Index})/\ \sigma_h^G$	$MPa^{-1}.\ m$

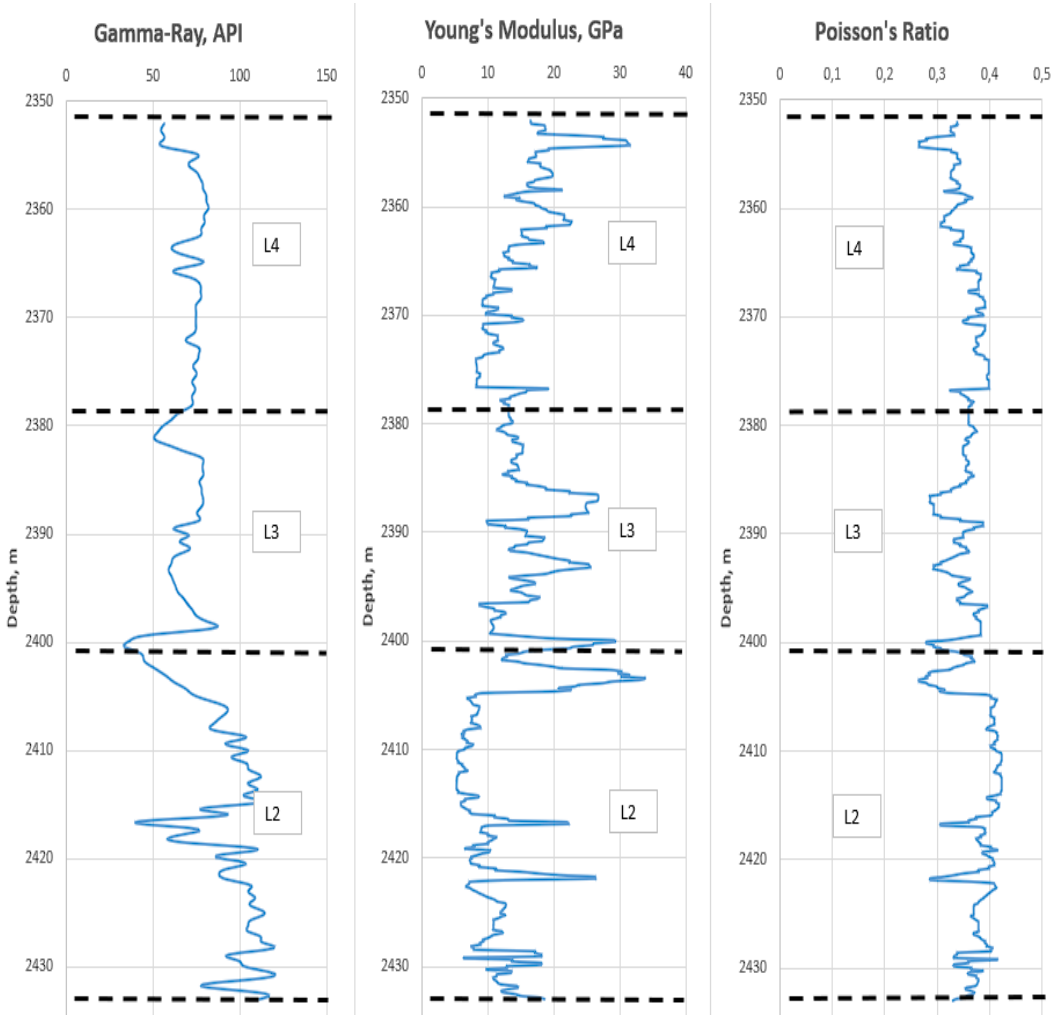

Figure 7.5 Profiles of Young's modulus and Poisson's ratio with respect to the profile of Gamma-ray log regarding Dadaş-I member.

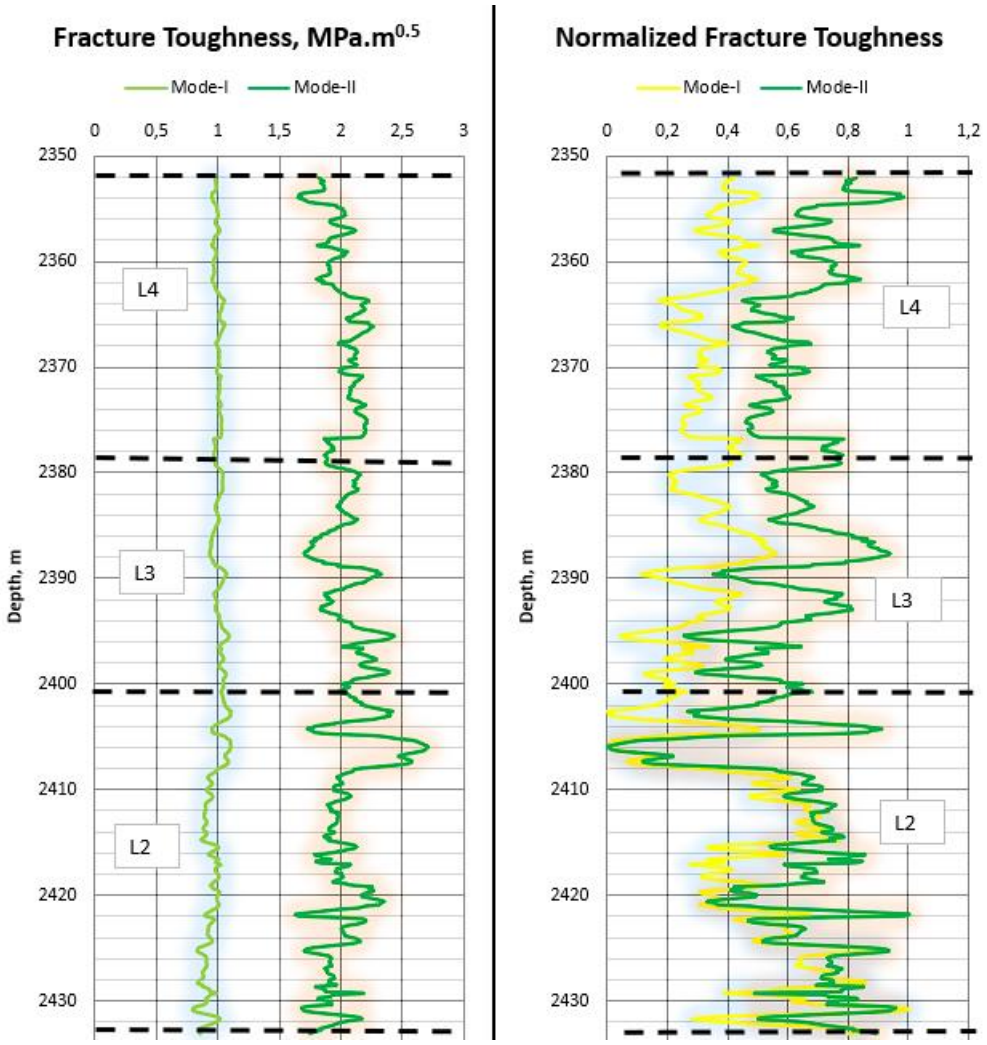

Figure 7.6 Profiles of fracture toughness and normalized fracture toughness regarding Dadaş-I member.

Rickman et al.'s conventional fracability model (**2008**) creates the infrastructure of the other three fracability models. Yuan et al.'s model (**2017**) presents a fracability equation including BI_{mech}, K_{IC} & K_{IIC}, and σ_h^G but neglecting Δσ. On the other hand, Dou et al.'s (**2022**) suggests a developed model by integrating the DHS (Δσ) into fracability model but the technique lacks the mode-II fracture toughness (K_{IIC}). It is an undeniable fact that DHS (Δσ) affects the structure of complex fracture networks and the size of stimulated reservoir volume (SRV) (**Dou et al., 2022; Lihong et al., 2019**), whereas the K_{IIC} is related to shear fracture growth and fracture conductivity (**He et al., 2019; Yuan et al., 2017**).

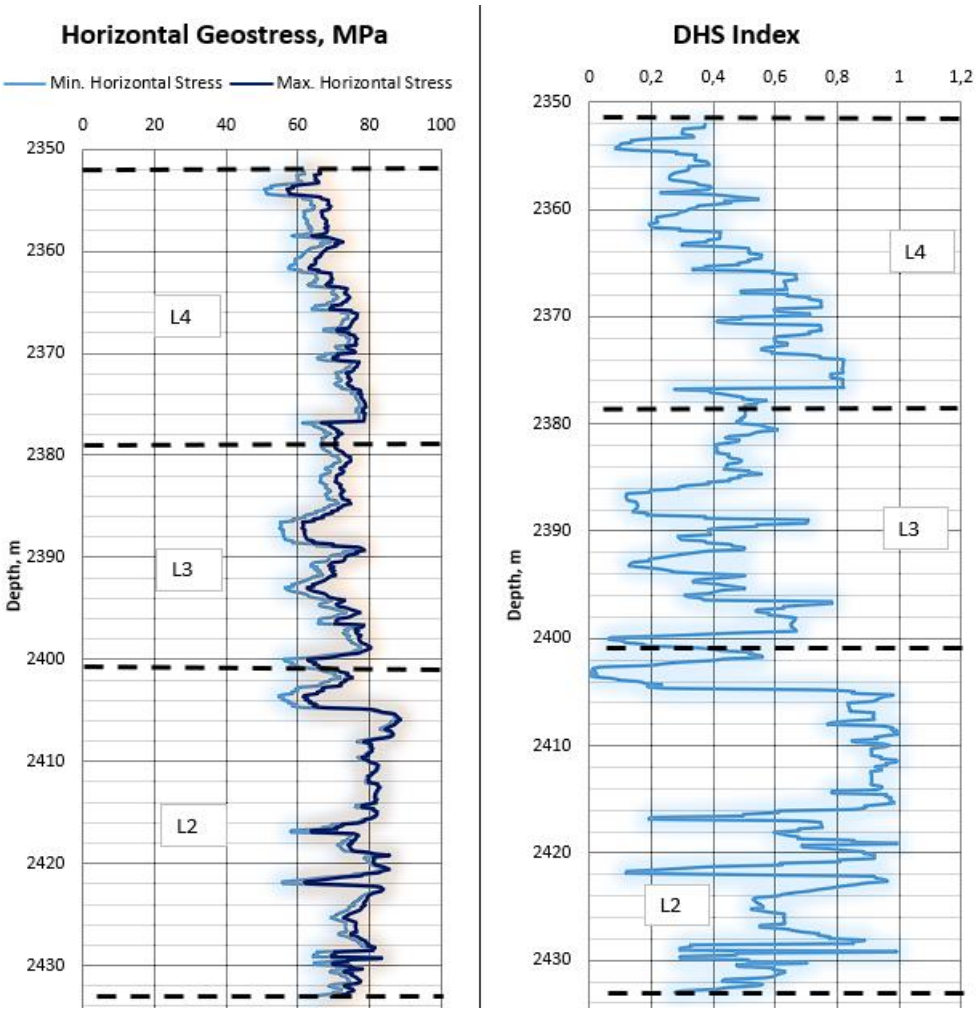

Figure 7.7 Profiles of horizontal geostresses and differential horizontal stress regarding Dadaş-I member.

Moreover, strike-slip (SS) faulting (notably) and reverse faulting (RF) (considerably) regimes are generally observed around Diyarbakir region according to the WSM data (**Merey et al., 2021**) and the study of Inan & Kavak (**2019**). In light of all the facts mentioned above, a new fracability model that integrates both K_{IIc} and $\Delta\sigma$ into the same fracability equation has been proposed mainly taking the study of Dou et al. (**2022**) as a reference. In this new model, mode-I and mode-II fracture toughness (K_{IC}, K_{IIC}) are assumed to have equal impacts on fracability as in Yuan et al.'s study (**2017**). Reasons for this assumption can be sorted as: the limited data on the studied formation, high uncertainty of fracture modes, no general opinion about the coefficients of fracture toughness in the fracability literature.

Before explaining ranges of fracability index models, it is worth noting that while fracture toughness is directly expressed in Yuan et al.'s model, but it is expressed with its normalized version in Dou et al.'s and newly Proposed models.

For the fracability evaluation, in Rickman et al.'s model, fracability index (FI) values vary between 0 and 1 (from the lowest to highest), yet there is no recommended range option for FI. On the other hand, Yuan et al.'s model presents a relative comparison among candidate zones without defining boundaries for FI instead of using specific ranges describing fracable and non-fracable spots. Unlike these two models, in Dou et al.'s model, candidate reservoir zones have been classified based on three distinct FI ranges as follows:

(1) Type-I: FI $\geqslant$ 0.3 MPa^{-1}. m. For this type, there is a high probability of obtaining a complex fracture network, a greater SRV, and high fracture conductivity. The fracability is ranked as high. Zones corresponding to this range are regarded as ideal spots for hydraulic fracturing (HF).

(2) Type-II: 0.22 MPa^{-1}. m $\leqslant$ FI < 0.3 MPa^{-1}. m. For this type, there is an intermediate probability of obtaining a complex fracture network and a greater SRV. The fracability is ranked as intermediate. The HF may be recommended for this type of zone, but not strongly supported.

(3) Type-III: FI < 0.22 MPa^{-1}. m. For this type, it is difficult to obtain a complex fracture network and a greater SRV. To this end, the fracability is ranked as low. This type of reservoir zone tends to behave as a fracture barrier and the HF is not advised in these zones.

As for the newly Proposed model, the aforementioned FI ranges in Dou et al.'s model was taken as a basis for fracability evaluation.

7.1 Deterministic Method

The deterministic method is a computation tool that creates a single output from particular inputs expressed by a single representative value. This method enables to users to obtain a specific answer by following a simple and certain way not including randomness or uncertainty. According to above-mentioned principles, geomechanical parameters were averaged over the zones to express the fracability in terms of a discrete, constant value of input constituents.

Table 7.3 shows the representative values of geomechanical properties used to evaluate the fracability index (FI) deterministically. Inserting averaged input parameters in ***Table 7.3*** into correlations in ***Table 7.1*** produced constant-valued fracability indexes (FIs) listed in ***Table 7.4***.

Table 7.3 The averaged input data of Dadaş-I for deterministic fracability evaluation.

Input Parameters	**Zones**		
	L4	**L3**	**L2**
Poisson's Ratio, ν	0.35	0.34	0.38
Young's Modulus, E (GPa)	14.55	16.37	11.17
Static Young's Modulus, E_S (GPa)	2.80	3.10	2.19
Biot's Constant, α	0.69	0.7	0.7
Pore Pressure Gradient, $P_{P,grad}$ (psi/ft)	0.871	0.871	0.871
Vertical Stress, σ_V (MPa)	59.14	60.36	60.76
Maximum Horizontal Stress, σ_H (MPa)	71.09	70.98	77.28
Minimum Horizontal Stress, σ_h (MPa)	67.38	66.63	75.04
Differential Horizontal Stress Index, $\Delta\sigma_{Index}$	0.49	0.40	0.68
Mechanical Brittleness Index, BI_{mech}	0.38	0.44	0.24
Mode-I Fracture Toughness (MPa x $m^{0.5}$)	1.00	1.01	0.95
Mode-II Fracture Toughness (MPa x $m^{0.5}$)	2.02	2.05	2.04

Table 7.4 Deterministic fracability index results of all zones in Dadaş-I for studied models.

Zones	Fracability Index			
	Rickman et al.	**Yuan et al.**	**Dou et al.**	**Proposed Model**
L4	0.377	0.404	0.611	0.683
L3	0.443	0.468	0.586	0.663
L2	0.237	0.241	0.629	0.660

For each reservoir zone, FI results were obtained in descending order as the Proposed model, Dou et al.'s model, Yuan et al.'s model, and Rickman et al.'s model. According to Rickman et al.'s and Yuan et al.'s model, L3 (in first place) and L4 (in second place) zones are found to be much better targets for HF operation compared to L2 zone. Interestingly, the FI values obtained from the conventional model (depends on normalized Young's modulus [YM] (E_N) and normalized Poisson's ratio [PR] (ν_N)) are found to be significantly close to the FI values obtained from Yuan et al.'s model (depends on normalized YM (E_N) and normalized PR (ν_N), mode-I & mode-II fracture toughnesses (K_{IC}, K_{IIC}), and minimum horizontal stress (σ_h)). In particular, the results obtained for the L2 zone from both approaches are found to be almost equal. This equality situation seems questionable because of the fact that all additional parameters included (K_{IC}, K_{IIC}, and σ_h) are theoretically inversely proportional to fracability and no directly proportional parameter to fracability exists against these inverse parameters in Yuan et al.'s model.

On the other hand, Dou et al.'s model and the Proposed model suggest that all studied zones are observed highly-fracable. Additionally, the FI results obtained from Dou et al.'s model and those obtained from the Proposed model are obviously higher than those offered by two other models. Accordingly, this may reflect that the differential horizontal stress ($\Delta\sigma$) has a strong effect on the fracability of Dadaş shale. Besides, it was observed that the results suggested by the Proposed model are highly close to the results obtained from Dou et al.'s model. This may suggest that mode-II fracture toughness (K_{IIC}) plays a small role in FI evaluation for Dadaş shale. The low effect

of K_{IIC} on FI may be attributed to the fact that the initiation and propagation of fractures are more related to tensile fractures rather than shear fractures.

Although Dadaş Shale mostly contains undesirable clay percentage (higher than >40%) according to various studies (***Table 7.5***), the mineralogical content of Dadaş has considerable similarity with some of the most productive shale formations in the U.S. (***Figure 7.8***), which show high HF performance.

Table 7.5 The mineralogical distribution of Dadaş Shale from various sources.

Data Source	Clay (%)	Quartz (%)	Carbonate (%)
(Ercengiz et al., 2014)	38	35	27
(Kara & Isik, 2021)	40	24	33
(Şen et al., 2021)	50	27	23
(Akkoca & Işık, 2018)	63	18	19
(Ozturk et al., 2016)	70	28	2

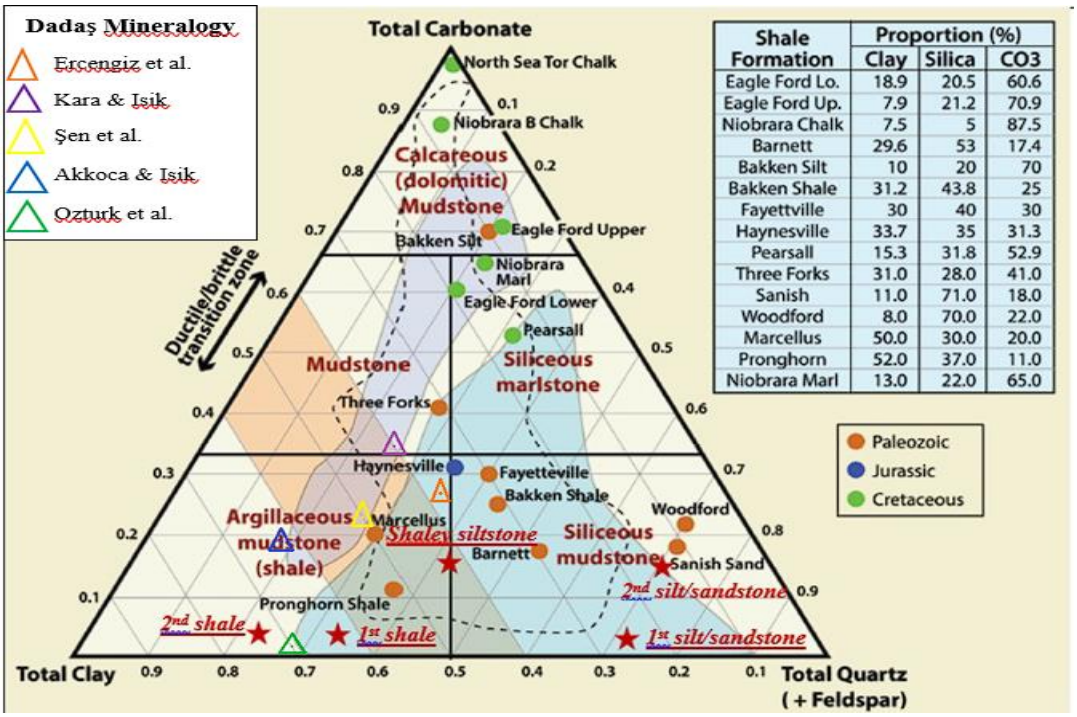

Shale Formation	Proportion (%)		
	Clay	Silica	CO3
Eagle Ford Lo.	18.9	20.5	60.6
Eagle Ford Up.	7.9	21.2	70.9
Niobrara Chalk	7.5	5	87.5
Barnett	29.6	53	17.4
Bakken Silt	10	20	70
Bakken Shale	31.2	43.8	25
Fayettville	30	40	30
Haynesville	33.7	35	31.3
Pearsall	15.3	31.8	52.9
Three Forks	31.0	28.0	41.0
Sanish	11.0	71.0	18.0
Woodford	8.0	70.0	22.0
Marcellus	50.0	30.0	20.0
Pronghorn	52.0	37.0	11.0
Niobrara Marl	13.0	22.0	65.0

Figure 7.8 A ternary diagram shows the comparison of Dadaş shale mineralogy (indicated by triangles) with some major North American "shale" plays (indicated by circles) and one European-origin Derbyshire shale (indicated by red stars) (Modified after Yildirim, 2019).

In a similar vein, the mechanical elasticity structure of Dadaş Shale possesses significantly lower Young's modulus and relatively higher Poisson's ratio (***Table 7.6***). On the other hand, as can be seen in ***Figure 7.9***, it was observed that Dadaş Shale reflects a parallel mechanical trend with some of the most productive shale formations in North America (having high HF performance). To explain more specifically, the mineralogical structure and the mechanical elasticity of Dadaş shale appear similar at a reasonable level with those of Marcellus shale (currently the most productive shale gas formation in the world, ***Figure 7.10***). Based on these findings, Marcellus Shale was taken as a reference to compare with Dadaş Shale, and the fracability of Marcellus Shale was examined in detail accordingly.

Table 7.6 Poisson's ratio and Young's modulus values of some of the most productive North American shales and Dadaş shale (Modified after Dobson & Houseworth, 2014).

** The mechanical elasticity properties of Dadaş were estimated from the average values of all Dadaş-I zones researched in this study.*

Shale Formations	Poisson's Ratio	Young's Modulus (GPa)
Barnett	0.26	34.51
Haynesville	0.29	25.09
New Albany	0.29	24.33
Antrim	0.34	15.71
Eagle Ford	0.26	33.78
Marcellus	0.30	22.28
Woodford	0.26	34.00
Monterey	0.22	54.66
Dadaş*	0.36	13.70

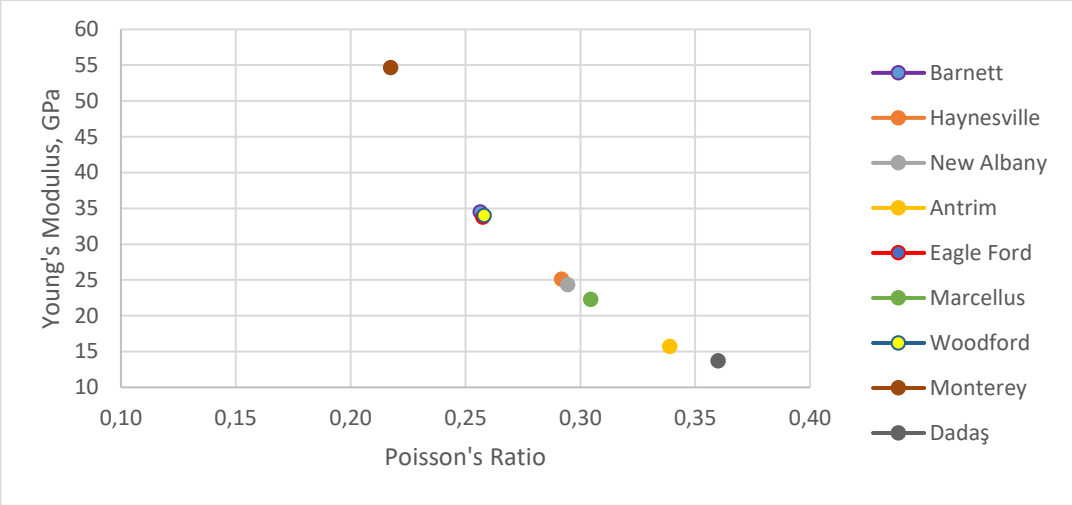

Figure 7.9 A graph showing the mechanical elasticity comparison between Dadaş shale and some major North American shales (Drawn by using the data of Dobson & Houseworth, 2014).

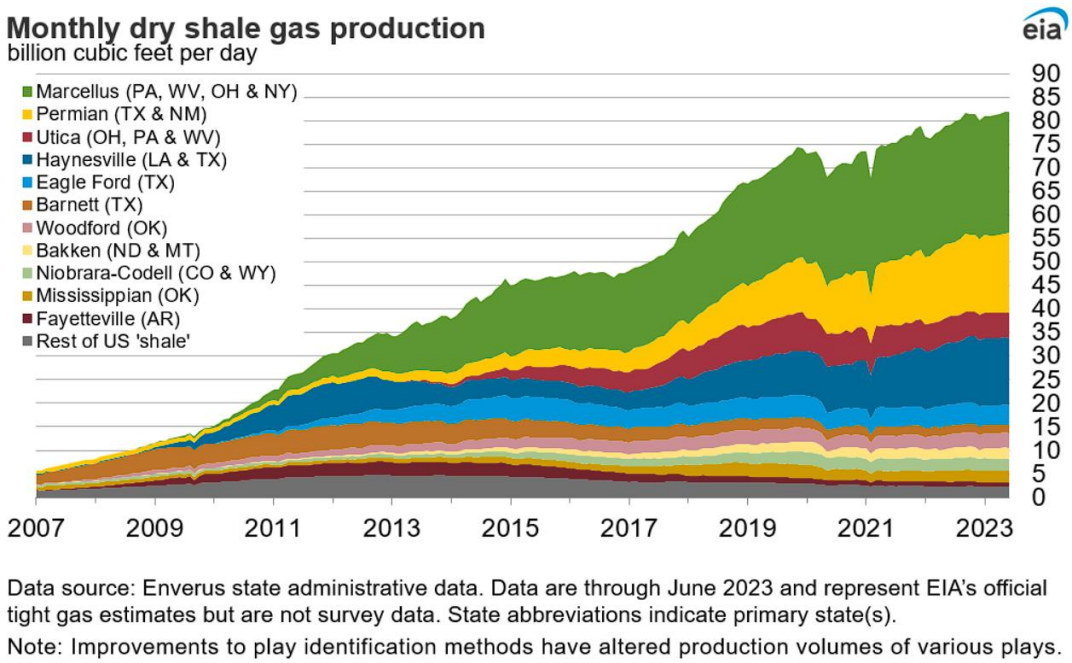

Figure 7.10 Dry Shale Gas Production of the U.S. Shale Formations from 2007 to 2023 (EIA, 2023c).

The geomechanical properties of Boggess-17H and MIP-3H wells (***Table 7.7***) drilled within the Marcellus shale were estimated by the same process applied to Dadaş shale. Expectedly, two wells in Marcellus showed equal or very similar geomechanical properties between each other. On the other hand, Marcellus shale presented considerable differences from the geomechanical aspect except for vertical stress and fracture toughness compared to Dadaş-I shale (***Table 7.7***).

Table 7.7 Averaged geomechanical input data of Dadaş-I (all zones) and Marcellus shales.

Input Parameters	**Dadaş-I (Caliktepe-2)**	**Marcellus (Boggess-17H)**	**Marcellus (MIP-3H)**
Poisson's Ratio, ν	0.36	0.25	0.25
Young's Modulus, E (GPa)	13.70	44.55	41.65
Static Young's Modulus, E_S (GPa)	2.64	10.01	9.02
Pore Pressure Gradient, $P_{P,grad}$ (psi/ft)	0.87	0.68	0.65
Vertical Stress, σ_V (MPa)	60.11	60.78	57.70
Maximum Horizontal Stress, σ_H (MPa)	73.52	53.44	50.42
Minimum Horizontal Stress, σ_h (MPa)	70.21	46.56	43.93
Differential Horizontal Stress Index, $\Delta\sigma_{Index}$	0.54	0.14	0.13
Mechanical Brittleness Index, BI_{mech}	0.34	0.59	0.56
Mode-I Fracture Toughness (MPa x $m^{0.5}$)	0.98	1.02	1.01
Mode-II Fracture Toughness (MPa x $m^{0.5}$)	2.04	1.92	1.90

The deterministic FI results **()** for Dadaş-I shale and Marcellus shale were obtained from geomechanical parameters listed in ***Table 7.7***. In all FI models, Marcellus wells indicated relatively high FI values in parallel with their effective and productive HF performances. From a comparative aspect, Marcellus shale has larger FI values than Dadaş-I shale in all studied models (especially in Rickman et al.'s model and Yuan et al.'s model). This can be explained by that Marcellus has a much more desirable geomechanical structure (***Table 7.7***) compared to Dadaş-I shale.

Table 7.8 Deterministic fracability index results of Dadaş-I shale (all zones) and Marcellus shale for all studied models.

Formations (Wells)	**Fracability Index**			
	Rickman et al.	**Yuan et al.**	**Dou et al.**	**Proposed Model**
Dadaş-I (Caliktepe-2)	0.340	0.356	0.611	0.669
Marcellus (Boggess-17H)	0.595	0.926	0.683	0.752
Marcellus (MIP-3H)	0,562	0.947	0.720	0.803

The fracability indexes (FIs) of some major shale formations in the U.S were calculated (***Table 7.9***) by the same process applied to Dadaş shale over newly Proposed model, and findings were shown with respect to mechanical brittleness index (BI_{mech}) in ***Figure 7.11***. The results showed that FI may not regularly increase as BI gets larger, which, means that there is not always positive correlation between FI and BI. It was also observed that all formations can be graded as highly fracable (> 0.3 MPa^{-1}. m) according to this model despite their relatively not much bigger BI values (between 0.3-0.6). This finding suggests that Dou et al.'s fracability model was verified by Proposed model when well-proven HF performances of productive shales in the U.S. are considered. Additionally, it can be inferred that Dadaş Shale may be hydraulically fractured in an effective manner.

Table 7.9 Fracability Index and mechanical brittleness index values of some of the most productive North American shales and Dadaş shale.

Note: The fracability index of Dadaş were calculated from the average values of all Dadaş-I zones examined in this study.

Shale Formation	Fracability Index	Mechanical Brittleness Index	Reference
Marcellus (Boggess 17-H)	0.75	0.59	(MSEEL, 2021)
Marcellus (MIP-3H)	0.80	0.56	(MSEEL, 2021)
Haynesville	0.49	0.30	(Saneifar et al., 2014)
Eagle Ford	1.05	0.56	(Mokhtari et al., 2016)
Bakken	0.97	0.43	(Parapuram et al., 2018)
Barnett	0.69	0.37	(Perez Altamar & Marfurt, 2014)
Dadaş-I	0.67	0.34	This study

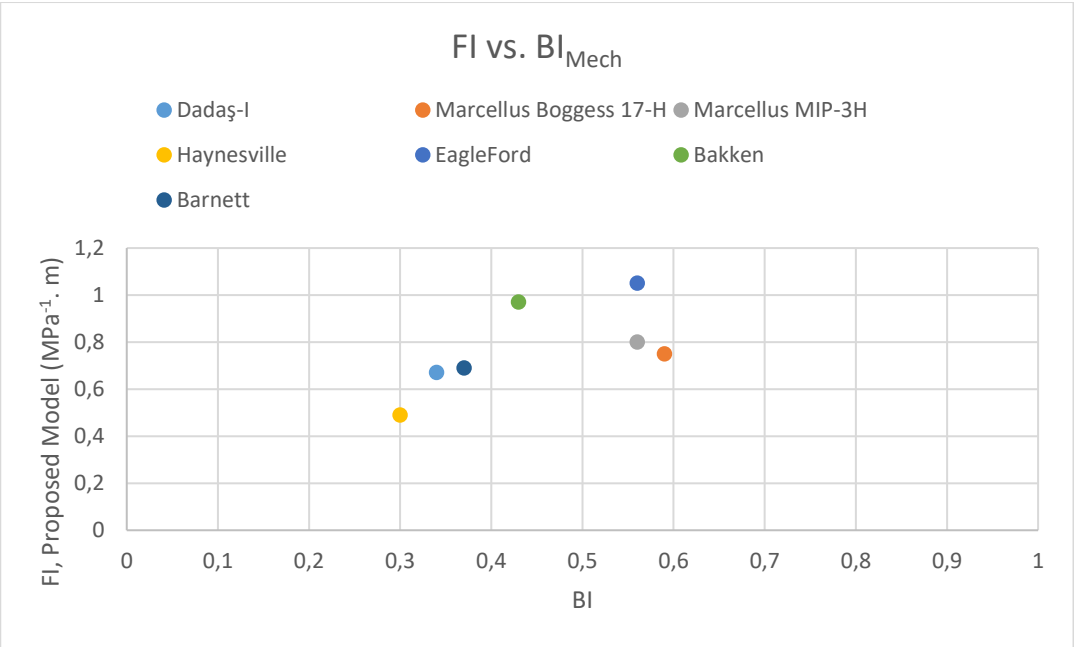

Figure 7.11 The comparison of FI and BImech for some shale formations in the U.S. and for Dadaş shale (all zones)(Drawn by using the data of references listed above).

7.2 Stochastic (Probabilistic) Method

The stochastic method is a mathematical process that estimates the probability of various outcomes from the random combination of uncertain inputs. In this method, a whole system is simulated through an iteration technique to derive a set of possible outcomes represented by their probability density functions.

The uncertainties that each mechanical input parameter has necessitated the utilization of a probabilistic model for a more reliable fracability evaluation process. To this end, after optimally fitting the input data to specific distributions using the @RISK software, probabilistic risk analysis has been performed by Monte Carlo simulation, which is one of the most widely used techniques in stochastic evaluation.

Best-fitted distribution type for each fracability component (***Table 7.10***) was selected among the distribution options automatically recommended by @RISK software.

Table 7.10 Distribution types of input parameters for each zone.

Input Parameters	**Dadaş-I Zones**		
	L4	**L3**	**L2**
Normalized YM	Pert	Pert	Exponential
Normalized PR	Triangular	Triangular	Exponential
Kıc (MPa x $m^{0.5}$)	Pert	Pert	Pert
Kııc (MPa x $m^{0.5}$)	Triangular	Triangular	Triangular
Normalized Kıc	Pert	Pert	Pert
Normalized Kııc	Pert	Pert	Pert
σ_h (MPa)	Triangular	Triangular	Triangular
DHS Index	Triangular	Triangular	Triangular

Whereas the normalized YM (E_N) and the normalized PR (ν_N) data in L2 zone are exponentially distributed, the optimum profiles in other zones followed the PERT distribution for the normalized Young's modulus (E_N), and the triangular distribution for the normalized Poisson's ratio (ν_N). The fracture toughness parameter in itself showed different distribution tendencies (for all zones; K_{Ic}: PERT distribution, and K_{IIc}: Triangular distribution). On the other hand, the normalized types of fracture toughness (K_{IC_N} & K_{IIC_N}) optimally matched with the PERT distribution in all zones. In addition, the data range for minimum horizontal stress (σ_h) and differential horizontal stress (DHS, $\Delta\sigma$) best fit in with triangular distribution for all zones.

As an interval of any normalized parameter is inherently bounded by 0 and 1, it is not a coincidence that fracability components are dominated by triangular and PERT distributions, which are highly suitable for bounded-interval inputs.

Before applying probabilistic analysis, distribution types used along the stochastic (probabilistic) process can be explained in a few words.

The exponential distribution is a special case of Gamma distribution and an analog of the Geometric distribution where input values show a continuous profile at a constant average rate (**Palisade, 2023a; Wikipedia, 2023a**).

Triangular distribution is a fundamental distribution type defined by minimum, most likely, and maximum values when the relationship between variables is known but limited sample data is available (**Palisade, 2023c; Wikipedia, 2023c**).

PERT distribution (corresponds to Program Evaluation & Review Technique), defined by the minimum, most likely, and maximum values as in the triangular distribution, is one of the most commonly used distributions in statistics. It is a particular form of the Generalized Beta distribution. PERT distribution has a smoothed curve structure, and therefore it may be used as an alternative to triangular distribution (**Palisade, 2023b; Wikipedia, 2023b**).

Considering Kara & Isik's findings (***Table 2.5***), and the list of critical values in shale rock characterization (***Table 2.1***), it can be easily observed that the L2 subunit is by far the most favorable zone among all studied subunits (L2, L3, and L4) of Dadaş-I member in terms of reservoir quality. More clearly, L3 and L4 zones contain high water saturation (73% and 50%, respectively), and low total organic carbon (TOC) (1.79% and 1.69%, respectively). From these facts, the probabilistic risk analysis has been performed over the L2 zone.

A comprehensive demonstration of distributions of fracability components is presented over the L2 zone as provided in ***Figure 7.12***, ***Figure 7.13***, ***Figure 7.14***, and ***Figure 7.15***.

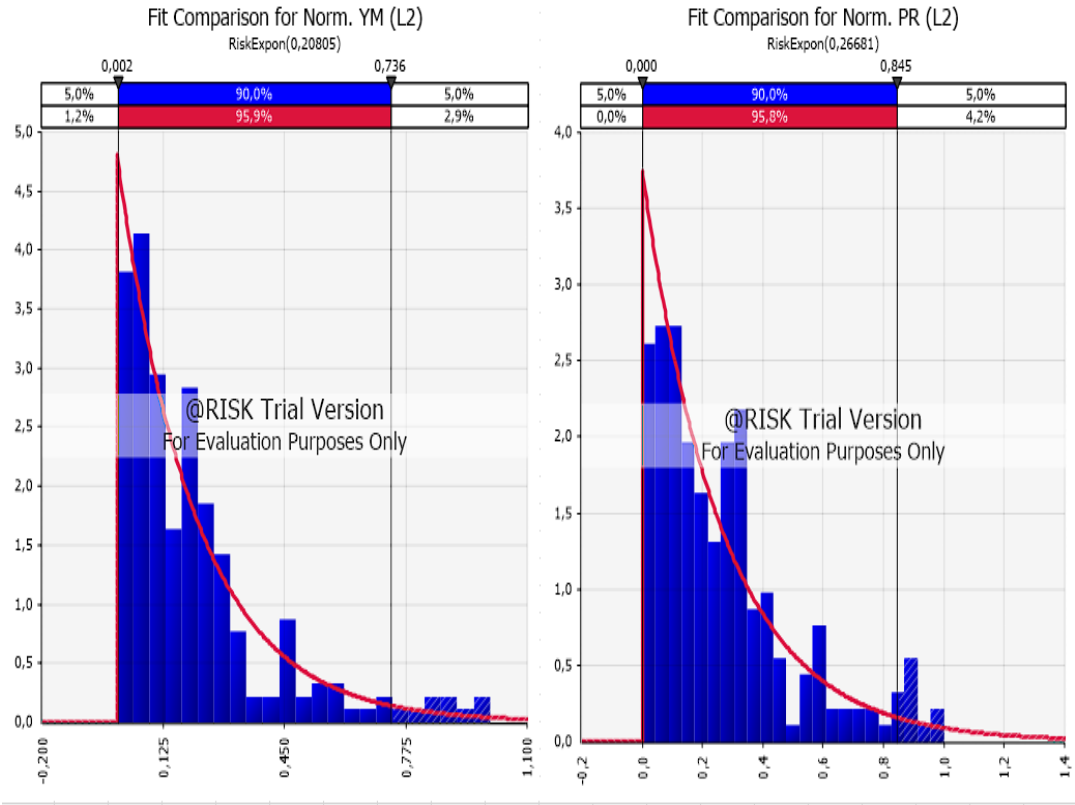

Figure 7.12 Distribution of normalized YM (EN) and PR (νN) for L2 zone.

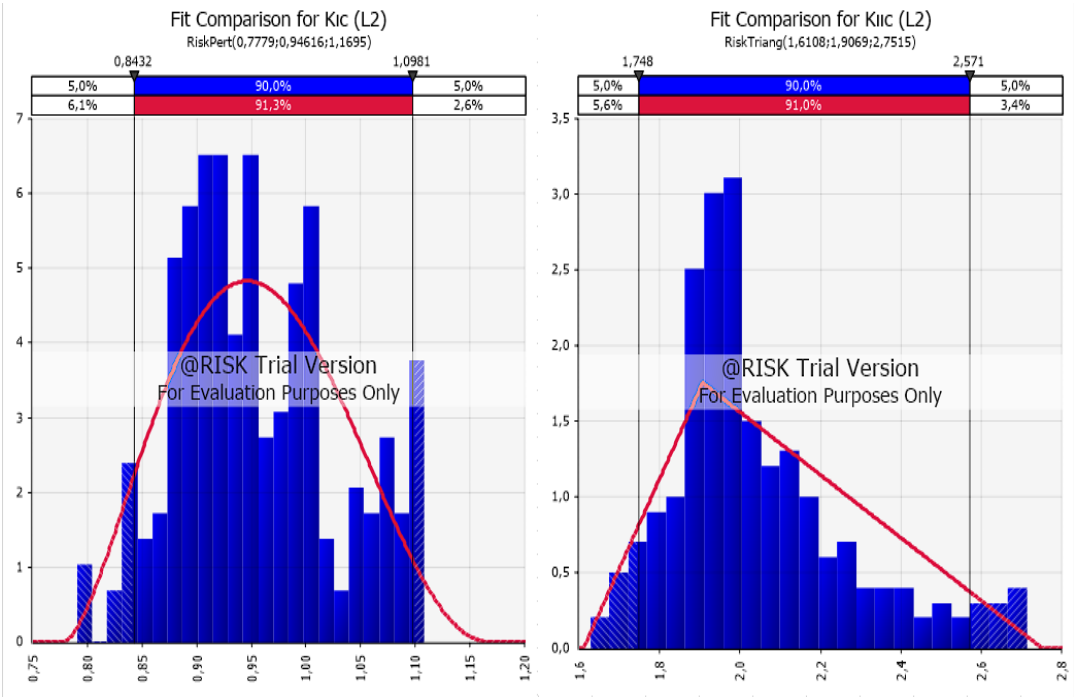

Figure 7.13 Distribution of mode-I (K_{IC}) and mode-II (K_{IIC}) fracture toughness for L2 zone.

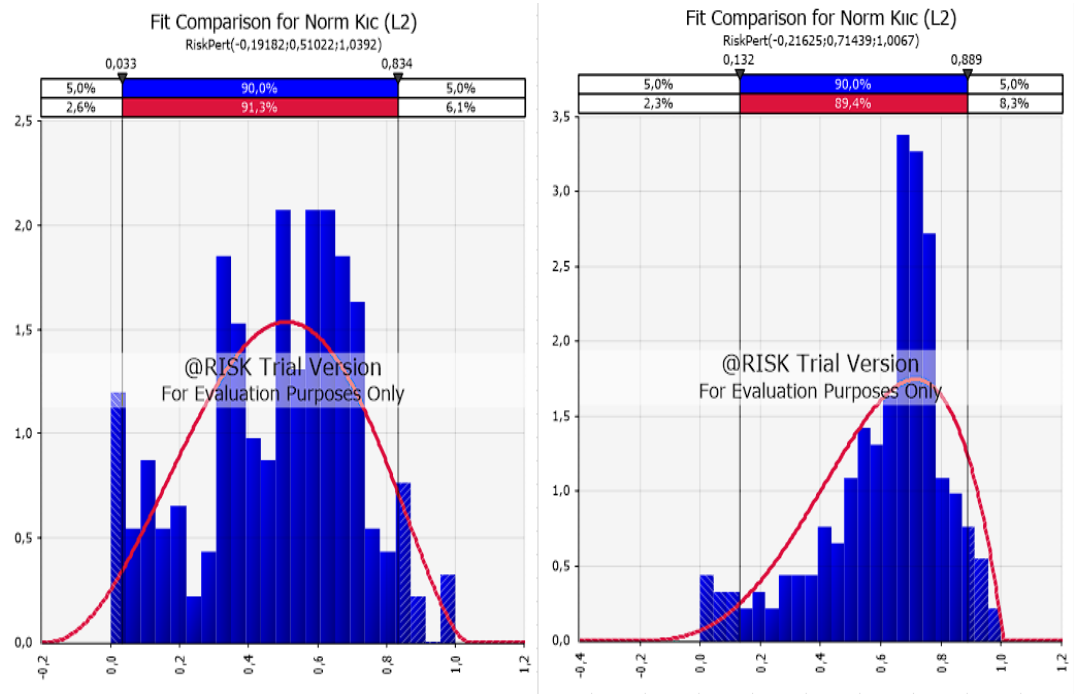

Figure 7.14 Distribution of normalized Kıc & Kıic for L2 zone.

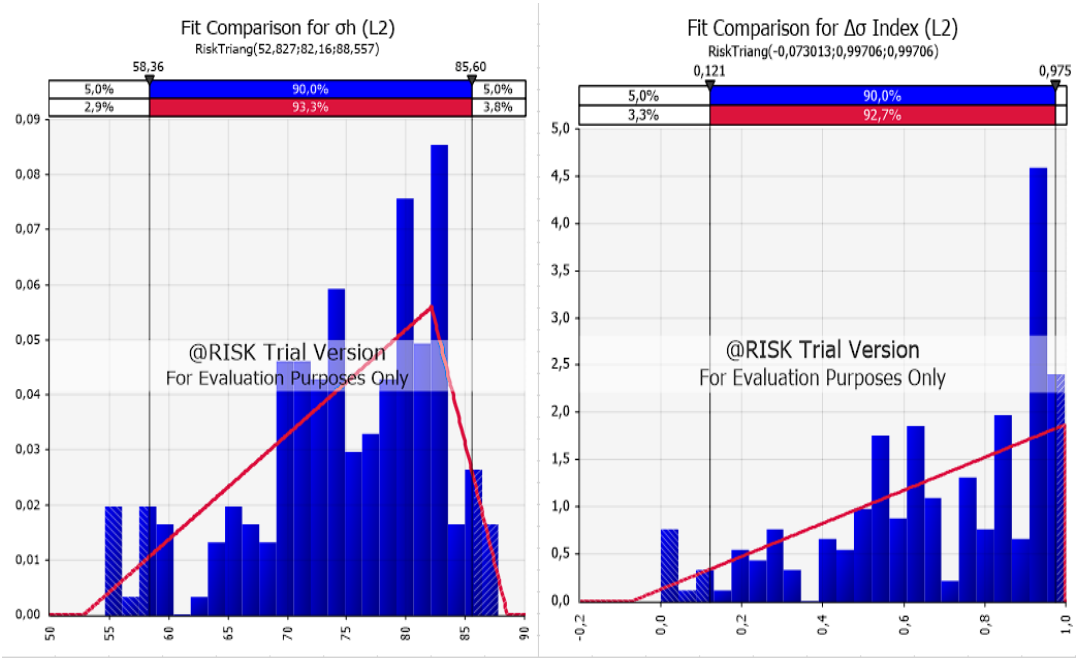

Figure 7.15 Distributions of MinHS (σ_h) and DHS ($\Delta\sigma$) index for L2 zone.

Subsequent to the distribution specification procedure, a Monte Carlo simulation with 10,000 iterations has been applied to evaluate the fracability index (FI) stochastically. In this context, the graphs of probability density functions (PDFs) and cumulative distribution functions (CDFs) were obtained for each fracability model. and presented in ***Figure 7.16*** and ***Figure 7.17*** (Rickman et al.'s model), ***Figure 7.18*** and ***Figure 7.19*** (Yuan et al.'s model), ***Figure 7.20*** and ***Figure 7.21*** (Dou et al.'s model), and ***Figure 7.22*** and ***Figure 7.23*** (Proposed model). All possible scenarios relating to FI were depicted by profiles of PDF and CDF graphs.

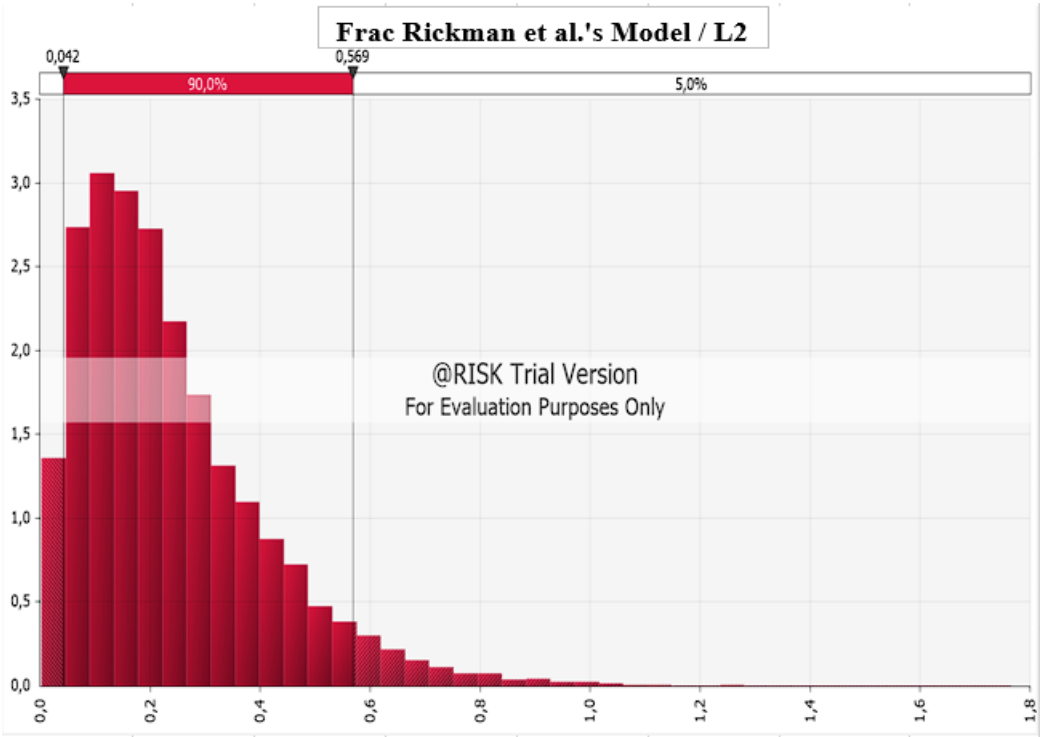

Figure 7.16 Distribution graph of the PDF for Rickman et al.'s model.

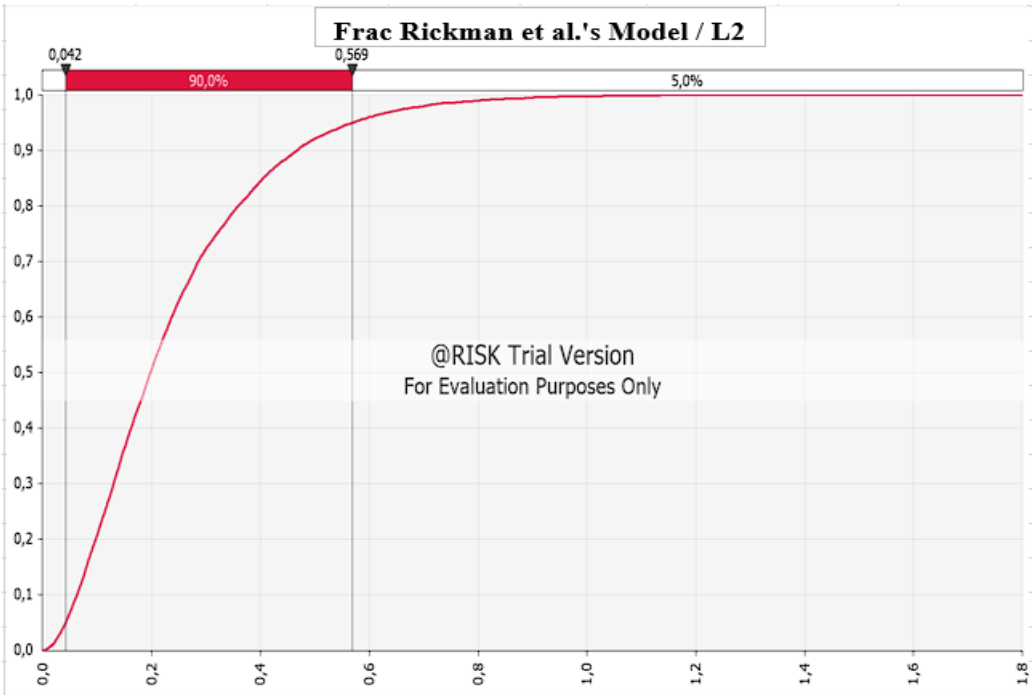

Figure 7.17 Distribution graph of the CDF for Rickman et al.'s model.

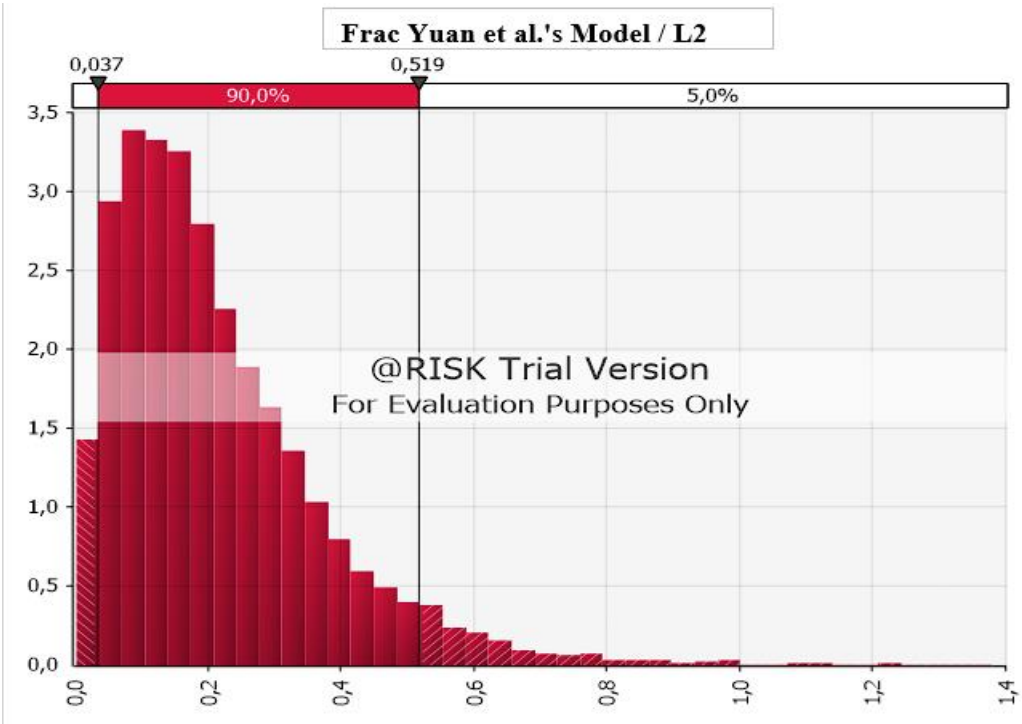

Figure 7.18 Distribution graph of the PDF for Yuan et al.'s model.

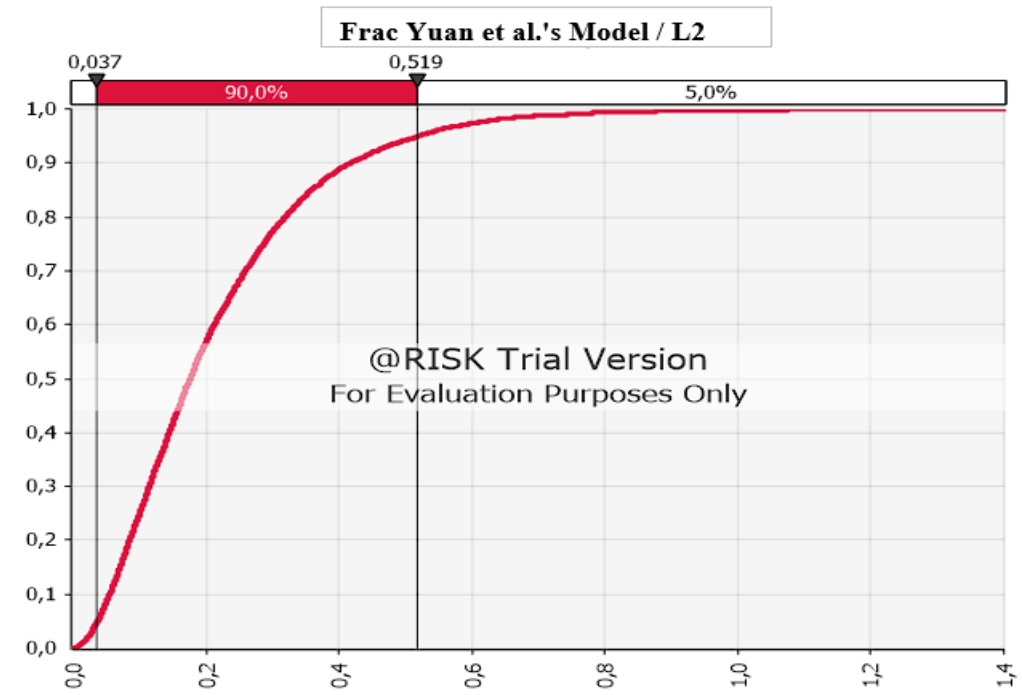

Figure 7.19 Distribution graph of the CDF for Yuan et al.'s model.

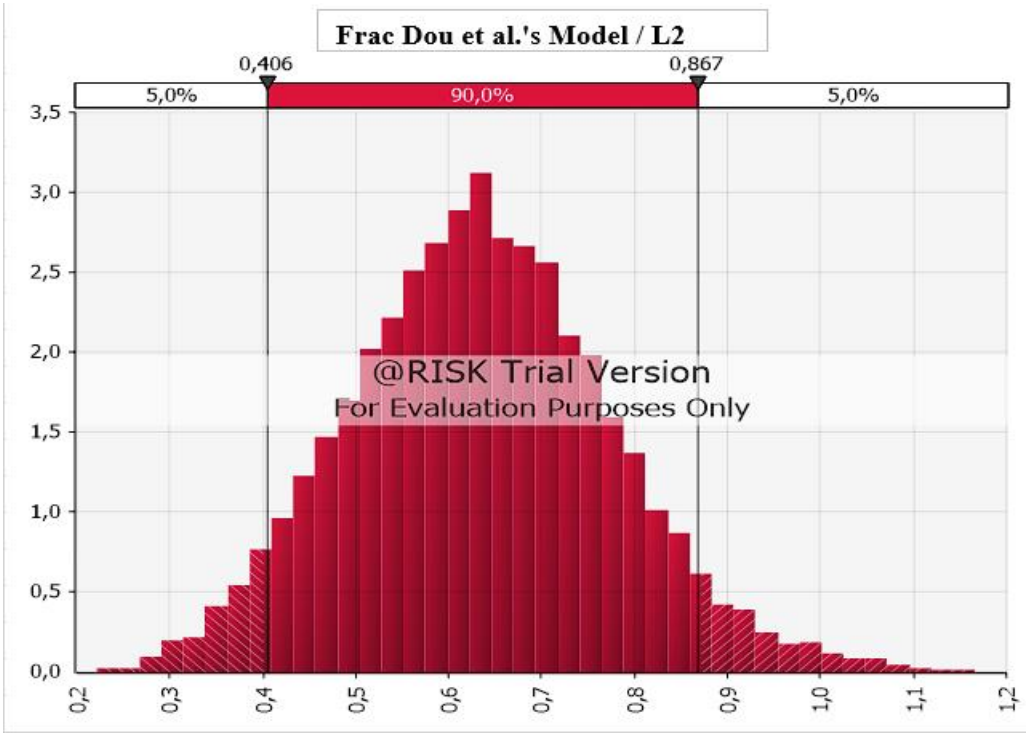

Figure 7.20 Distribution graph of the PDF for Dou et al.'s model.

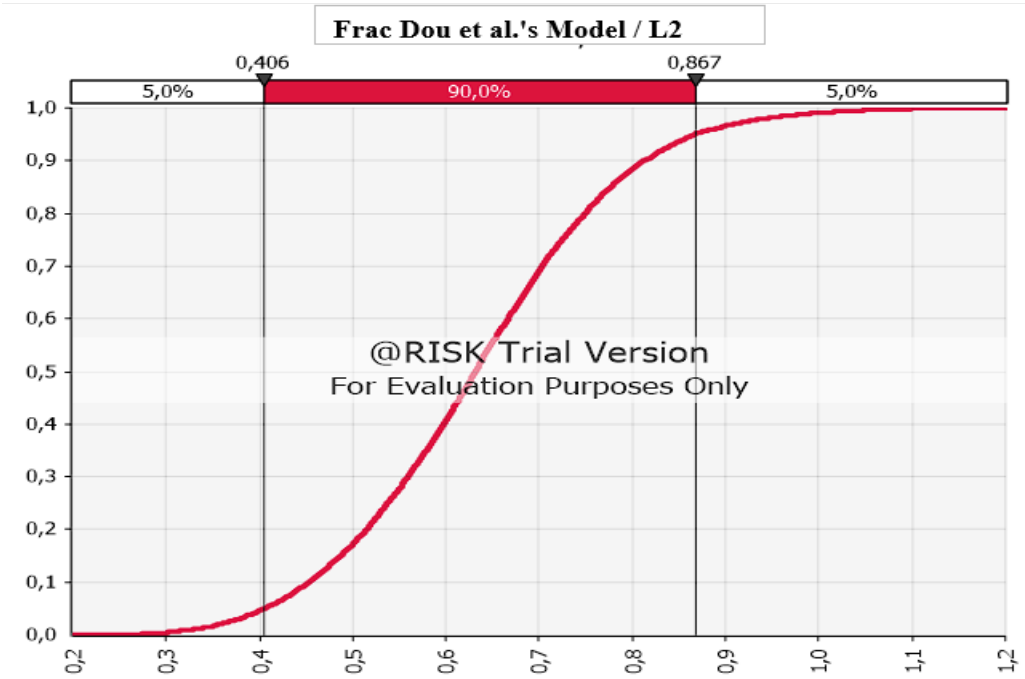

Figure 7.21 Distribution graph of the CDF for Dou et al.'s model.

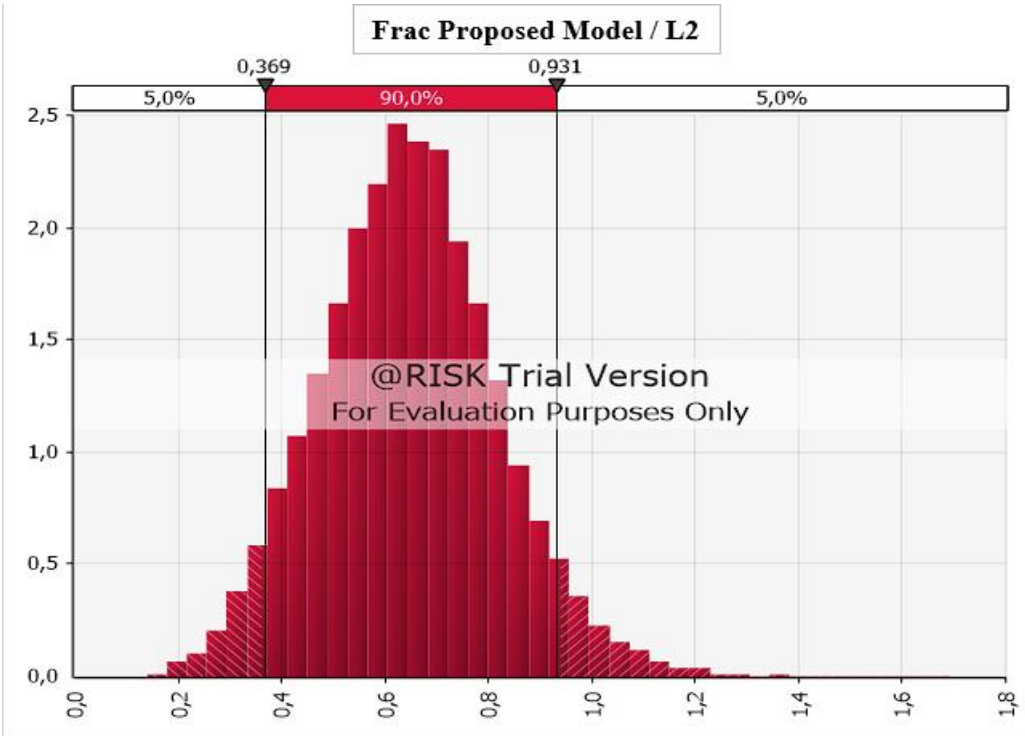

Figure 7.22 Distribution graph of the PDF for Proposed model.

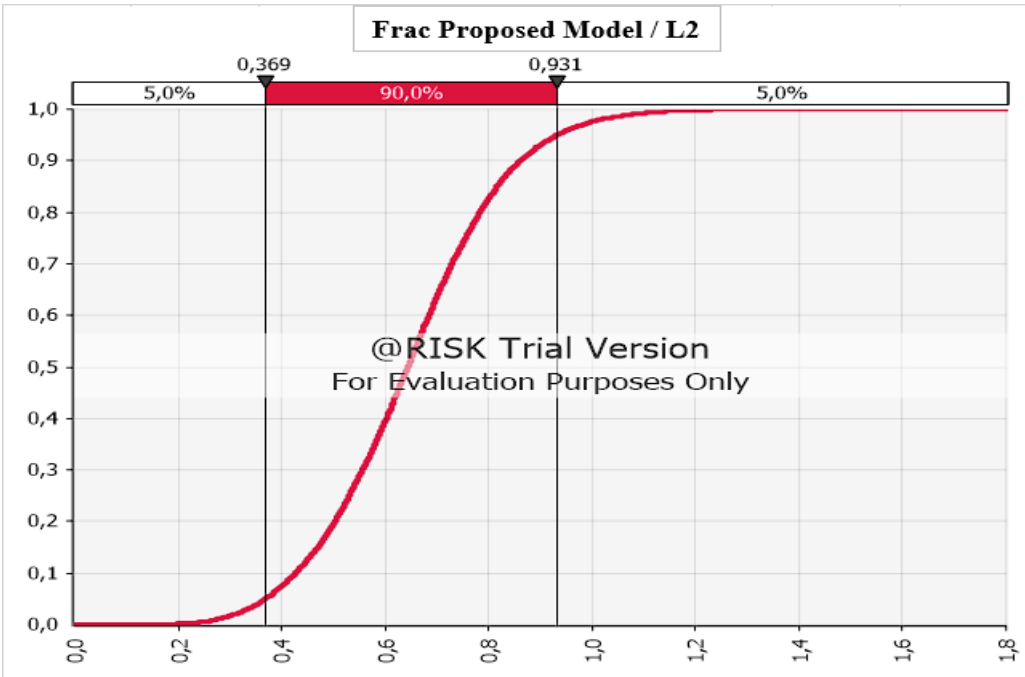

Figure 7.23 Distribution graph of the CDF for Proposed model.

The behavior of output data in response to changing input data can be examined by performing a sensitivity analysis. By ranking the inputs quantitatively, the sensitivity analysis facilitates evaluating the relative effect of different factors and identifying the most critical factor in fracability evaluation. Accordingly, an input with a greater impact score on a sensitivity assessment tool includes more uncertainty, requiring risk mitigation and developed investigation and modeling studies (**Lumivero, 2023c**). Tornado charts and spider graphs can represent the analysis visually to make more informed and sound judgments. As the bar length of an input parameter increases on the tornado chart, its impact on the FI increases. In a similar vein, as the line steepness of an input parameter increases on the spider chart, its impact on the FI increases. A spider chart presents more information than a tornado diagram since a tornado diagram reflects only the overall change in output value. However, a spider chart informs about the change rate in output value as the input data changes within its range (**Lumivero, 2023a, 2023b**).

Tornado and spider graphs for four fracability models were generated to analyze how the model inputs affect the behavior of the FI in L2 zone.

In Rickman et al.'s conventional fracability model, which consists of only two parameters, the normalized PR (ν_N) is observed to be slightly more effective on FI than the normalized YM (E_N) (***Figure 7.24*** & ***Figure 7.25***). As expected, the profile of possible FI outcomes is aligned with the exponential distribution as such in the normalized YM (E_N) and the normalized PR (ν_N).

For Yuan et al.'s model, normalized PR (ν_N) and normalized YM, (E_N) have the by far the largest impact score on FI (***Figure 7.26*** & ***Figure 7.27***). This result matches up with the fact that the PDF of the FI resembles the exponential distribution, which is best fitted for normalized YM (E_N) and normalized PR(ν_N).

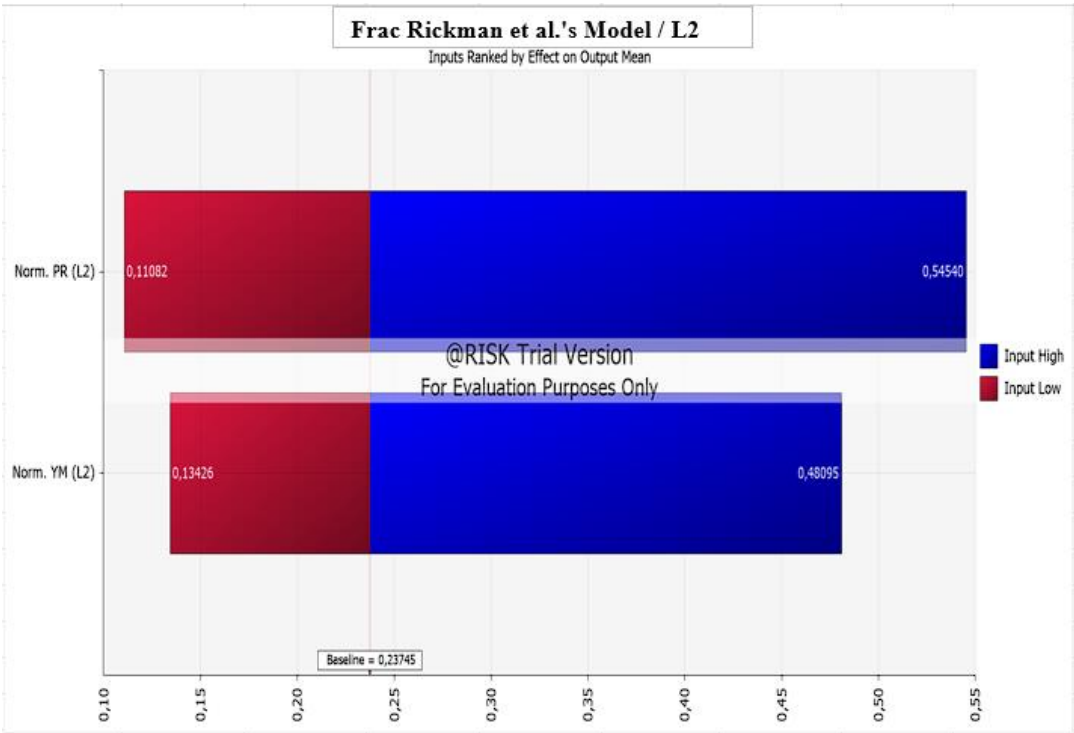

Figure 7.24 Tornado chart of L2 zone for Rickman et al.'s model.

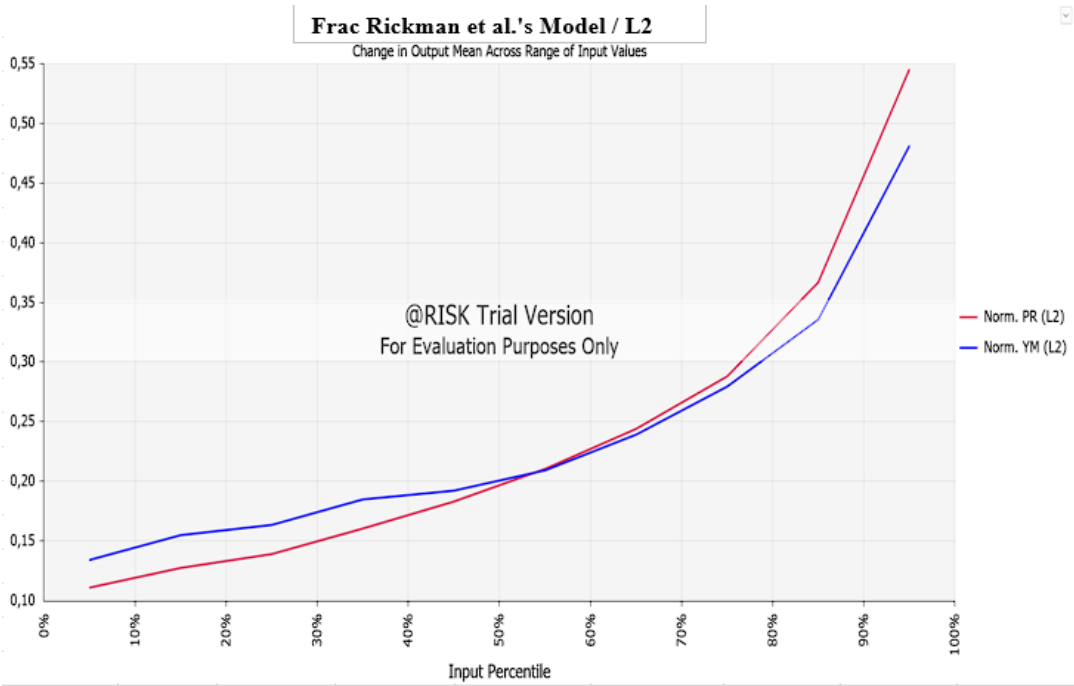

Figure 7.25 Spider chart of L2 zone for Rickman et al.'s model.

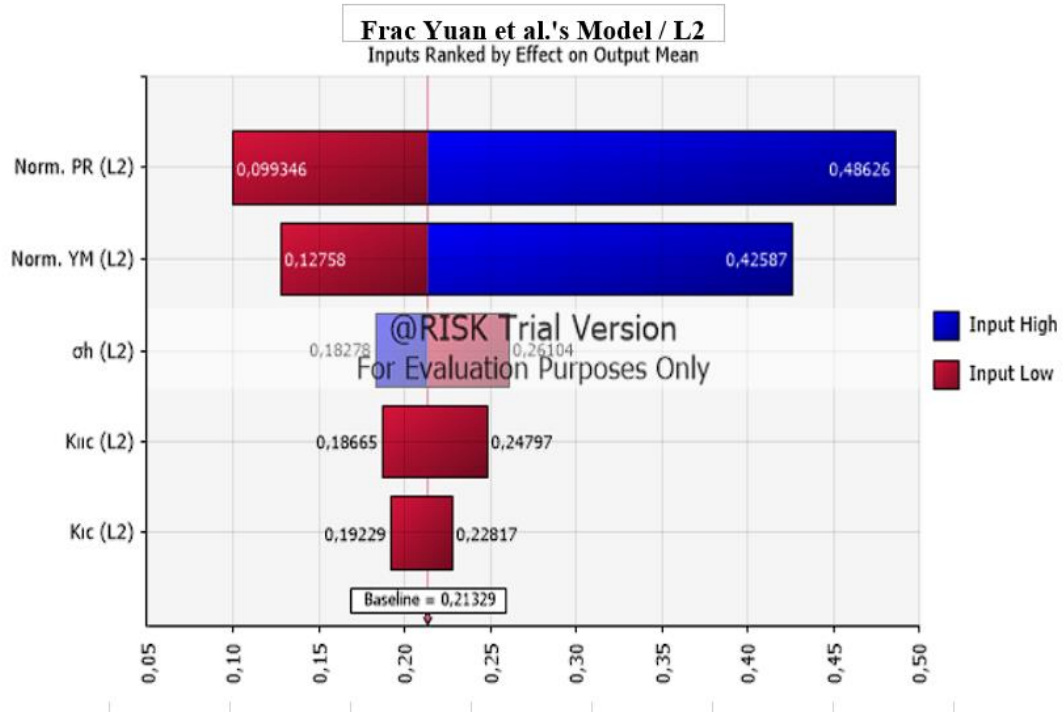

Figure 7.26 Tornado chart of L2 zone for Yuan et al.'s model.

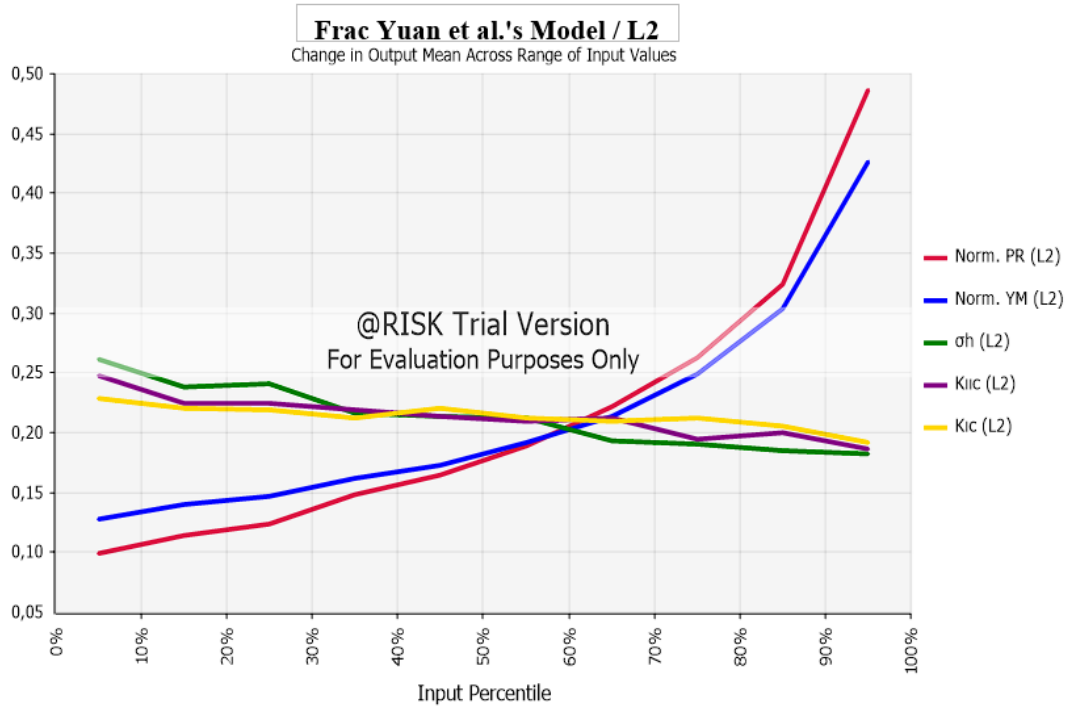

Figure 7.27 Spider chart of L2 zone for Yuan et al.'s model.

In Dou et al.'s model, the FI is found to be mostly sensitive to (at an almost equal rate) the DHS index ($\Delta\sigma$) and normalized mode-I fracture toughness (K_{IC_N}) (***Figure 7.28*** & ***Figure 7.29***). Thus, it is an expected result that the FI profile seems as the projection of the combination of Triangular and PERT distributions. Also, the minimum horizontal stress (σ_h), the normalized PR (ν_N), and the normalized YM (E_N) (in descending order) have a considerable level of impact on the sensitivity analysis.

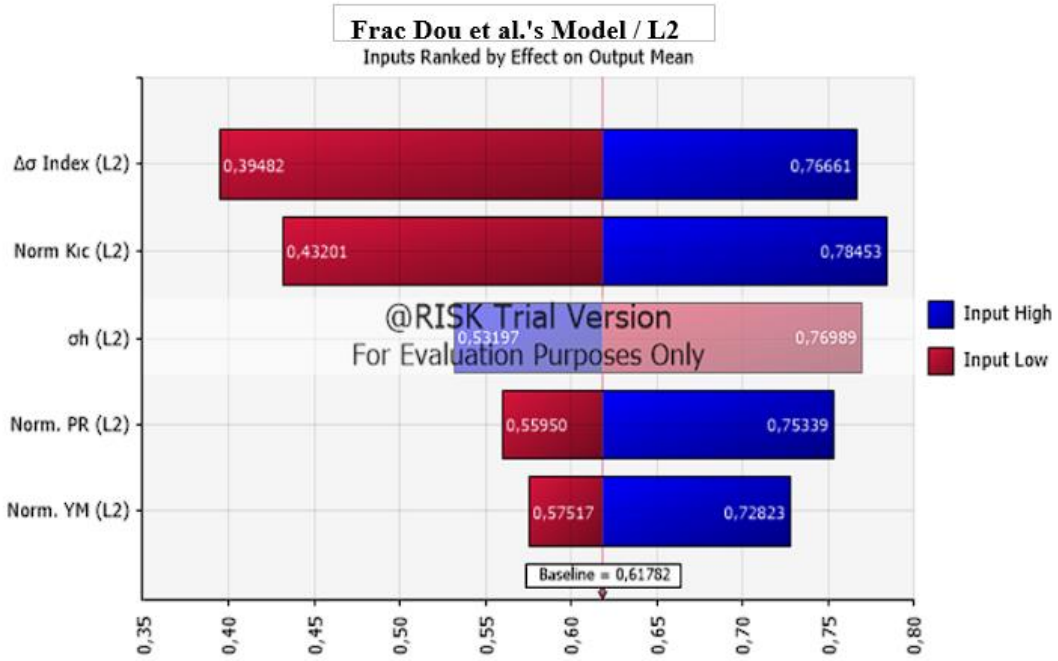

Figure 7.28 Tornado chart of L2 zone for Dou et al.'s model.

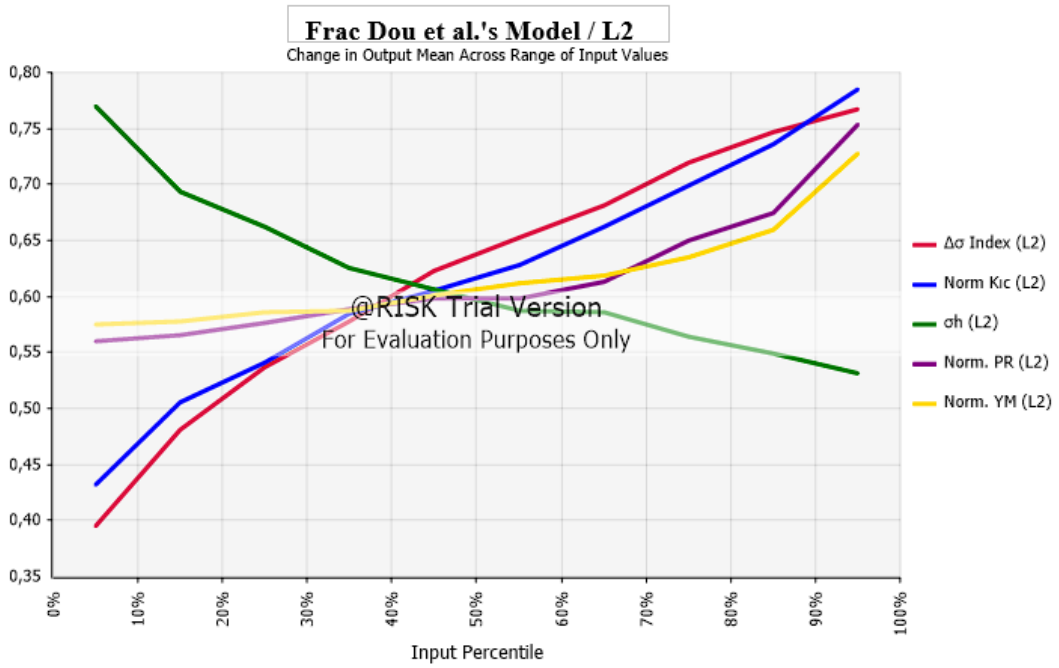

Figure 7.29 Spider chart of L2 zone for Dou et al.'s model.

As for the Proposed model in this research, since the DHS index (Δσ) has the largest bar on the tornado graph (***Figure 7.30***) and has the steepest line on the spider graph (***Figure 7.31***), it may be easily inferred that FI distribution is predominantly affected by the uncertainty in DHS index (Δσ). Minimum horizontal stress (σ_h) ranks number two at the effect ranking on the FI after the DHS index (Δσ). The rest of the input parameters almost share the same portion at the scale. In addition, the shape of the PDF distribution of FI in this model nearly corresponds to the triangular distribution, which accords with the distribution of the predominant input parameter (DHS index, (Δσ)).

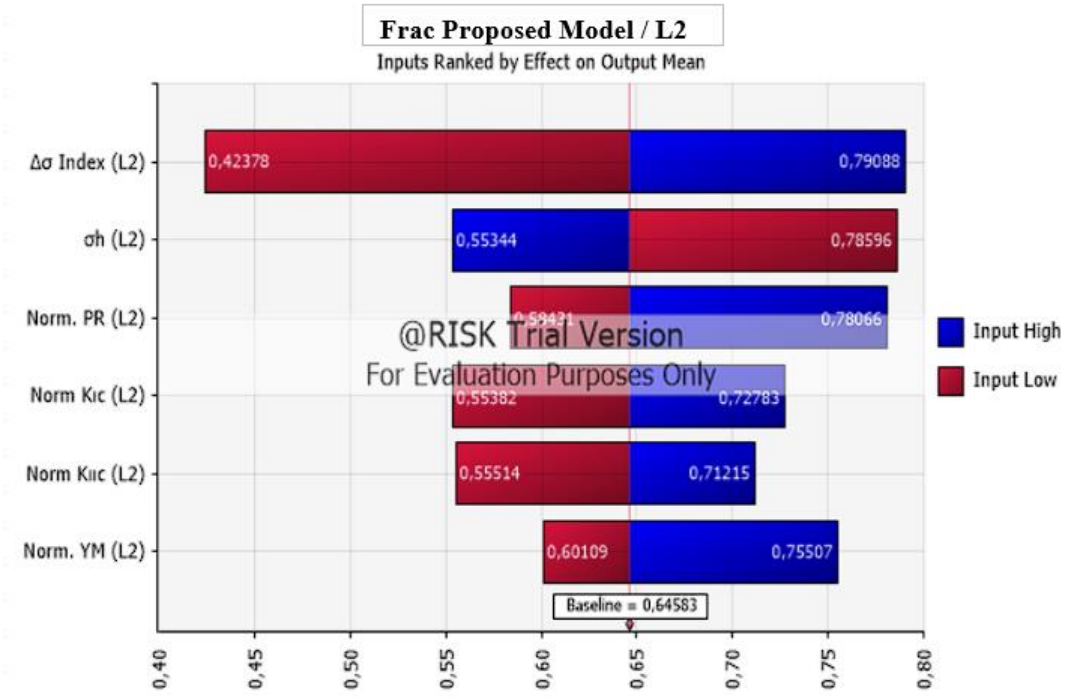

Figure 7.30 Tornado chart of L2 zone for Proposed model.

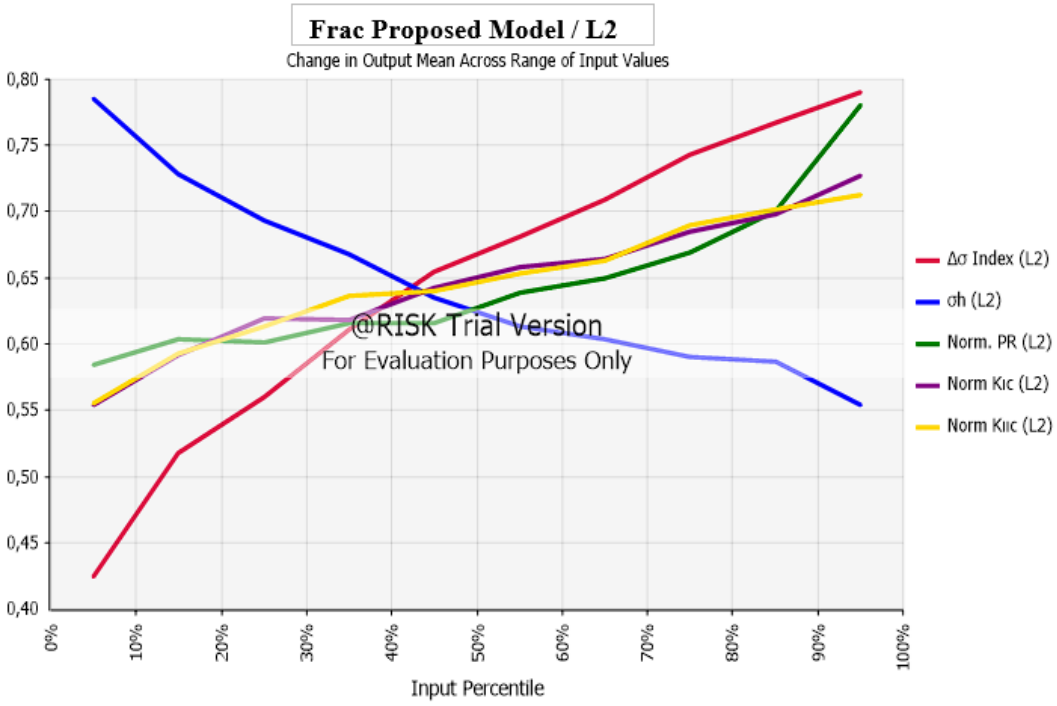

Figure 7.31 Spider chart of L2 zone for Proposed model.

CHAPTER 8

CONCLUSIONS

The fracability index (FI) values of Dadaş-I member were calculated by implementing four different FI models deterministically and stochastically, and the results are detailed in ***Table 8.1***.

Table 8.1 The collective fracability index (FI) results of L2 zone for all models.

Value Type	Rickman et al.	Yuan et al.	Dou et al.	Proposed Model
Mean Value	0.237	0.213	0.618	0.646
P50 Value	0.198	0.177	0.612	0.644
Deterministic Value	0.237	0.241	0.629	0.660
Stochastic Corresponding Value of Deterministic Value	P60	P65	P53	P54

The deterministic FI results for L2 zone were listed in descending order as the Proposed model, Dou et al.'s model, Yuan et al.'s model, and Rickman et al.'s model. On the other hand, the probabilistic analysis indicates that FI values from the largest to the smallest are as the Proposed model, Dou et al.'s model, Rickman et al.'s model, and Yuan et al.'s model.

Deterministic and probabilistic FI results for each model generally showed no big difference. To clarify, slight but noticeable differences in Rickman et al.'s model and in Yuan et al.'s model were observed. The deterministic FI values for Rickman et al.'s model (0.237) and for Yuan et al.'s model (0.241 MPa^{-2}. $m^{0.5}$) correspond to the P60 and P65 percentiles in stochastic distribution, respectively. As for Dou et al.'s model and Proposed model, the deterministic FI values (0.629 MPa^{-1}. m and 0.660

MPa^{-1}. m, respectively) correspond to the P53 and P54 percentiles in the stochastic approach, respectively. Both for Dou et al.'s model and for the Proposed model, the stochastic approach suggested that P50 values are almost equal to statistical mean values. On the other hand, considerable differences were observed between the mean value and P50 value both for Rickman et al.'s model and Yuan et al.'s model.

According to the model comparison analysis, all deterministic and probabilistic FI values obtained from Dou et al.'s model and Proposed model are much bigger than those of the two other models. This, indeed, may imply that the fracability of Dadaş shale is highly affected by differential horizontal stress (DHS, $\Delta\sigma$). Besides, it was observed that the results of the Proposed model are highly close to the results of Dou et al.'s model. This may suggest that the mode-II fracture toughness (K_{IIC}), which is mainly correlated with the shear failure, plays a small role in FI evaluation for Dadaş shale.

The relatively high deterministic FI results of Marcellus shale may be used as a supportive argument for successful hydraulic fracturing (HF) operations applied in this formation. Besides, when Dou et al.'s model and the Proposed model were reviewed, it was understood that deterministic FI results of Marcellus shale indicated close values with those of Dadaş-I shale. Supportively, the results of the Proposed fracability model for Dadaş-I shale are found to be consistent with those of Dou et al.'s model. It was also observed that all studied formations in the United States (Marcellus, Barnett, Haynesville, Bakken, and Eagle Ford) were found to be highly fracable (> 0.3 MPa^{-1}. m) according to Proposed model despite their relatively not much bigger BI values (between 0.3-0.6). This finding suggests that Dou et al.'s fracability model was verified by Proposed model when well-proven HF performances of productive shales in the U.S. are considered. Additionally, it was found that Dadaş Shale shows a similar tendency with Barnett Shale and Haynesville Shale in regards to FI and BI_{mech}. The results also showed that FI may not regularly increase as brittleness index (BI) gets bigger, which, means that there is not always positive correlation between FI and BI.

In light of such information, the Proposed model may be presented as an alternative fracability index approach for assessing candidate zones in HF operations. The Proposed model emphasizes the importance of differential horizontal stress (DHS, $\Delta\sigma$) as well as the type-II fracture toughness (K_{IIC}) parameter in fracability evaluation of shale reservoirs, which especially reside in strike-slip (SS) faulting and reverse faulting (RF) environments (e.g., Dadaş shale).

All in all, according to Rickman et al.'s model and Yuan et al.'s model, the L2 zone has low-fracable structure, and it is difficult to obtain an effective HF performance from this zone. However, it should not be forgotten that the Rickman et al.'s model only contains the mechanical brittleness in the FI equation. Additionally, Yuan et al.'s model inspires not much confidence due to the absence of differential horizontal stress in fracability equation. But not limited to this, although Yuan's et al.'s model includes three additional parameters (K_{IC}, K_{IIC}, and σ_h) compared to Rickman et al.'s model, FI values obtained from Yuan et al.'s model are significantly close to the FI values in Rickman et al.'s model. On the other hand, for L2 zone, Dou et al.'s model and the Proposed model suggested a highly promising picture regarding obtaining a complex fracture network, a greater stimulated reservoir volume (SRV), and a higher fracture conductivity. Besides, as opposed to all other zones, L2 zone has favorable petrophysical and geochemical properties in addition to its geomechanical properties. From this viewpoint, it was concluded that L2 zone is the most likely ideal option in the matter of the effective stimulation of Dadaş shale by HF. In the near future, the results obtained from this research, along with the proposed fracability model, may be extended and used to evaluate the fracability of unconventional shale reservoirs in Turkey.

CHAPTER 9

RECOMMENDATIONS

Uncertainties of geomechanical properties and preexisting fracture networks, resulting from the heterogeneous reservoir conditions in shale formations need further and rigorous study for the optimization of hydraulic fracturing (HF) operations. In this respect,

- experimental research must be carried out on actual core samples to increase the reliability degree of geomechanical parameters derived from well-logs
- numerical modelling research should be carried out to describe and quantify the relationship between hydraulic fractures (hFs) and natural fractures (nFs) in a more real-like way.
- the field-scale real HF and production data related to Dadaş shale should be evaluated, which, then, might be used to validate the outcomes of this research on the fracability index (FI).

However, in Turkey, the limitation of public data, financial difficulties, technical inadequacies, and the distinct lack of interest in geomechanics area obstruct the implementation of such detailed studies in fracability research.

In short, this research is expected to contribute to the existing knowledge about unconventional Dadaş shale in Southeast (SE) Turkey, and to pave the way for creating a reliable mechanical earth model (MEM) for the improvement of literature on the unconventional reservoir geomechanics in Turkey. In the near future, the results and findings obtained from this research may be extended by experimental activities and numerical modelling studies. These efforts should be supported for a better and more accurate understanding of the geomechanical structure of unconventional reservoirs in Turkey.

REFERENCES

Addis, M. A., Bordoloi, S., Franquet, J. A., Hooyman, P. J., Hurt, R. S., Kowan, J. E., Khaksar, A., Nagel, N. B., & Ong, S. H. (2016). Chapter 9 - Role of Geomechanical Engineering in Unconventional Resources Developments. In U. Ahmed & D. N. Meehan (Eds.), *Unconventional Oil and Gas Resources: Exploitation and Development*. Taylor & Francis. https://www.routledge.com/Unconventional-Oil-and-Gas-Resources-Exploitation-and-Development/Ahmed-Meehan/p/book/9781498759403

Afsari, M., Ghafoori, M. R., Roostaeian, M., Haghshenas, A., Ataei, A., & Masoudi, R. (2009). Mechanical earth model (MEM): An effective tool for borehole stability analysis and managed pressure drilling (case study). *SPE Middle East Oil and Gas Show and Conference, MEOS, Proceedings*, *1*, 87–98. https://doi.org/10.2118/118780-ms

Ahmad, A., & Rezaee, R. (2015). Pore Pressure Prediction for Shale Formations Using Well Log Data. In *Fundamentals of Gas Shale Reservoirs* (pp. 139–167). https://doi.org/https://doi.org/10.1002/9781119039228.ch7

Akkoca, D. B., & Işık, Ü. (2018). Geochemistry of paleozoic dadaş shales from the foreland of southeastern Turkey, Bismil, Diyarbakır. *Periodico Di Mineralogia*, *87*(3), 207–225. https://doi.org/https://doi.org/10.2451/2018PM683

Altindag, R. (2010). Assessment of some brittleness indexes in rock-drilling efficiency. *Rock Mechanics and Rock Engineering*, *43*(3), 361–370. https://doi.org/10.1007/s00603-009-0057-x

Alzahabi, A., Al Qahtani, G., Soliman, M. Y., Bateman, R. M., Asquith, G., & Vadapalli, R. (2015). Fracturability index is a mineralogical index: A new approach for fracturing decision. *Society of Petroleum Engineers - SPE Saudi*

Arabia Section Annual Technical Symposium and Exhibition, 1–32. https://doi.org/10.2118/178033-ms

Anderson, T. L. (2005). *Fracture Mechanics: Fundamentals and Applications, Third Edition*. Taylor & Francis. https://books.google.com.tr/books?id=MxrtsC-ZooQC

Ardila, S., Corzo, R., Rubio, N., & Arias, H. (2019). Brittleness, Fracability and Stresses Evaluation to Define the Completion Quality in Unconventional Reservoirs. In S. Montoya & A. Roa (Eds.), *Eighth International Symposium Geomechanics*.

Aydemir, A. (2011). Comparison of mississippian barnett shale, northern-central texas, USA and silurian dadas formation in southeast Turkey. *Journal of Petroleum Science and Engineering*, *80*(1), 81–93. https://doi.org/10.1016/j.petrol.2011.10.009

Bai, M. (2016). Why are brittleness and fracability not equivalent in designing hydraulic fracturing in tight shale gas reservoirs. *Petroleum*, *2*(1), 1–19. https://doi.org/10.1016/j.petlm.2016.01.001

Baiyegunhi, T. L., Baiyegunhi, C., & Pharoe, B. K. (2022). Global Research Trends on Shale Gas from 2010–2020 Using a Bibliometric Approach. *Sustainability (Switzerland)*, *14*(6). https://doi.org/10.3390/su14063461

Bassiouni, Z. (1994). *Theory, measurement, and interpretation of well logs*. Henry L. Doherty Memorial Fund of AIME, Society of Petroleum Engineers Richardson, TX. https://doi.org/LK - https://worldcat.org/title/30899531

Belyadi, H., Fathi, E., & Belyadi, F. (2017). Chapter Thirteen - Rock Mechanical Properties and In Situ Stresses. In *HYDRAULIC FRACTURING IN UNCONVENTIONAL RESERVOIRS Theories, Operations, and Economic Analysis* (pp. 207–224). Gulf Professional Publishing. https://doi.org/https://doi.org/10.1016/B978-0-12-849871-2.00013-7

Berard, T., & Prioul, R. (2016). The Defining Series: Mechanical Earth Model. *Schlumberger - Oilfield Review*, *1*, 2.

Blanton, T. L. (1982). An experimental study of interaction between hydraulically induced and pre-existing fractures. *Society of Petroleum Engineers - SPE Unconventional Gas Recovery Symposium, UGR 1982*, 559–562. https://doi.org/10.2523/10847-ms

Blanton, T. L. (1986). Propagation of hydraulically and dynamically induced fractures in naturally fractured reservoirs. *Society of Petroleum Engineers - SPE Unconventional Gas Technology Symposium, UGT 1986*, 613–621. https://doi.org/10.2118/15261-ms

Bowers, G. L. (1995). Pore Pressure Estimation From Velocity Data: Accounting for Overpressure Mechanisms Besides Undercompaction. *SPE Drilling & Completion*, *10*(02), 89–95. https://doi.org/10.2118/27488-PA

Brocher, T. M. (2005). Empirical relations between elastic wavespeeds and density in the Earth's crust. *Bulletin of the Seismological Society of America*, *95*(6), 2081–2092. https://doi.org/10.1785/0120050077

Bruner, K. R., & Smosna, R. (2011). A comparative study of the Mississippian Barnett Shale, Fort Worth Basin, and Devonian Marcellus Shale, Appalachian Basin. In *US DoE Report*.

CASMO - World Stress Map. (2016). https://www.world-stress-map.org/casmo

Chang, C., Zoback, M. D., & Khaksar, A. (2006). Empirical relations between rock strength and physical properties in sedimentary rocks. *Journal of Petroleum Science and Engineering*, *51*(3–4), 223–237. https://doi.org/10.1016/j.petrol.2006.01.003

Chen, J., Deng, J., Yuan, J., Yan, W., Yu, B., & Tan, Q. (2015). Determination of fracture toughness of modes I and ii of shale formation. *Yanshilixue Yu Gongcheng Xuebao/Chinese Journal of Rock Mechanics and Engineering*, *34*,

1101–1105. https://doi.org/10.13722/j.cnki.jrme.2014.1187

Chen, P., & Rahman, M. M. (2015). A novel approach to predict interaction between hydraulic fracture and natural fracture using artificial neural networks. *Society of Petroleum Engineers - SPE/IATMI Asia Pacific Oil and Gas Conference and Exhibition, APOGCE 2015*. https://doi.org/10.2118/176143-ms

Chen, P., Rahman, M. M., & Sarma, H. K. (2014). Interaction between hydraulic fracture and natural fracture - A new prediction model by adaptive neuro-fuzzy inference system (ANFIS). *Society of Petroleum Engineers - 30th Abu Dhabi International Petroleum Exhibition and Conference, ADIPEC 2014: Challenges and Opportunities for the Next 30 Years*, *4*(1997), 2671–2686. https://doi.org/10.2118/171927-ms

Chong, K. K., Grieser, W. V., Passman, A., Tamayo, C. H., Modeland, N., & Burke, B. (2010). A completions guide book to shale-play development: A review of successful approaches towards shale-play stimulation in the last two decades. *Society of Petroleum Engineers - Canadian Unconventional Resources and International Petroleum Conference 2010*, *1*, 68–94. https://doi.org/10.2118/133874-ms

Dargahi, H. J., & Rezaee, R. (2013). Evaluation of the Carynginia Formation as a Potential Gas Shale Reservoir at Perth Basin, Western Australia. In *SPE/AAPG/SEG Unconventional Resources Technology Conference* (p. URTEC-1540748-MS). https://doi.org/10.1190/urtec2013-275

Dobson, P., & Houseworth, J. (2014). *Inventory of Shale Formations in the US, Including Geologic, Geochemical, Hydrological, Mechanical, and Thermal Characteristics*. https://escholarship.org/uc/item/1vb4c0vh#author

Dong, K., Liu, H., Wang, S., & Jiang, M. (2015). Experiment and simulation research on hydraulic fracture propagation characteristic under interface layer influence. *Society of Petroleum Engineers - SPE/IATMI Asia Pacific Oil and*

Gas Conference and Exhibition, APOGCE 2015, 1–10. https://doi.org/10.2118/176130-ms

Dou, L., Zuo, X., Qu, L., Xiao, Y., Bi, G., Wang, R., & Zhang, M. (2022). A New Method of Quantitatively Evaluating Fracability of Tight Sandstone Reservoirs Using Geomechanics Characteristics and In Situ Stress Field. *Processes*, *10*(5), 1040. https://doi.org/10.3390/pr10051040

Eaton, B. A. (1975). *The Equation for Geopressure Prediction from Well Logs*. https://doi.org/10.2118/5544-ms

EIA. (2013). *Technically Recoverable Shale Oil and Shale Gas Resources: An Assessment of 137 Shale Formations in 41 Countries Outside the United States*. https://www.eia.gov/analysis/studies/worldshalegas/pdf/overview.pdf

EIA. (2015). *Technically Recoverable Shale Oil and Shale Gas Resources: Turkey*. https://www.eia.gov/analysis/studies/worldshalegas/pdf/Turkey_2013.pdf

EIA. (2016). *Maps: Oil and Gas Exploration, Resources, and Production*. https://www.eia.gov/maps/maps.htm

EIA. (2022). *U.S. energy facts explained - consumption and production*. https://www.eia.gov/energyexplained/us-energy-facts/

EIA. (2023a). *Frequently Asked Questions (FAQs) - How much shale (tight) oil is produced in the United States?* https://www.eia.gov/tools/faqs/faq.php?id=847&t=6

EIA. (2023b). *Frequently Asked Questions (FAQs) - How much shale gas is produced in the United States?* https://www.eia.gov/tools/faqs/faq.php?id=907&t=8

EIA. (2023c). *Natural Gas Data - U.S. Energy Information Administration (EIA)*. https://www.eia.gov/naturalgas/data.php

Enderlin, M. B., Alsleben, H., & Beyer, J. A. (2011). Predicting fracability in shale

reservoirs. *AAPG Annual Convention and Exhibition, Houston, Texas, USA*, *20*, 10–13.

Ercengiz, S. A., Alper, M. Z., Sancay, R. H., Blair, G. J., & Ekinci, M. K. (2014). Characteristics of Lower Silurian Rocks as an Unconventional Resource in Diyarbakir Basin, SE Turkey. *International Conference & Exhibition*. https://www.searchanddiscovery.com/abstracts/html/2014/90194ice/abstracts/1948896.html

Fernandez Rojas, L., Quintero Peña, Y., & Calderon Carrillo, Z. H. (2016). Brittleness analysis: A methodology to identify sweet spots in shale gas reservoirs. *Society of Petroleum Engineers - SPE Argentina Exploration and Production of Unconventional Resources Symposium*. https://doi.org/10.2118/180955-ms

Fjær, E., Holt, R. M., Horsrud, P., Raaen, A. M., & Risnes, R. (2008). Chapter 5 Elastic wave propagation in rocks. In *Petroleum Related Rock Mechanics 2nd Edition* (Vol. 53, pp. 175–218). Elsevier. https://doi.org/https://doi.org/10.1016/S0376-7361(07)53005-0

Gholinezhad, J., Fianu, J. S., & Galal Hassan, M. (2018). Shale Gas Reservoirs—A Comparative Approach. In *Challenges in Modelling and Simulation of Shale Gas Reservoirs* (pp. 1–11). Springer International Publishing. https://doi.org/10.1007/978-3-319-70769-3_1

Govindarajan, S., Gokaraju, D. V., Mitra, A., Patterson, R., & Aldin, M. (2017). Evaluation of fracability index for reservoir rock - A laboratory study. *51st US Rock Mechanics / Geomechanics Symposium 2017*, *2*, 1424–1434.

Grieser, B., & Bray, J. (2007). Identification of production potential in unconventional reservoirs. *SPE Production and Operations Symposium, Proceedings*, 243–248. https://doi.org/10.2523/106623-ms

Guo, B., Liu, X., & Tan, X. (2017). Hydraulic Fracturing. In *Petroleum Production Engineering* (2nd ed., pp. 389–501). Elsevier. https://doi.org/10.1016/B978-0-

12-809374-0.00014-3

Guo, J. C., Luo, B., Zhu, H. Y., Wang, Y. H., Lu, Q. L., & Zhao, X. (2015). Evaluation of fracability and screening of perforation interval for tight sandstone gas reservoir in western Sichuan Basin. *Journal of Natural Gas Science and Engineering*, *25*, 77–87. https://doi.org/10.1016/j.jngse.2015.04.026

He, R., Yang, Z., Li, X., Li, Z., Liu, Z., & Chen, F. (2019). A comprehensive approach for fracability evaluation in naturally fractured sandstone reservoirs based on analytical hierarchy process method. *Energy Science and Engineering*, *7*(2), 529–545. https://doi.org/10.1002/ese3.303

Heidbach, O., Rajabi, M., Cui, X., Fuchs, K., Müller, B., Reinecker, J., Reiter, K., Tingay, M., Wenzel, F., Xie, F., Ziegler, M. O., Zoback, M. Lou, & Zoback, M. (2016). The World Stress Map database release 2016: Crustal stress pattern across scales. *Tectonophysics*, *744*, 484–498. https://doi.org/10.1016/j.tecto.2018.07.007

Higgins-Borchardt, S., Sitchler, J., & Bratton, T. (2016). Chapter 7 - Geomechanics for Unconventional Reservoirs. In Y. Zee Ma & S. A. Holditch (Eds.), *Unconventional Oil and Gas Resources Handbook* (pp. 199–213). Elsevier. https://doi.org/10.1016/B978-0-12-802238-2.00007-9

Hilchie, D. W. (1982). *Applied Openhole Log Interpretation (for Geologists and Engineers)*. https://books.google.com.tr/books?id=vN8xAQAAIAAJ

Horsrud, P. (2001). Estimating mechanical properties of shale from empirical correlations. *SPE Drilling and Completion*, *16*(2), 68–73. https://doi.org/10.2118/56017-PA

Hosgor, İ., & Yilmaz, İ. Ö. (2022). The Paleozoic petroleum system of the Molla-Bismil area (Diyarbakır Basin, Turkey) and source rock properties of Lower Silurian (Llandovery) organic-rich shale. *Marine and Petroleum Geology*, *143*(June). https://doi.org/10.1016/j.marpetgeo.2022.105762

Huang, C., Tianyang, X. U., Yiwen, J. U., Zhu, H., Liting, J. U., & Wuyang, L. I. (2019). Fracability Evaluation of Shale of the Wufeng-Longmaxi Formation in the Changning Area, Sichuan Basin. *Acta Geologica Sinica*, *93*(4), 996–1004. https://doi.org/10.1111/1755-6724.13877

Huang, Z. X., Yang, K., Peng, C. Y., Ai, C. Z., Jiang, M., Deng, J. T., & Liu, W. J. (2021). How to identify the best candidate fracturing zone: A review of current fracability evaluation method. *IOP Conference Series: Earth and Environmental Science*, *861*(6). https://doi.org/10.1088/1755-1315/861/6/062071

Hughes, J. D. (2021). *Shale Reality Check 2021: Drilling Into the U.S. Government's Optimistic Forecasts for Shale Gas & Tight Oil Production Through 2050*. https://www.postcarbon.org/publications/shale-reality-check-2021/

IEA. (2021). *Turkey 2021 Energy Policy Review*. https://www.iea.org/reports/turkey-2021

Inan, M. A., & Kavak, O. (2019). Shale resource potential of the Silurian Dadas Formation in Diyarbakır (SE Anatolia of Turkey) and its surroundings. *Arabian Journal of Geosciences*, *12*(22). https://doi.org/10.1007/s12517-019-4837-7

Irwin, G. R. (1957). Analysis of Stresses and Strains Near the End of a Crack Traversing a Plate. *Journal of Applied Mechanics*, *24*(3), 361–364. https://doi.org/10.1115/1.4011547

Iyare, U. C., Blake, O. O., & Ramsook, R. (2022). Fracability evaluation of the upper Cretaceous Naparima Hill Formation, Trinidad. *Journal of Petroleum Science and Engineering*, *208*(PD), 109599. https://doi.org/10.1016/j.petrol.2021.109599

Jahandideh, A., & Jafarpour, B. (2014). Optimization of hydraulic fracturing design under spatially variable shale fracability. *Society of Petroleum*

Engineers - SPE Western North American and Rocky Mountain Joint Meeting. https://doi.org/10.2118/169521-ms

Jarvie, D. M., Hill, R. J., Ruble, T. E., & Pollastro, R. M. (2007). Unconventional shale-gas systems: The Mississippian Barnett Shale of north-central Texas as one model for thermogenic shale-gas assessment. *American Association of Petroleum Geologists Bulletin*, *91*(4), 475–499. https://doi.org/10.1306/12190606068

Jin, X., Shah, S. N., Roegiers, J.-C., & Zhang, B. (2014). *Fracability Evaluation in Shale Reservoirs-An Integrated Petrophysics and Geomechanics Approach*. 4–6. http://onepetro.org/SPEHFTC/proceedings-pdf/14HFTC/All-14HFTC/SPE-168589-MS/1525823/spe-168589-ms.pdf/1

Jin, Y., Chen, M., & Zhang, X. (2001). Determination of fracture toughness for deep well rock with geophysical logging data. *Yanshilixue Yu Gongcheng Xuebao/Chinese Journal of Rock Mechanics and Engineering*, *20*, 454–456.

Jin, Y., Yuan, J., Chen, M., Chen, K. P., Lu, Y., & Wang, H. (2011). Determination of Rock Fracture Toughness KIIC and its Relationship with Tensile Strength. *Rock Mechanics and Rock Engineering*, *44*(5), 621–627. https://doi.org/10.1007/s00603-011-0158-1

Kara, B., & Isik, V. (2021). Reservoir characteristics and unconventional oil potential of Silurian aged Dadaş shale in southeast Turkey. *Journal of Petroleum Science and Engineering*, *200*(December 2020), 108365. https://doi.org/10.1016/j.petrol.2021.108365

Labani, M., & Rezaee, R. (2015). Petrophysical Evaluation of Gas Shale Reservoirs. In R. Rezaee (Ed.), *Fundamentals of Gas Shale Reservoirs* (pp. 117–137). https://doi.org/https://doi.org/10.1002/9781119039228.ch6

Lal, M. (1999). Shale stability: Drilling fluid interaction and shale strength. *Society of Petroleum Engineers - SPE Asia Pacific Oil and Gas Conference and Exhibition 1999, APOGCE 1999*. https://doi.org/10.2523/54356-ms

Lee, K. S., & Kim, T. H. (2016). Chapter 1 - Introduction. In *Integrative Understanding of Shale Gas Reservoirs* (pp. 1–19). Springer International Publishing. https://doi.org/10.1007/978-3-319-29296-0_1

Lihong, Z., Xuewei, L., Daqi, F., Dongping, L., Xingsong, L., Shengchuan, Z., Gongquan, C., Min, Z., Fuchun, T., Yudong, Z., Xiugang, P., Jianfeng, L., & Shunli, Y. (2019). *Evaluation and application of influencing factors on the fracturability of continental shale oil reservoir : a case study of Kong 2 Member in Cangdong sag*. *24*(5).

Lu, C., Ma, L., Guo, J., Li, X., Zheng, Y., Ren, Y., Yin, C., Li, J., Zhou, G., Wang, J., Du, Z., Meng, X., Song, M., & Yang, B. (2021). Novel method and case study of a deep shale fracability evaluation based on the brittleness index. *Energy Exploration and Exploitation*. https://doi.org/10.1177/01445987211033656

Lumivero. (2023a). *Spider Graphs*. https://help.palisade.com/v8/en/@RISK/Graphing/Spider-Graphs.htm?Highlight=spider

Lumivero. (2023b). *Tornado Graphs*. https://help.palisade.com/v8/en/@RISK/Graphing/Tornado-Graphs.htm?Highlight=tornado

Lumivero. (2023c). *What is Sensitivity Analysis and How Does it Work*. https://lumivero.com/software-features/sensitivity-analysis/

MENR. (2022). *Türkiye National Energy Plan*. https://enerji.gov.tr//Media/Dizin/EIGM/tr/Raporlar/TUEP/Türkiye_Ulusal_Enerji_Planı.pdf

Merey, Ş. (2019). Analysis of the effect of experimental adsorption uncertainty on CH4 production and CO2 sequestration in Dadas shale gas reservoir by numerical simulations. *Journal of Petroleum Science and Engineering*, *178*, 1051–1066. https://doi.org/10.1016/j.petrol.2019.04.022

Merey, S., Polat, C., & Eren, T. (2021). Design of horizontal wellbore in Dadas shales of Turkey by considering wellbore stability and reservoir geomechanics. *Proceedings of the SPE/IADC Middle East Drilling Technology Conference and Exhibition*, *2021-May*. https://doi.org/10.2118/202183-MS

Mews, K. S., Alhubail, M. M., & Barati, R. G. (2019). A review of brittleness index correlations for unconventional tight and ultra-tight reservoirs. *Geosciences (Switzerland)*, *9*(7). https://doi.org/10.3390/geosciences9070319

Mokhtari, M., Honarpour, M. M., Tutuncu, A. N., & Boitnott, G. N. (2016). Characterization of Elastic Anisotropy in Eagle Ford Shale: Impact of Heterogeneity and Measurement Scale. *SPE Reservoir Evaluation & Engineering*, *19*(03), 429–439. https://doi.org/10.2118/170707-PA

MSEEL. (2021). *mseel.org - /data/Wells_Datasets/*. http://mseel.org/data/Wells_Datasets/

Nacht, P. K., Oliveira, M. F. F. De, Roehl, D. M., & Costa, A. M. (2010). Investigation of geological fault reactivation and opening. *Asociacion Argentina de Mécanica Computaticioonal*, *XXIX*(January), 8684–8697.

Nalley, S., & Larose, A. (2021). *IEO2021 Highlights*. https://www.eia.gov/outlooks/ieo/pdf/IEO2021_ReleasePresentation.pdf

Ozturk, S. S., Demirel, I. H., & Günay, Y. (2016). Petroleum source rock potential of the Silurian Dadaş shales in the Hazro and Korudağ regions of Southeast Anatolia, Turkey. *Marine and Petroleum Geology*, *75*, 53–67. https://doi.org/10.1016/j.marpetgeo.2016.04.007

Palisade. (2023a). *RiskExpon*. https://help.palisade.com/v8/en/@RISK/Function/1-Distribution/RiskExpon.htm

Palisade. (2023b). *RiskPert*. https://help.palisade.com/v8/en/@RISK/Function/1-Distribution/RiskPert.htm

Palisade. (2023c). *RiskTriang*. https://help.palisade.com/v8/en/@RISK/Function/1-Distribution/RiskTriang.htm

Parapuram, G., Mokhtari, M., & Ben Hmida, J. (2018). An Artificially Intelligent Technique to Generate Synthetic Geomechanical Well Logs for the Bakken Formation. In *Energies* (Vol. 11, Issue 3). https://doi.org/10.3390/en11030680

Perez Altamar, R., & Marfurt, K. (2014). Mineralogy-based brittleness prediction from surface seismic data: Application to the Barnett Shale. *Interpretation*, *2*(4), T255–T271. https://doi.org/10.1190/INT-2013-0161.1

Rasouli, V. (2015). Geomechanics of Gas Shales. In R. Rezaee (Ed.), *Fundamentals of Gas Shale Reservoirs* (pp. 169–190). https://doi.org/https://doi.org/10.1002/9781119039228.ch8

Rickman, R., Mullen, M., Petre, E., Grieser, B., & Kundert, D. (2008). A practical use of shale petrophysics for stimulation design optimization: All shale plays are not clones of the Barnett Shale. *Proceedings - SPE Annual Technical Conference and Exhibition*, *2*(Wang), 840–850. https://doi.org/10.2118/115258-ms

Sahai, R. (2022). Chapter 1 - Field development and asset management. In R. G. Moghanloo (Ed.), *Unconventional Shale Gas Development Lessons Learned* (pp. 1–31). Gulf Professional Publishing. https://doi.org/https://doi.org/10.1016/B978-0-323-90185-7.00019-4

Salah, M., Ibrahim Mohamed, M., Ibrahim, M., & Pieprzica, C. (2019). A Newly Developed Approach to Evaluate Rock Brittleness and Fracability for Hydraulic Fracturing Optimization in Shale Gas. *SPE Western Regional Meeting*, 23–26. https://doi.org/10.2118/195196-MS

Saneifar, M., Aranibar, A., & Heidari, Z. (2014). Rock classification in the Haynesville Shale based on petrophysical and elastic properties estimated from well logs. *Interpretation*, *3*(1), SA65–SA75. https://doi.org/10.1190/INT-2013-0198.1

Şen, Ş., Aysal, N., & Kaygısız, E. (2021). Mineralogical Composition of the Silurian (Llandovery) Dadaş Hot Shales: Implication to Hydraulic Fracture Propagation. In O. Parlak, K. Sayit, B. L. Mesci, H. Akilli, & M. Akyildiz (Eds.), *73rd Geological Congress of Turkey with International Participation*. https://www.researchgate.net/publication/351971786_Mineralogical_Composition_of_the_Silurian_Llandovery_Dadas_Hot_Shales_Implication_to_Hydraulic_Fracture_Propagation

Sen, S., & Kozlu, H. (2020). Impact of maturity on producible shale oil volumes in the Silurian (Llandovery) hot shales of the northern Arabian plate, southeastern Turkey. *AAPG Bulletin*, *104*(3), 507–524. https://doi.org/10.1306/05141917201

Sondergeld, C. H., Newsham, K. E., Comisky, J. T., Rice, M. C., & Rai, C. S. (2010). Petrophysical considerations in evaluating and producing shale gas resources. *Society of Petroleum Engineers - Canadian Unconventional Resources and International Petroleum Conference 2010*, *1*, 1–34. https://doi.org/10.2118/131768-ms

Sui, H., Gao, W., & Hu, R. (2019). A new evaluation method for the fracability of a shale reservoir based on the structural properties. *Geofluids*, *2019*, 10–12. https://doi.org/10.1155/2019/2079458

Sui, L., Zheng, J., Yu, J., & Wang, X. (2015). Comprehensive evaluation on shale fracability using principal component analysis. *Electronic Journal of Geotechnical Engineering*, *20*(13), 5965–5976.

Suriamin, F., & Ko, L. T. (2022). Chapter 2 - Geological characterization of unconventional shale-gas reservoirs. In R. G. Moghanloo (Ed.), *Unconventional Shale Gas Development Lessons Learned* (pp. 33–70). Gulf Professional Publishing. https://doi.org/https://doi.org/10.1016/B978-0-323-90185-7.00006-6

The Geological Society of America. (2022). *GSA Geologic Time Scale*.

https://www.geosociety.org/GSA/GSA/timescale/home.aspx

Thiercelin, M. C., & Roegiers, J.-C. (2000). Chapter 3 - Formation Characterization: Rock Mechanics. In M. J. Economides & K. G. Nolte (Eds.), *Reservoir Stimulation* (3rd ed.). Wiley New York.

Topcu, G. Y. (2013). *Quantification of the uncertainties in shale gas reservoirs, a case study for Dadas shale formation* [Master's thesis, Middle East Technical University]. https://open.metu.edu.tr/handle/11511/22702

TPAO. (2023). *Operations: Unconventional*. https://www.tpao.gov.tr/en/unconventional

Tugan, M. F. (2017). *Assessing uncertainties and managing risks in shale gas projects* [Doctoral dissertation, Middle East Technical University]. https://open.metu.edu.tr/handle/11511/26887

Wang, D., Ge, H., Wang, X., Wang, J., Meng, F., Suo, Y., & Han, P. (2015). A novel experimental approach for fracability evaluation in tight-gas reservoirs. *Journal of Natural Gas Science and Engineering*, *23*, 239–249. https://doi.org/10.1016/j.jngse.2015.01.039

Wang, F. P., & Gale, J. F. W. (2009). Screening criteria for shale-gas systems. *Gulf Coast Association of Geological Societies Transactions*, *59*, 779–793. http://archives.datapages.com/data/gcags_pdf/2009/WangGale.pdf

Wang, H. Y. (2016). Numerical investigation of fracture spacing and sequencing effects on multiple hydraulic fracture interference and coalescence in brittle and ductile reservoir rocks. *Engineering Fracture Mechanics*, *157*(February 2016), 107–124. https://doi.org/10.1016/j.engfracmech.2016.02.025

Wikipedia. (2023a). *Exponential distribution*. https://en.wikipedia.org/wiki/Exponential_distribution

Wikipedia. (2023b). *PERT distribution*. https://en.wikipedia.org/wiki/PERT_distribution

Wikipedia. (2023c). *Triangular distribution*. https://en.wikipedia.org/wiki/Triangular_distribution

Worldometer. (2023). *Oil Production by Country*. https://www.worldometers.info/oil/oil-production-by-country/

Yasin, Q., Du, Q., Sohail, G. M., & Ismail, A. (2018). Fracturing index-based brittleness prediction from geophysical logging data: application to Longmaxi shale. *Geomechanics and Geophysics for Geo-Energy and Geo-Resources*, *4*(4), 301–325. https://doi.org/10.1007/s40948-018-0088-4

Yildirim, B. (2019). *An Experimental and Numerical Investigation Into Hydraulic Fracture Propagation in Naturally Fractured Shale Gas Reservoirs* [Doctoral Dissertation, Imperial College London]. https://spiral.imperial.ac.uk/handle/10044/1/80287

Yildirim, B. (2022). *Interaction of Hydraulic Fracture with Natural Fractures*. https://odtuclass2021s.metu.edu.tr/

Yuan, J., Deng, J., Zhang, D., Li, D., Yan, W., Chen, C., Cheng, L., & Chen, Z. (2013). Fracability evaluation of shale-gas reservoirs. In *Shiyou Xuebao/Acta Petrolei Sinica* (Vol. 34, Issue 3, pp. 523–527). https://doi.org/10.7623/syxb201303015

Yuan, J., Zhou, J., Liu, S., Feng, Y., Deng, J., Xie, Q., & Lu, Z. (2017). An improved fracability-evaluation method for shale reservoirs based on new fracture toughness-prediction models. *SPE Journal*, *22*(5), 1704–1713. https://doi.org/10.2118/185963-pa

Zee Ma, Y. (2016). Chapter 1 - Unconventional Resources from Exploration to Production. In Y. Zee Ma & S. A. Holditch (Eds.), *Unconventional Oil and Gas Resources Handbook Evaluation and Development* (pp. 3–52). Gulf Professional Publishing. https://doi.org/https://doi.org/10.1016/B978-0-12-802238-2.00001-8

Zendehboudi, S., & Bahadori, A. (2017a). Chapter One - Shale Gas: Introduction, Basics, and Definitions. In *SHALE OIL AND GAS HANDBOOK Theory, Technologies, and Challenges* (pp. 1–26). Gulf Professional Publishing. https://doi.org/https://doi.org/10.1016/B978-0-12-802100-2.00001-0

Zendehboudi, S., & Bahadori, A. (2017b). *Chapter Two - Shale Gas Characteristics* (S. Zendehboudi & A. B. T.-S. O. and G. H. Bahadori (Eds.); pp. 27–79). Gulf Professional Publishing. https://doi.org/https://doi.org/10.1016/B978-0-12-802100-2.00002-2

Zhang, F., Zhang, H., Yuan, F., Wang, Z., Chen, S., Li, C., & Han, X. (2015). Geomechanical mechanism of hydraulic fracturing and fracability evaluation of natural fractured tight sandstone reservoir in keshen gasfield in Tarim Basin. *Society of Petroleum Engineers - Abu Dhabi International Petroleum Exhibition and Conference, ADIPEC 2015*. https://doi.org/10.2118/177457-ms

Zhang, G., Wang, H., Li, F., Wang, D., Li, N., & He, S. (2022). Effects of Hydration during Drilling on Fracability of Shale Oil Formations: A Case Study of Da'anzhai Section Reservoir in Sichuan Basin, China. *Processes*, *10*(11). https://doi.org/10.3390/pr10112313

Zoback, M. (2007a). Chapter 1 - The tectonic stress field. In *Reservoir Geomechanics* (pp. 3–26). Cambridge University Press. https://doi.org/10.1017/CBO9780511586477.002

Zoback, M. (2007b). Chapter 4 - Rock failure in compression, tension and shear. In *Reservoir Geomechanics* (pp. 84–139). Cambridge University Press. https://doi.org/10.1017/CBO9780511586477.005